THERMOTOGA MARITIMA GLYCEROL DEHYDROGENASE AS A CATALYST FOR DIHYDROXYACETONE PRODUCTION: ENZYME CHARACTERIZATION, ENGINEERING AND COFACTOR IMMOBILIZATION

By

Justin Liam Beauchamp

A DISSERTATION

Submitted to
Michigan State University
In partial fulfilment of the requirements
For the degree of

Cell and Molecular Biology—Doctor of Philosophy

2015

ABSTRACT

THERMOTOGA MARITIMA GLYCEROL DEHYDROGENASE AS A CATALYST FOR DIHYDROXYACETONE PRODUCTION: ENZYME CHARACTERIZATION, ENGINEERING AND COFACTOR IMMOBILIZATION

By

Justin Liam Beauchamp

NAD-dependent dehydrogenases facilitate a diverse range of hydride transfer reactions in many areas of cellular metabolism. Dehydrogenases catalyze about 12% of metabolic reactions and are classified into 4 different groups: the medium-chain dehydrogenase superfamily, the short-chain dehydrogenase superfamily, the long-chain dehydrogenases, and the family III metal-dependent polyol dehydrogenases. The broad range of reactions catalyzed makes them attractive catalysts for synthetic process, especially since many produce chiral products. However, their use as catalysts has been limited by the requirement that the NAD cofactor be supplied in stoichiometric amounts. Enzymatic cofactor regeneration has been used for synthesis of high value products, but is not applicable to many processes because providing an extra enzyme increases costs. Electrochemical cofactor regeneration could be a lower cost alternative to enzymatic regeneration. Our overall goal is to immobilize *Thermotoga maritima* glycerol dehydrogenase (TmGlyDH) and its NAD cofactor onto an electrode for catalytic production of dihydroxyacetone (DHA) from glycerol where the electrode regenerates NAD^+. Glycerol is a waste product of the biodiesel industry, while DHA is a more valuable synthetic precursor and sunless tanning agent.

TmGlyDH's kinetics, stability and activity were characterized to provide acceptable operating conditions for an electrochemical reactor. TmGlyDH showed cooperative rather than Michaelis-Menten kinetics with glycerol and DHA, so the Hill equation was used to determine

limiting rate (V_{max}), half saturating substrate concentration ($K_{0.5}$) and Hill coefficient (n). The optimum pH for glycerol oxidation was 7.9. We tested alternative substrates similar to glycerol and TmGlyDH was able to produce 1,2-propanediol from hydroxyacetone at greater than 99% enantiomeric excess. To test if TmGlyDH can use immobilized NAD, the NAD analogue N^6-carboxymethyl-NAD (N^6-CM-NAD) was synthesized and immobilized on amino-linker-modified sepharose beads (NAD-sepharose). TmGlyDH had low activity with N^6-CM-NAD and mutants were produced to increase activity with the NAD analog 10-fold, but both TmGlyDH mutants and wild-type showed similar activity with NAD-sepharose. The length of the linker between NAD and sepharose had no effect on coenzymic activity. To see if other dehydrogenases can use N^6-immobilized NAD, we tested 6 different dehydrogenases and 5 of the 6 used NAD-sepharose as a cofactor; structural analysis of the enzymes binding pockets predicted activity with soluble N^6-carboxymethyl-NAD, but not with NAD-sepharose.

In a catalytic system, the longevity of the catalyst is important because renewing the catalyst is costly. We observed that TmGlyDH gets inactivated by its product, DHA. TmGlyDH inactivation by DHA is a result of the enzyme getting modified by Maillard reactions between the Lys and Arg residues and DHA. We identified which Lys and Arg residues get modified by DHA and prepared mutants to improve stability in the presence of DHA. The mutant most stable to DHA at 50°C was K361Q, maintaining activity twice as long as the wild-type enzyme in the presence of DHA at 50°C.

In summary, TmGlyDH has been characterized and engineered towards use in a bioelectronic catalytic system. Our immobilization method of NAD is suitable for use by a wide variety of dehydrogenases, indicating a working bioelectronic system would be adaptable to many novel applications.

Dedicated to the memory of my father, Michael Beauchamp. He was thrilled that I chose to go to graduate school, always excited to hear about my progress and would have loved to see me finish.

ACKNOWLEDGEMENTS

I would like to thank all former and current members of Dr. Vieille's lab. In particular, I would like to thank former postdoc Hoon Soon Song for mentoring me during my first couple years in the lab and for teaching me many of the lab skills I still use today. I would like to thank former postdocs (Dr. JJ Park and Dr. Sanhana Lal) and current and former graduate students (Dr. Bryan Schindler, Nik McPherson, and Rajasi Joshi) for being helpful and supportive lab members. I would like to thank Maris Laivenieks for sharing his considerable experience and knowledge with me and helping with many technical aspects of my project. I thank Ian Bloomquist for cloning the TmGlyDH gene prior to my joining the lab. I would like to thank the undergraduate researchers that worked with me on my project (Phillip Gross, Christopher Blum, and Mohamed Esa). Especially, I would like to thank Phillip Gross for his countless hours of work and dedication to the project.

I would like to thank Dr. R. Mark Worden, Dr. Scott Calabrese Barton, Dr. Brian Hassler, Dr. Hanzi Li, Dr. Rui Li and Dr. Chloe Liu, my collaborators in chemical engineering, for many constructive conversations, suggestions and insight into my project. I would like to thank Dr. Dan Jones, Dr. Lijun Chen and Dr. Scott Smith, members of MSU RTSF Mass Spectrometry Facility for their technical help with my project. I would like to thank Dr. Michael Feig and Dr. Srinivasa Gopal for help with the structural protein modeling aspects of my project. I would like to thank Arving Jagnathan for helping me get started with the NAD analog synthesis.

I would like to thank my committee members. Dr. R. Mark Worden, Dr. Eric Hegg, Dr. Shelagh Ferguson-Miller and Dr. Kevin Walker for their time and constructive guidance.

I would like to thank my friends and family for being there when needed. I thank my wife, Sami for her unwavering support and encouragement. I am grateful for the friends I have made while here at MSU; I think of them as part of my extended family.

Lastly I thank my advisor Dr. Claire Vieille. I am honored to have had her as my advisor. She has always been available when needed and has been very supportive and helpful. I appreciate the many hours she has spent editing my writing and helping me improve as a writer. Her insight and guidance has helped me to become a better scientist.

TABLE OF CONTENTS

LIST OF TABLES

LIST OF FIGURES

KEY TO ABBREVIATIONS

2°ADH, secondary alcohol dehydrogenase

ADH, alcohol dehydrogenase

B3APA, bis(3-aminopropyl)amine

bGDH, Bovine liver type III L-glutamate dehydrogenase

BsGlyDH, *Bacillus stearothermophilus* glycerol dehydrogenase

CBA, Carboxyphenylboronic acid

CboFDH, *Candida boidinii* formate dehydrogenase

CHES, 2-(cyclohexylamino)ethanesulfonic acid

CV, column volumes

DETA, diethylene triamine

DHA, dihydroxyacetone

e.e., enantiomeric excess

ED, ethylene diamine

ESI-TOF, electrospray ionization time of flight

GlyDH, glycerol dehydrogenase

IAA, iodoacetamide

LDR, long-chain dehydrogenases/reductases

LmG6PDH, *Leuconostoc mesenteroides* glucose-6-phosphate dehydrogenase

MDR, medium-chain dehydrogenases/reductases

N^1-CM-NAD, N^1-carboxymethyl-NAD

N^6-CM-NAD, N^6-carboxymethyl-NAD

PEG, poly(ethylene glycol)

PQQ, pyrroloquinoline quinone

PseFDH, *Pseudomonas* sp.101 formate dehydrogenase

PTDH, phosphite dehydrogenase

rLDH, Rabbit muscle type XI L-lactate dehydrogenase

SDR, short-chain dehydrogenases/reductases

TBO, toluidine blue O

TFA, trifluoroacetic acid

TmGlyDH, *Thermotoga maritima* glycerol dehydrogenase

TmMtDH, *Thermotoga maritima* mannitol dehydrogenase

yADH, *Saccharomyces cerevisiae* alcohol dehydrogenase

CHAPTER 1. Introduction – Dehydrogenases as catalysts

1.1 INTRODUCTION

My project started as a collaboration between the Vieille laboratory in the Department of Microbiology and Molecular Genetics, and the Worden and Calabrese Barton laboratories in the Department of Chemical Engineering and Material Science at Michigan State University. Our goal was to develop a dual-chamber bioelectrocatalytic reactor that uses dehydrogenase enzymes to catalyze chemical reactions. The two enzymes selected for this project were *Thermotoga maritima* mannitol dehydrogenase (TmMtDH) that interconverts mannitol and fructose and *T. maritima* glycerol dehydrogenase (TmGlyDH) that interconverts glycerol and dihydroxyacetone (DHA). In a reactor, the enzymes and NAD(H) cofactors would be immobilized on electrodes that have been modified to allow electron transfer to/from NAD(H). TmMtDH was supposed to catalyze fructose conversion to mannitol in the cathode compartment, and TmGlyDH was supposed to convert glycerol to DHA in the anode compartment. The electrons and protons released in the anode compartment were going to be used to regenerate NADH in the cathode compartment (Figure 1.1), with the protons traveling through a proton-permeable membrane and the electrons traveling through the external electrical circuit. I Studied the enzymes and devoloped a method to immobilize NAD(H) onto an electrode surface. Partway into my project, we were not able to reproduce early results of NAD^+ electrochemical reduction, although NADH oxidation was reproducible and new methods to increase the oxidation rate at lower overpotentials were promising. Therefore, we decided to focus our project on the anode reaction, for which a single chamber flow-through reactor may be ideal (Figure 1.2). For my part of the project, it meant focusing on the study of TmGlyDH and NAD immobilization rather than on both TmGlyDH and TmMtDH.

Figure 1.1: Two-chamber bioelectrocatalytic system for DHA and mannitol enzymatic production.

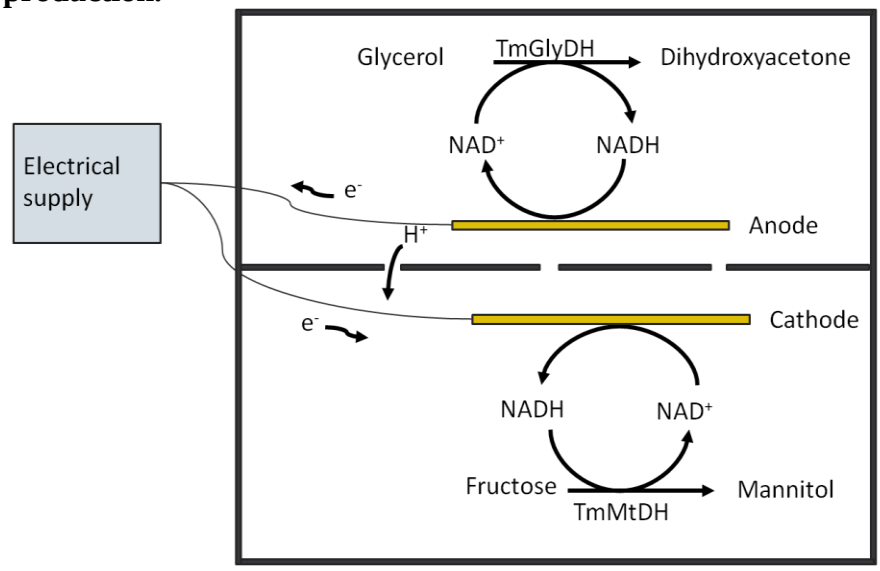

Figure 1.2: A single-chamber flow-through reactor for DHA enzymatic production from glycerol.

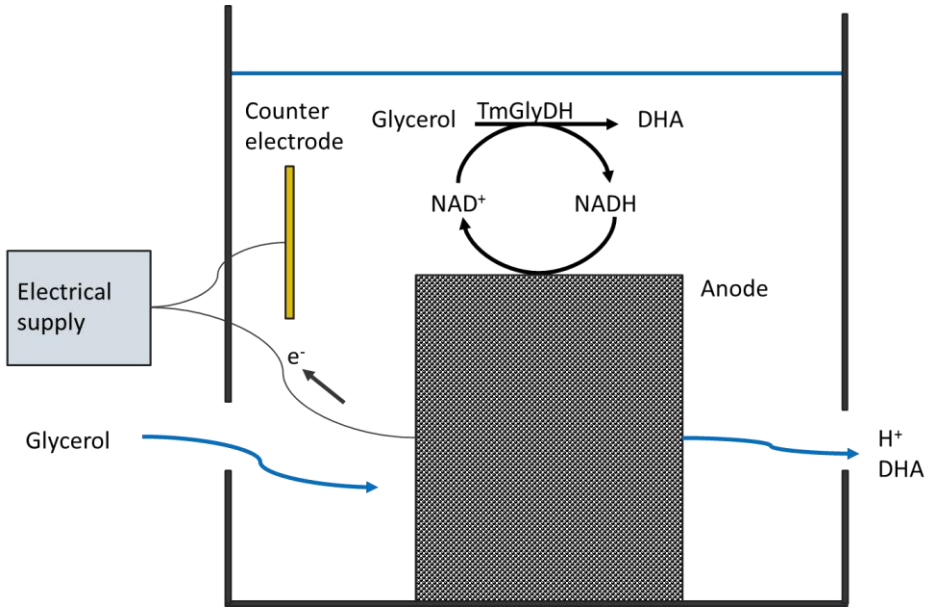

For dehydrogenase-based bioelectrocatalysis to be viable there needs to be (1) rapid electron transfer between the electrode, mediator, cofactor, and enzyme; (2) rapid proton transfer; (3) rapid mass transfer of reactants; and (4) rapid enzyme kinetics (69). Immobilization

of the enzyme and cofactor will eliminate the need for regenerated NAD(H) to diffuse through the bulk liquid to the enzyme, reducing mass transfer limitations and allowing catalytic quantities of enzyme and cofactor to be used (15). However, for immobilization to be successful, two conditions must be met. First, NAD must be immobilized in an orientation that allows enzyme binding. Second, the immobilized enzyme must retain high levels of activity. Another requirement for bioelectrocatalysis is that the products should be of higher value than the reactants. In the following sections, I am reviewing the background knowledge on NAD(P)-dependent dehydrogenases, glycerol dehydrogenases, DHA as a high value-added chemical, cofactor regeneration methods, and methods for cofactor and enzyme immobilization methods, before introducing the main objectives of my project.

1.2 DEHYDROGENASE DIVERSITY AND FAMILIES

Dehydrogenases catalyze oxido-reduction (redox) reactions that transfer an electron pair and a proton between a cofactor such as NADH and a substrate (68). These enzymes play an important role in metabolism and are responsible for over 12% of all metabolic reactions in *Escherichia coli* (50). NAD(P)-dependant dehydrogenases and reductases belong to one of four groups, short-chain dehydrogenases/reductases (SDR) (21), medium-chain dehydrogenases/reductases (MDR) (48), long-chain dehydrogenases/reductases (LDR) (22, 23), and family III metal-dependent polyol dehydrogenases (52), based on size, sequence, structure, and features of their catalytic mechanism (21-23, 48, 52). All characterized dehydrogenases share the NAD binding Rossman fold motif and catalyze a hydride transfer (21, 48). Of note, aldo-keto reductases, which evolved separately, do not share sequence similarity with dehydrogenases, do not have a Rossman fold, and belong to the TIM barrel protein family, still

have active sites that are nearly superimposable to those of dehydrogenases (2, 21). Most known dehydrogenases belong to either the MDR or SDR groups (21, 48).

1.2.1 The long-chain dehydrogenases

The LDR group is small, consisting of only 66 members as of 2003 (22). LDRs range in size from 357 to 544 amino acids, and are primarily categorized based on their sequence containing the Lys-X_4-Asn-X_2-His motif (X is any amino acid) (22). In general, LDRs are not well characterized, but they are primarily active as monomers, are not metal dependent, have a conserved lysine in their catalytic site, and are distinct structurally and mechanistically from the MDRs and SDRs (21-23).

1.2.2 The medium-chain dehydrogenases

The MDR superfamily is composed of many large families, and smaller groups, many of which are zinc dependent (48). MDRs use a catalytic zinc, and members of the alcohol dehydrogenase (ADH) family also have an additional, structural zinc. There are two main structural domains in MDRs, a substrate-binding domain and a Rossman fold NAD-binding domain. The catalytic site sits in a deep cleft in the protein with the cofactor binding site. MDRs can be monomers or multimers with different numbers of subunits and each monomer is typically composed of about 350 amino acids. Most known MDRs can be grouped into 8 families, but it is estimated that there are 500 different MDR families (48).

1.2.3 The short-chain dehydrogenases

There are at least 140 different SDRs, making up about ¼ of all dehydrogenases, and they are found in all domains of life (21). SDRs are unique because they are made up of only one domain that is about 250 amino acids long. Most of them have a catalytic tyrosine in their active site, but no residue is completely conserved. The one unifying factor is their NAD(P)-binding Rossman fold. SDRs catalyze a broad range of reactions, being found in half of the different enzyme class types (21).

1.2.4 The family III polyol dehydrogenases

The family III metal-dependent polyol dehydrogenases, formerly called iron-containing dehydrogenases are metal and NAD-dependent cytoplasmic enzymes (52). They can either have zinc or iron bound in their active site, or require iron in solution for activity (49). Many have similar activity to the medium chain dehydrogenases, but do not show sequence similarity (52).

Although structurally different, all the dehydrogenase families share the Rossman fold for NAD binding. The similarity in cofactor binding pocket is advantageous because a cofactor immobilization method that works for one dehydrogenase is likely adaptable to many different dehydrogenases.

1.3 GLYCEROL DEHYDROGENASES

Glycerol dehydrogenase (GlyDH) is a promising enzyme catalyst for DHA production from glycerol. Glycerol dehydrogenases can be classified into four groups. The first group is composed of cytoplasmic zinc-dependent enzymes that belong to the NAD-dependent family II polyol dehydrogenases in the MDR superfamily (74). The second group comprises cytoplasmic

zinc-dependent enzymes that are part of the NAD-dependent family III metal-dependent polyol dehydrogenases formerly called iron-containing dehydrogenases (52). Although similar in activity, groups one and two GlyDHs do not show any sequence similarity (52). The third group has not been well studied and comes from molds and filamentous fungi; these enzymes are NADP-dependent and can reduce both DHA and glyceraldehyde to glycerol (32). The final group represents membrane-bound pyrroloquinoline quinone (PQQ)-containing enzymes found in many bacterial species. These enzymes are hard to purify and are unstable once purified (25). In contrast, NAD-dependent cytoplasmic GlyDHs can be expressed and purified in high yields.

To reduce costs associated with dehydrogenase-based catalysis and to optimize reaction conditions to an industrial setting, thermostable dehydrogenases are being investigated. Part of the reduction in cost comes from simple purification of overexpressed proteins via heat treatment. (56) Thermostable enzymes also increase operational temperatures for enzymatic processes by reducing mass transfer limitations, reducing viscosity, increasing substrate and product solubility, and reducing microbial contamination (8, 64). We chose to study the GlyDH from *T. maritima* (TmGlyDH). *T. maritima* is a hyperthermophilic bacterium that grows optimally at 80°C, and we expected TmGlyDH to be highly thermostable. TmGlyDH is a family III NAD-dependent GlyDH whose crystal structure had been solved (7, 58) as part of a structural genomics project targeting the *T. maritima* proteome, but whose catalytic properties remained unstudied.

Family III NAD-dependent GlyDHs use zinc in their active site and share the Rossman fold. Many have broad substrate specificity, showing high activity levels on 1,2-ethanediol, 1,2-propanediol, 2-3-butanediol, 3-mercapto-1,2-propanediol, 3-chloro-1,2-propanediol, 1,2,3-propanetriol monoacetate, 3-amino-1,2-propanediol, and 3-methoxy-1,2-propanediol (27, 57,

60). These enzymes have also been shown to produce a variety of (R) or (S) diols at 98% or greater enantiomeric excess (e.e.) (73).

1.4 DHA PRODUCTION AND APPLICATIONS

We chose to synthesize DHA, because it is a value-added product that can be produced from glycerol, a waste product of the biodiesel industry. DHA is the only FDA-approved active ingredient used in sunless tanning creams (19), and it is used as a precursor for many valuable products. DHA can be used as a precursor to 1,2-propylene glycol, which is used in antifreeze, brake fluids, and as a precursor to polyurethanes and polypropylene glycols (59). DHA is also a precursor of anti-ulcer, antihypertensive anti-inflammatory, analgesic (47), anti-ischemic, and α-2-adrenergic receptor agonist drugs (11). Many chiral, optically active epoxide-based drugs (75), pesticides (59), and sweeteners (6) use DHA as a precursor. The DHA global market was about 2,000 tons per year as of 2007 (45).

DHA is currently produced by glycerol oxidation in a large stirred tank using *Gluconobacter oxydans* (16). A batch-fed process is used so that glycerol and DHA can be kept below inhibitory concentrations (16). Glycerol oxidation to DHA needs large quantities of oxygen, so aeration levels must be kept high using oxygen-enriched air (16). An industrial strain of *G. oxydans* optimized to overcome DHA inhibition produced DHA at a rate of 3.6 g L^{-1} h^{-1} with a 85% yield in a two-step fed-batch process (3). *G. oxydans* has been further optimized to produce DHA at a rate ranging from 12 g L^{-1} h^{-1} at a concentration of 100 g/L glycerol to 9.5 g L^{-1} h^{-1} at a concentration of 140 g/L glycerol with a 96% yield. In addition the productivity based on cell dry weight increased by 140% (31). Although optimization of the DHA production process has increased yields and rate of production, the cost of DHA remains relatively high

because of the batch-fed process, high aeration levels required, and downstream purification costs. A bioelectrocatalytic system has potential to reduce the production and purification costs of DHA.

1.5 ENZYMATIC COFACTOR REGENERATION METHODS

Because of the variety of reactions catalyzed by dehydrogenases, these enzymes have potential as catalysts for the production of many different compounds including chiral compounds and pharmaceutical precursors (67, 68). In cells, the activity of dehydrogenases is driven by cofactor regeneration in complementary pathways. In vitro, though, dehydrogenase reactions depend on the cofactor being supplied in stoichiometric amounts or somehow regenerated. This limitation has significantly hindered dehydrogenase-based industrial applications (67, 68).

1.5.1 Formate dehydrogenase

Several methods have been developed to regenerate the cofactor, reducing overall cost. For high value products such as chiral compounds, NADH can be regenerated by coupling the desired reaction with another enzymatic reaction (67, 68). A promising enzyme for regenerating NADH is formate dehydrogenase (FDH), which converts formate to CO_2 while reducing NAD^+ to NADH (55). For example, formate dehydrogenase was first used as a NADH regeneration system to produce lactate (79% yield after 15 days) from pyruvate using D-lactate dehydrogenase, producing D-lactate in 92% enantiomeric excess (55). This NADH regeneration method is useful because CO_2 is poorly soluble in water and easily removed from the reaction, making the formate dehydrogenase reaction almost irreversible. Cofactor recycling with FDH

can thus be used to drive thermodynamically unfavorable reactions and formate has little effect on dehydrogenase activity (67).

The use of FDH to regenerate the reduced cofactor has been limited by the low stability of the enzyme (61). FDHs have Cys residues whose modification or oxidation, quickly inactivates the enzyme. Also, FDH does not natively use NADP as a cofactor, enzyme production costs are high, and specific activity is low. FDH has been extensively engineered to alleviate these problems. The two most studied FDHs are from *Candida boidinii* (CboFDH) and *Pseudomonas* sp.101 (PseFDH). PseFDH is the most active native FDH with a specific activity of 10 U per mg (k_{cat} = 7.3 s^{-1}). Several of the PseFDHs Cys residues have been mutated resulting in a 1,000-fold increased chemical stability. Directed evolution has been used to increase thermal stability of PseFDH enough to allow a heat treatment step during purification, reducing purification cost. The cofactor specificity has also been changed to allow FDH to be used with NADP-dependent enzymes, although the activitiesare only about 10% of the wild-type enzyme with NAD (61). Overall, with the exception of the PseFDH chemical stabilization, improvement in FDH thermostability, activity levels, and activity with NADP have been incremental, though.

1.5.2 Phosphite dehydrogenase

Another promising cofactor-recycling enzyme is phosphite dehydrogenase (PTDH) (77). PTDH catalyzes the oxidation of phosphite to phosphate, reducing NAD to NADH in the process. With an equilibrium constant of 10^{11}, the reaction is essentially irreversible (65). PTDH has been engineered for increased activity with NADP, yielding a mutant enzyme with a 1,000-fold increased catalytic efficiency with NADP (70), and a k_{cat} with NADP reaching almost 50% of the k_{cat} with NAD (70). Interestingly, the catalytic efficiency of the mutant enzyme with NAD

also increased 3.6-fold. PTDH's thermostability has been increased by directed evolution, increasing the half-life at 45°C 7,000-fold (18). PTDH is likely a better recycling enzyme than FDH for reactions involving NADP, because the catalytic efficiency of PTDH with NADP is 39-fold higher than that of the commercially available mutant PseFDH while the k_{cat} is comparable (70).

1.5.3 Regeneration of oxidized cofactors

Regeneration of the oxidized cofactor $NAD(P)^+$ has not been as well studied as regeneration of the reduced form because the reduced form is used more often, in particular to drive enzymatic reactions that produce chiral compounds (63). Regenerating the oxidized cofactor could allow dehydrogenases to be used for clarifying racemic mixtures of enantiomers, or synthesizing difficult-to-prepare aldehydes and ketones. Glutamate dehydrogenase, which is active with both NAD and NADP, could be used to recycle the oxidized cofactor by reducing α-ketoglutarate. NAD^+ could also be recycled using NADH oxidase. Many NADH oxidases produce hydrogen peroxide, which can damage proteins, so the addition of catalase would be required. But certain NADH oxidases produce water instead and would be preferred.

A major limitation of enzyme-based cofactor regeneration is the added cost of using two enzymes and two reactants while still producing only one product. Several other enzymes have been used to regenerate NADH including glucose-6-phosphate dehydrogenase, glucose dehydrogenase, alcohol dehydrogenase, and hydrogenase, (67). All of these enzymes require extra reaction components, often complicating product purification and increasing overall cost. Regenerating NAD(H) with electrical current could be a lower cost alternative, allowing new dehydrogenase-based catalytic systems to be developed.

1.6 ELECTROCHEMICAL COFACTOR REGENERATION

1.6.1 Direct cofactor regeneration

There are two electrochemical methods of regenerating NAD(H), direct electron transfer and mediated electron transfer. Direct electron transfer involves electrons being transferred directly between the electrode and NAD(H). Carbon electrodes can be used to oxidize NADH at moderate potentials (ca 0.64 V vs standard hydrogen electrode [SHE]) (35), but the reaction kinetics are quite poor and NAD adsorbs onto the electrode surface, interfering with activity (35). Using high overpotentials of around 1V greater than the formal potential (-320 mV vs SHE) (10, 35) increases the catalytic rate but can lead to unwanted reactions taking place, cofactor degradation, and electrode fouling (4, 5). Direct NADH oxidation has been combined with different dehydrogenases in biosensors to detect ethanol, lactate, glutamate, hydroxybutyrate, and cholic acid with the NAD either in solution, entrapped under a membrane, or covalently attached (35). In general these biosensors had low stability (losing most activity after a few days to a few weeks) and used applied voltages of ca ~1 V (vs SHE) (35). In contrast, FAD-dependent enzymes such as glucose oxidase readily allow direct electron transfer (17, 35, 71).

Direct electrochemical reduction of NAD^+ also requires high overpotentials and requires two electrons for each NAD^+ molecule (53, 54). A radical intermediate forms during direct reduction because electrons are transferred one by one (53, 54). Two NAD radicals can then react together to form an inactive dimer (Figure 1.3) (53, 54).

Figure 1.3: Electrochemical reduction of NAD^+. R= Adenosine diphosphate ribose.

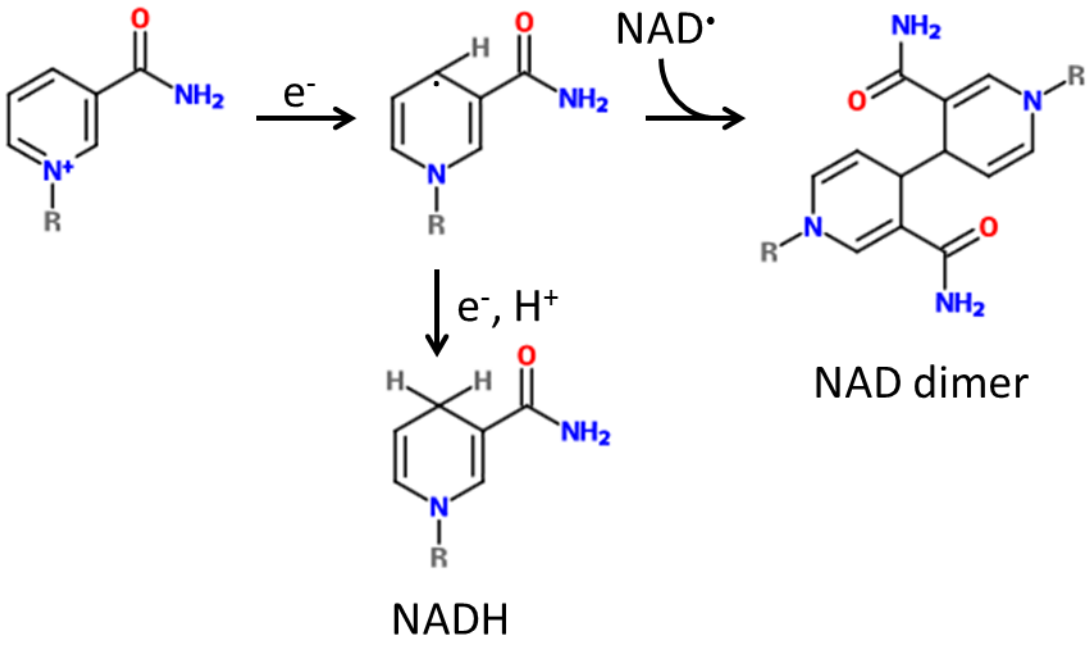

1.6.2 Mediated cofactor regeneration

The problems associated with direct electrochemical oxidation of NADH have been addressed using mediated electron transfer. Mediators accept electrons from NADH and then diffuse to the electrode surface where they are oxidized at a lower potential than NADH (35). The most studied mediators are quinones, quinoneimines, and azines such as phenazine**.** One azine mediator that can be readily covalently bound to an electrode through carbodiimide coupling is toluidine blue O (TBO) (14, 15). TBO has been coimmobilized with the cofactor and alcohol dehydrogenase and used for the electrochemical detection of alcohol. Mediated transfer has also been combined with the enzyme diaphorase (10). Diaphorase regenerates NAD^+ with a benzyl viologen (10) or ferrocene mediator (66), transferring electrons from the electrode to diaphorase where NADH is oxidized. Diaphorase-coupled regeneration is less desirable than

using a chemical mediator because diaphorase is oxygen sensitive and adding a second enzyme increases cost.

Similarly, the electrode surface can be directly modified with a catalyst that can activate NADH oxidation. The difference between a mediator and a catalyst can be unclear at times, but generally a mediator will carry electrons to a distance from the electrode while a catalyst will be incorporated into the electrode surface. Adding carbon nanotubes to an electrode lowers the overpotential required for NADH oxidation and increases the surface area of the electrode (76). A carbon nanotube-modified electrode worked as a glucose biosensor, which operated continually for 25 hours without a significant reduction in current and maintained 64% of activity after being stored dry for 1.5 months (76). NADH oxidation took place readily at voltages of ca 180 mV vs SHE, which is 300 mV lower than a bare glassy carbon electrode (76). Adding a mediator/catalyst, such as an azine can increase current density and further lower the oxidation potential (30).

Methylene green and TBO have also been electropolymerized onto a carbon nanotube-modified electrode, catalyzing NADH oxidation (30). Polymethylene green was a more effective NADH oxidation catalyst than polyTBO. Electropolymerization takes place by cycling the potential of the electrode from low potential (ca -0.7 V vsSHE) to high potential (c a1.3 V vs SHE) for many cycles, where the polymerization takes place around 1V. Methylene green polymerized onto a carbon nanotube-modified electrode is promising as a NAD^+ regeneration system. In addition, electroactivation of carbon electrodes can increase the catalytic rate of NADH oxidation (29). Electroactivation works by cycling the potential of the electrode from ca -1.7 V to 2.3 V vs SHE for twenty cycles, where at the higher voltage the carbon can oxidize forming a variety of functional groups, of which the formation of quinones is the main

contributor to NADH oxidation. In addition, carbon nanotubes can be electroactivated, increasing the surface area and further increasing the catalytic rate. Adding methylene green and polymethylene green can lead to current densities of 7.0 mA/cm^2 and 3.8 mA/cm^2, respectively, in 20 mM NADH at ca 28 mV vs SHE (29). The high current densities produced make electrochemical regeneration of NAD^+ feasible for a dehydrogenase-based catalytic reactor.

1.7 MODIFYING ELECTRODES FOR IMMOBILIZATION OF MEDIATOR AND COFACTOR

Two approaches to modifying electrodes can be used. In the first approach, a small chemical with a carboxyl group (e.g., cysteine or glycine) is electrolytically deposited or polymerized on the electrode, while the second approach involves depositing on the electrode polymers that have reactive groups that can be further modified; such methods for carbon electrodes are currently being developed in the Worden and Calabrese-Barton laboratories (Department of Chemical Engineering and Materials Science, Michigan State University). The first approach has already been used for cysteine on gold electrodes (15). Firest, a self-assembling monolayer of cysteine was prepared on a gold electrode. The mediator (TBO) was then bound to cysteine's carboxylic group, and the boronate linker carboxyphenyl boronic acid was bound to cysteine's amino group using amide linkages (Figure 1.4) (15). Then NAD(P) was bound to the boronate linker through its cis-diols. This interface with immobilized NAD was tested with *Saccharomyces cerevisiae* ADH, and immobilized NADP was tested with *Thermoanaerobacter ethanolicus* secondary ADH (2°ADH). The enzymes were immobilized onto the interface using glutaric dialdehyde fixation (15). Current was observed to increase linearly from 0 to 25 mM of enzyme substrate (ethanol for ADH and 2-propanol for 2°ADH).

The 2°ADH interface lost only 2% of its activity after 24 hours of continuous operation at room temperature and it could be stored dry for 3 weeks without activity loss. The interface started to lose 5% of activity per rinse after 10 rinses (15).

Figure 1.4: Two possible NAD binding orientations on a boronate linker. Methionine (Met) is directly bound to the electrode, carboxyphenylboronic acid (CBA) and TBO are bound to MET through amide bonds, and NAD is bound to CBA through its cis-diols. The dotted lines represent the limits between different molecules.

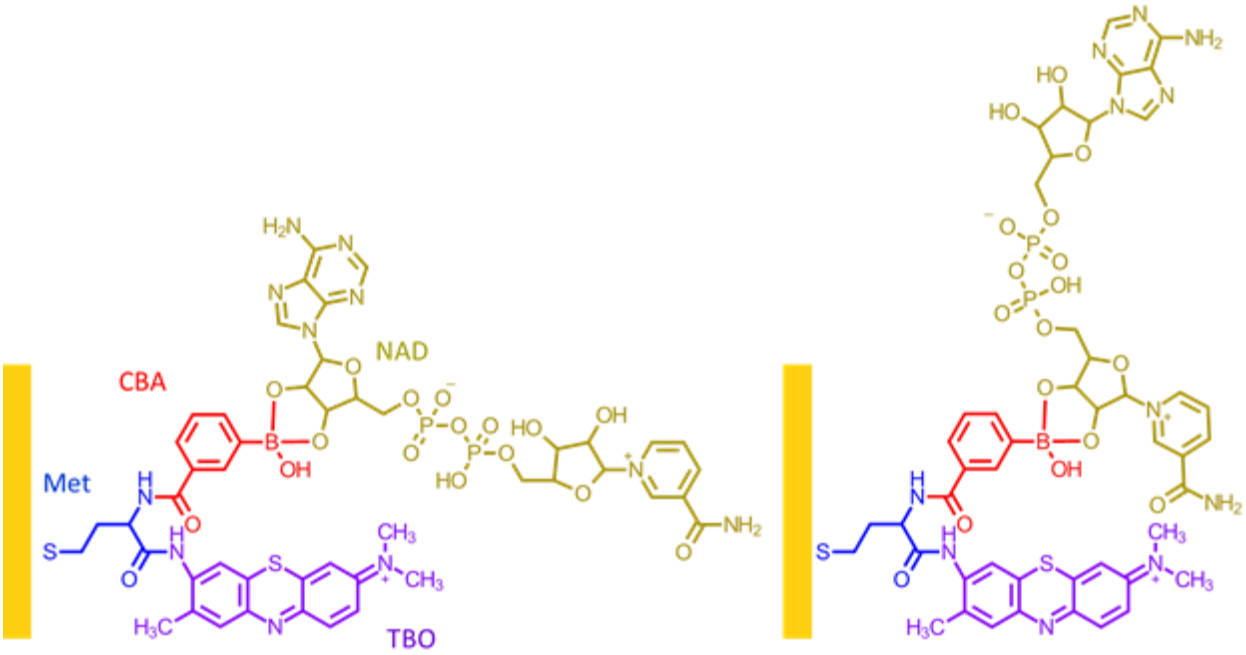

The second approach was designed to make easily renewable and higher loading interfaces. This method involves a layer-by-layer build up using polyelectrolyte polymers (14). Polymers with carboxylic or amine groups are layered, alternating between positively and negatively charged polymers. After 3-mercaptopropionic acid attaches to the electrode, the TBO mediator is bound to its terminal carboxylic group, then a layer of poly(ethyleneimine) is added to the electrode. A linker such as carboxyphenyl boronic acid can then be attached to the terminal

amine groups in a reaction with N-(3-dimethylaminopropyl)-N′-ethylcarbodiimide hydrochloride (EDC), followed by NAD binding (14). A 0.1 M HCl solution can be used to remove the poly(ethyleneimine)-attached NAD and allow the electrode interface to be renewed. Then a new layer can be applied, restoring electrode activity. After regeneration, the saturation current, sensitivity, and turnover rate were reduced by 8.3%, 16%, and 5% respectively (14). Saturation current is the maximum current measured as the enzyme substrate is increased and sensitivity is the change in current observed after a change in substrate concentration. The layer-by-layer build up method could also be used for an amine-containing linker, if the final polymer layer contains carboxylic groups.

In both of these methods, a boronate linker was used to attach NAD, but boronate-based linkages have two problems for the applications proposed for the current work. First, NAD has two cis-diols, so NAD can bind to the boronate in two possible conformations which could affect its ability to bind to the enzyme and affect catalytic efficiency (Figure 1.2) (15).

Second, the bond formed between boronate and NAD is relatively unstable, with a dissociation constant (K_d) of 5.9×10^{-3} (1). Boronate also has affinity for cis-diols found on sugars and sugar alcohols; the K_d for mannitol is similar to that for NAD and the K_d for fructose is smaller than that for NAD (1). In a catalytic reactor using TmGlyDH glycerol will be present in high concentrations. Because the K_d for glycerol is likely in the same order of magnitude as that for NAD, the boronate linkage would be unstable, with high concentrations of glycerol displacing NAD. For a catalytic reactor, stability is a particularly important issue because the catalytic interface would need to be stable over a long period of time (several days to several weeks).

1.8 COFACTOR IMMOBILIZATION

For dehydrogenase-based catalysis to be economically feasible on a large scale, the cofactor needs to be easily regenerated and recovered. Cofactor regeneration during the reaction allows products to accumulate using only small quantities of NAD, while NAD recovery after the reaction allows it to be used again. Recovering the soluble cofactor for reuse in another reaction can be difficult and increases reaction costs. Immobilization of the cofactor and enzyme is ideal, because it allows reuse of the entire catalytic system. In an electrochemical recycling system the cofactor would ideally be bound to the electrode surface together with the enzyme to facilitate electron transfer from the electrode to the enzyme active site. Physically entrapping the cofactor in a matrix is not ideal, because the NAD can slowly diffuse away from the electrode (40). Membranes have been used to entrap enzyme and cofactor at the electrode surface successfully for biosensors (24, 28, 46). Using membranes in a catalytic reactor is not ideal, though, because the membrane would have to be selective to allow reactant and product to diffuse while preventing cofactor and enzyme from diffusing, and the membrane can reduce mass transfer rates (34). Covalent attachment of the cofactor to an electrode is more promising for catalytic use because it is adaptable to high surface area electrodes and the immobilization process allows the addition of a linker molecule that can reduce steric hindrance between the enzyme and the surface to which NAD is bound.

1.8.1 Modification of NAD's N^1 and N^6-amines

Covalent modification of NAD was studied heavily in the 1970s and 1980s (9, 37). Some of the earliest NAD immobilizations involved directly coupling NAD to a carboxyl-containing polymer matrix using a carbodiimide coupler (26) or directly coupling NAD to CNBr-activated agarose

(38). The first well-characterized NAD^+ analogue was synthesized by Lindberg et al. (33). The authors alkylated NAD^+ with iodoacetic acid to form N^1-carboxymethyl-NAD^+, which then rearranges to N^6-CM-NAD^+ under alkaline conditions (Figure 1.5). N^1-CM-NAD^+ was reported to have a broad-shouldered absorbance maximum at 259 nm. N^6-CM-NAD^+ was reported to have an absorbance maximum at 266 nm, as opposed to a shoulderless absorbance maximum at 260 nm for NAD^+. N^6-CM-NAD^+ was also coupled to 1,6-diaminohexane using a carbodiimide-coupling reagent giving NAD^+-N^6-[N-(6-aminohexyl)-acetamide] while maintaining the absorbance maximum at 266 nm. The NAD^+-N^6-[N-(6-aminohexyl)-acetamide] was then immobilized by reacting with CNBr-activated sepharose. The sepharose-bound NAD^+ was stable, retaining activity as a functioning cofactor and affinity chromatography matrix for several months. When tested in enzyme assays with three dehydrogenases (horse liver ADH, beef heart type III lactate dehydrogenase, and pig heart malate dehydrogenase), N^6-CM-NAD^+ showed 55-75% of activity as compared to native NAD^+, while the NAD^+-N^6-[N-(6-aminohexyl)-acetamide] analogue showed 50-100% activity as compared to native NAD^+. Enzyme activity with the sepharose-bound cofactor was also tested with a three-enzyme system where malate dehydrogenase converted malate to oxaloacetate, citrate synthase converted oxaloacetate to citrate, and lactate dehydrogenase recycled the cofactor. The reaction rate increased after the addition of the cofactor recycling enzyme. As an affinity chromatography matrix, sepharose-bound NAD^+ was able to bind ADH and lactate dehydrogenase, while bovine serum albumin passed through the column (33).

Figure 1.5: NAD$^+$ structure. The N^6-amine, phosphate backbone, and cis diols are possible immobilization points.

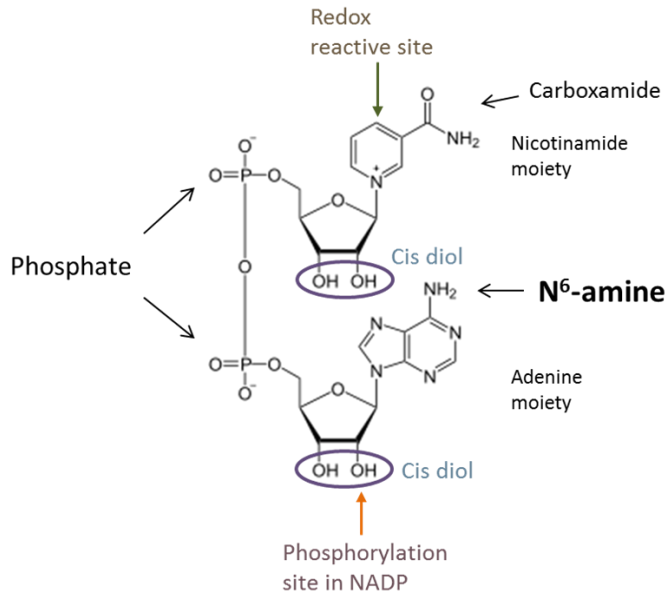

Building on the early work by Lindberg et al. (33), NAD was modified at the N^1-amine by various reactive species (i.e., iodoacetic acid, aziridine, propionolactone, and epoxides), creating a terminal carboxyl, amino, or vinyl group that could be used for immobilization (37). The N^1-modified NAD could then be immobilized, or rearranged into N^6-modified NAD via alkaline Dimroth rearrangement. One disadvantage of using the N^1-modified analogue is that it is unstable at basic pH, because the Dimroth rearrangement will take place slowly under mild alkaline conditions. The stability is low enough that, when the alkylation reaction is performed over fifteen days at pH 9.0, the main product is the N^6-derivative instead of the N^1-derivative formed at pH 6.5 (44). Recently, a mixture of chitosan-immobilized N^1-CM-NAD and chitosan-immobilized glucose dehydrogenase in a water solution of carbon nanotubes was dried on an electrode and used as a glucose biosensor (76). The addition of a Nafion membrane over the sensor increased the sensitivity and current density, giving a sensitivity of 1.8 mA M^{-1} cm^{-2} with

a linear range of 0.02-2.0 mM. The Nafion-modified electrodes were quite stable, maintaining 100% of activity over 24 hours and 64% of activity after storage for 1.5 months (76).

Another way to modify the N^6-position is to use an NAD derivative containing a 6-chloro- or 6-mercapto-modified adenine and use nucleophilic substitution by an amine-containing compound (37). This approach is not ideal, however, because it requires starting with an NAD analogue. Direct acylation of the N^6-amine is also possible, but the acylated derivative is poorly stable above pH 7 (72). NAD derivatives modified at the C^8 of the adenine ring have also been synthesized, but they generally have lower coenzymic activity than the N^1 or N^6 derivatives (37). The N^6-amine group on NAD(H) is a promising candidate for linkage, as it can be modified to have a terminal carboxyl group (33, 39). NAD(P)'s N^6 amine has been used to attach large molecules like poly(ethylene glycol) (PEG) to NAD to facilitate NAD reuse and removal from an enzymatic reaction (20, 43).

Recently, NAD has also been immobilized onto silica nanoparticles using the bifunctional linker glycidoxypropyltrimethoxysilane in which the epoxide is able to alkylate NAD at the N^1-amine and the silane group can be attached to silica (34). Nanoparticle-bound cofactor, nanoparticle-bound bovine glutamate dehydrogenase, and nanoparticle-bound rabbit lactate dehydrogenase were prepared by amine reaction with the epoxide-modified nanoparticles. A mixture of all three types of nanoparticles allowed the two enzymes to recycle the cofactor, while Brownian motion allowed the cofactor to be transferred between the two kinds of enzyme-particles. A similar method was used to immobilize NAD through its N^6-amine into a sol-gel-based biosensor (66). In this case, a diaphorase and ferrocene mediator were used to electrochemically sense and regenerate the cofactor on the electrode, in the presence of a co-immobilized dehydrogenase. The epoxide of glycidoxypropyltrimethoxysilane was used to

modify NAD at the N^6-amine and the silane was covalently incorporated into the sol-gel matrix. This biosensor assembly worked for D-sorbitol dehydrogenase, D-glucose dehydrogenase, and L-lactate dehydrogenase. Polyethyleneimine was added to stabilize the diaphorase and sorbitol dehydrogenase, and ferrocene was immobilized to the polyethyleneimine (66).

1.8.2 Immobilized NAD in affinity chromatography

N^6-immobilized NAD has been thoroughly studied for affinity chromatography using a kinetic locking-on strategy (13, 41, 42, 62). In this strategy, NAD is immobilized on a resin and NAD-dependent enzymes can be "locked on" to the NAD-resin in the presence of a competitive inhibitor, typically a substrate analogue.Thus, if NAD^+ is used, a non-reactive oxidized substrate analogue will also be used (41). This approach helps the enzyme form a ternary enzyme-substrate-cofactor complex but no reaction takes place, holding the enzyme onto the NAD-resin. A variety of NAD immobilization methods have been tested for this purpose, including 8'-azo, N^6, S^6, N^1, and linkages to NAD's phosphate backbone (13). Enzyme retention was the strongest for five of the six dehydrogenases tested when N^6-immobilized NAD was used as part of the affinity matrix compared to the other linkages (13). The one enzyme that did not follow this pattern was bovine glutamate dehydrogenase, which showed strong binding to the S^6- and 8'-azo-linked NAD but not to NAD bound through the N^6-amine. All of the linkages for immobilizing NAD showed some ability to be used for affinity chromatography. The N^6 linkage showed higher NAD loading and higher levels of enzyme redox-active NAD (up to 2.1 µmol/g wet sepharose resin) (13), indicating that N^6 linkages are the best. Because of the apparent broad acceptance for binding of N^6-immobilized NAD by dehydrogenases, immobilization of NAD through the N^6-amine was selected for this project.

1.8.3 Direct coupling of NAD

An alternative method of immobilizing NAD involves direct coupling of NAD to a carboxy-terminating spacer arm (42). This method results in NAD immobilized primarily through its phosphate groups, but because adenine can be directly coupled to carboxy-sepharose, some immobilization likely takes place through the N^6-amine as well (42). To elucidate the point of attachment, NAD, NADP, adenine, and inosine were immobilized by direct coupling in different conditions (42). When coupled in pyridine using dicyclohexylcarbodiimide, immobilization appeared to occur at the ribosyl hydroxyls, but coupling in water at pH 4.8 using EDC seemed to take place through NAD's pyrophosphate backbone or NADP's phosphate. In water at pH 4.8, inosine could not be coupled directly, indicating that the ribosyl moiety is not involved in immobilization. Adenine could be coupled directly in water at pH 4.8, with an observed absorbance maximum shift from 260 nm to 230 nm. In affinity chromatography, phenylalanine dehydrogenase did not bind to directly immobilized NAD, but it could bind to N^6-immobilized NAD, indicating a different mode of attachment. The absorption maximum of directly coupled NAD shifted to around 245 nm, indicating that some coupling took place through the adenine ring (42).

Although simple to prepare, directly coupled cofactors were somewhat unstable, losing between 30-70% of coupled NAD over a 1 month time and the absorbance maximum slowly shifted from 245 nm to 260 nm over a 3 month time (42). The amount of enzyme bound to the affinity chromatography matrix was generally lower with directly coupled NAD than with N^6-immobilized NAD. The lower stability and potential mixture of immobilized products would make it difficult to characterize directly coupled NAD-modified electrodes. Direct coupling also yields lower levels of accessible NAD than linking to N^6-CM-NAD (13, 42). However, it could

be useful because it eliminates the need to synthesize and purify N^6-CM-NAD, simplifying the linkage synthesis process. In addition, the lower NAD loading may not affect our electrode system because enzyme loading might be the limiting factor for catalytic rate, since the enzyme is substantially larger than NAD.

1.9 ENZYME IMMOBILIZATION

Enzymes can be immobilized through adsorption, covalent binding, affinity immobilization, and entrapment (12). Generally, immobilized enzymes maintain activity and are more stable. Immobilization can increase storage stability, thermostability, and stability in organic solvents, and reduce proteolysis, aggregation, and product inhibition (12, 51). Some of the support matrices used for enzyme immobilization include chitosan, collagen, carrageenan, gelatin, cellulose, starch, pectin, sepharose, and other synthetic polymers and inorganic support materials (12). Enzyme adsorption includes both liquid adsorption and drying an enzyme solution on a matrix. Adsorption of enzymes results from salt bridges, hydrophobic interactions and hydrogen bonds depending on the matrix used (12). Although generally, adsorbed enzymes slowly leach from the matrix, the interaction can be irreversible if the right matrix is used. Fibers with good water holding capacity work well for adsorbing enzymes (12). Covalent immobilization involves using a matrix with reactive groups that can react with protein side chains such as Lys and Glu (12). Often a matrix is modified by a reactive species followed by the addition of enzyme. A variety of linking agents have been used, but glutaraldehyde is often used because it can bind the enzyme to the matrix and stabilize the enzyme by forming crosslinks (12). Enzymes can be immobilized by entrapping them in gels, fibers, or under membranes (12). Entrapped enzymes are physically held in the matrix by the structure of the matrix. Enzymes

entrapped in gels and fibers often leach out of the matrix, but selecting different support materials has somewhat alleviated these problems (12). Affinity immobilization results from the enzyme having affinity for the support matrix (12). The matrix can be modified to carry an enzyme ligand, or the enzyme can be modified to have affinity to the matrix. An example would be adding streptavidin to an enzyme and attaching biotin to the matrix or vice versa.

1.9.1 Immobilization of glycerol dehydrogenase

The glycerol dehydrogenases from *Geobacillus stearothermophilus*, *citrobacter braakii*, and *cellulomonas* sp have recently been covalently immobilized on agarose (51). Agarose activated by CNBr, agarose activated with glyoxyl groups, and agarose with a combination of glyoxal and amine groups were tested. Immobilization was tested in two buffers (sodium bicarbonate and CAPS) and with two additives (glycerol and PEG600). GlyDH immobilized on the CNBr-activated agarose gave higher activity levels (42-65%) than on glyoxyl-modified agarose (5-29%). The addition of glycerol or PEG to the glyoxal immobilization reaction increased activity, but glycerol hampered the glyoxal chemistry. The half-life of the immobilized enzymes increased up to 4 times. Of the three enzymes tested, *G. stearothermophilus* GlyDH was the least stable in soluble form, but was the most stable after immobilization, retaining 100% of its activity after 18 hours at 65°C (51).

In our reactor system, we foresee that the cofactor will be covalently immobilized on the electrode first, followed by binding the enzyme to the immobilized cofactor by affinity. Then glutaraldehyde fixation can be used to covalently attach and stabilize the enzyme. Glutaraldehyde has been shown to immobilize other dehydrogenases while maintaining their activity and increasing their stability (15, 36).

1.10 INTRODUCTION TO PROJECT

A large part of my project has been the characterization of TmGlyDH. Although TmGlyDH had been previously crystallized, the enzyme had not been kinetically characterized. In Chapter 2, I describe the characterization of TmGlyDH and demonstrate that the enzyme was able to use N^6-immobilized NAD. Kinetic characterization is important for determining what conditions are suitable for a bioelectronic reactor, and the enzymes kinetic data can be compared to electrochemical rates. Another part of my project was to immobilize NAD while maintaining its coenzymic activity (Chapter 2). Although a bioelectronic interface had been previously set up in the Worden laboratory, NAD was immobilized onto a boronate linker through its cis-diols, which—as I described earlier—is unstable in the presence of other cis-diols. I chose a different method (modifying NAD at the N^6-amine) of immobilizing NAD and then ensured that the enzyme maintained activity with the immobilized NAD. In Chapter 3, I describe testing several different dehydrogenases with the immobilized NAD to show that N^6-immobilized NAD in an electrochemical system will likely be usable for many other dehydrogenases; I also check if the structure of the enzymes' binding pocket can predict activity with the immobilized cofactor. In Chapter 4, I describe how TmGlyDH is inactivated by its product (DHA), and engineer the enzyme for higher stability in the presence of DHA. In Chapter 5, I discuss the suitability of using TmGlyDH in a bioelectronic system, the suitability of N^6-immobilized NAD, and recommended future work on the project.

REFERENCES

REFERENCES

1. **Bailon, P., G. K. Ehrlich, W.-J. Fung, and W. Berthold (ed.).** 2000. Methods in molecular biology: affinity chromatography methods and protocols, vol. 147. Humana Press Inc, Totowa NJ.

2. **Barski, O. A., S. M. Tipparaju, and A. Bhatnagar.** 2008. The aldo-keto reductase superfamily and its role in drug metabolism and detoxification. Drug. Metab. Rev. **40:**553–624.

3. **Bauer, R., N. Katsikis, S. Varga, and D. Hekmat.** 2005. Study of the inhibitory effect of the product dihydroxyacetone on *Gluconobacter oxydans* in a semi-continuous two-stage repeated-fed-batch process. Bioprocess Biosys. Engin. **28:**37–43.

4. **Bergel, A., and M. Comtat.** 1991. Thin-layer spectrochemical study of the reversible reaction bewteen nicotinamide adenine dinucleotide and flavin adenine dinucleotide. J. Electroanal. Chem. **302:**219–231.

5. **Blaedel, W. J., and R. A. Jenkins.** 1975. Study of the electrochemical oxidation of reduced nicotinamide adenine dinucleotide. Anal. Chem. **47:**1337–1343.

6. **Bliznak, J. B., and R. E. Harcarufka.** 1981. Sweetener and flavoring compositions and method of producing same. United States Patent**:**4,277,511.

7. **Brinen, L. S., J. M. Canaves, X. Dai, A. M. Deacon, M. A. Elsliger, S. Eshaghi, R. Floyd, A. Godzik, C. Grittini, S. K. Grzechnik, C. Guda, L. Jaroszewski, C. Karlak, H. E. Klock, E. Koesema, J. S. Kovarik, A. Kreusch, P. Kuhn, S. A. Lesley, D. McMullan, T. M. McPhillips, M. A. Miller, M. D. Miller, A. Morse, K. Moy, J. Ouyang, A. Robb, K. Rodrigues, T. L. Selby, G. Spraggon, R. C. Stevens, H. v. d. Bedem, J. Velasquez, J. Vincent, X. Wang, B. West, G. Wolf, S. S. Taylor, K. O. Hodgson, J. Wooley, and I. A. Wilson.** 2003. Crystal structure of a zinc-containing glycerol dehydrogenase (TM0423) from *Thermotoga maritima* at 1.5 Å resolution. Proteins: Struct., Funct., Bioinf. **50:**371–374.

8. **Bruins, M., A. Janssen, and R. Boom.** 2001. Thermozymes and their applications. Appl. Biochem. Biotechnol. **90:**155–186.

9. **Bückmann, A., and G. Carrea.** 1989. Synthesis and application of water-soluble macromolecular derivatives of the redox coenzymes NAD(H), NADP(H) and FAD. Adv. Biochem. Eng. Biotechnol. **39:**97–152.

10. **Calabrese Barton, S., J. Gallaway, and P. Atanassov.** 2004. Enzymatic biofuel cells for implantable and microscale devices. Chem. Rev. **104:**4867–4886.

11. **Cossement, E., J. P. Geerts, J. Gobert, P. Michel, and E. Wulfert.** 1990. Substituted 1-(1H-imidazol-4-yl)alkyl-benzamides as anti-ischemics and as α-2-adrenergic receptor agonists. United States Patent**:**4,923,865

12. **Datta, S., L. R. Christena, and Y. R. S. Rajaram.** 2013. Enzyme immobilization: an overview on techniques and support materials. Biotech. **3:**1–9.

13. **Forde, J., L. Oakey, L. Jennings, and P. Mulchahy.** 2005. Fundamental differences in bioaffinity of amino acid dehydrogenases for N^6- and S^6-linked immobilized cofactors using kinetic-based enzyme capture strategies. Anal. Biochem. **338:**102–112.

14. **Hassler, B. L., N. Kohli, J. G. Zeikus, I. Lee, and R. M. Worden.** 2007. Renewable dehydrogenase-based interfaces for bioelectronic applications. Langmuir **23:**7127–7133.

15. **Hassler, B. L., and R. M. Worden.** 2006. Versatile bioelectronic interfaces based on heterotrifunctional linking molecules. Biosens. Bioelectron. **21:**2146–2154.

16. **Hekmat, D., R. Bauer, and J. Fricke.** 2003. Optimization of the microbial synthesis of dihydroxyacetone from glycerol with *Gluconobacter oxydans*. Bioprocess Biosys. Eng. **26:**109–116.

17. **Jasti, L. S., S. R. Dola, N. W. Fadnavis, U. Addepally, S. Daniels, and S. Ponrathnam.** 2014. Co-immobilized glucose oxidase and β-galactosidase on bovine serum albumin coated allyl glycidyl ether (AGE)-ethylene glycol dimethacrylate (EGDM) copolymer as a biosensor for lactose determination in milk. Enzyme Microb. Technol. **64–65:**67–73.

18. **Johannes, T. W., R. D. Woodyer, and H. Zhao.** 2005. Directed evolution of a thermostable phosphite dehydrogenase for NAD(P)H regeneration. Appl. Environ. Microbiol. **71:**5728–5734.

19. **Johnson, J. A., and R. M. Fusaro.** 1994. Alteration of skin surface protein with dihydroxyacetone: A useful application of the Maillard browning reaction, p. 114–119. *In* T. P. Labuza, G. A. Reineccius, V. M. Monnier, J. O'Brien, and J. W. Baynes (ed.), Maillard Reactions in Chemistry, Food, and Health. The Royal Society of Chemistry, Cambridge.

20. **Katayama, N., I. Urabe, and H. Okada.** 1983. Steady-state kinetics of coupled two-enzyme reactor with recycling of poly(ethylene glycol)-bound NAD. Eur. J. Biochem. **132:**403–409.

21. **Kavanagh, K. L., H. Jörnvall, B. Persson, and U. Oppermann.** 2008. The SDR superfamily: functional and structural diversity within a family of metabolic regulatory enzymes. Cell. Mol. Life Sci. **65:**3895–3906.

22. **Kavanagh, K. L., M. Klimacek, B. Nidetzky, and D. K. Wilson.** 2003. Crystal structure of *Pseudomonas fluorescens* mannitol 2-dehydrogenase: evidence for a very divergent long-chain dehydrogenase family. Chem.-Biol. Interact. **143–144:**551–558.

23. **Klimacek, M., and B. Nidetzky.** 2002. A catalytic consensus motif for D-mannitol 2-dehydrogenase, a member of a polyol-specific long-chain dehydrogenase family, revealed by kinetic characterization of site-directed mutants of the enzyme from *Pseudomonas fluorescens*. Biochem. J. **367:**13–18.

24. **Kulys, J. J., U. Bilitewski, and R. D. Schmid.** 1991. Reagentless biosensors for substrates of dehydrogenases. Anal. Lett. **24:**181–189.

25. **Lapenaite, I., A. Ramanaviciene, and A. Ramanavicius.** 2006. Current trends in enzymatic determination of glycerol. Crit. Rev. Anal. Chem. **36:**13–25.

26. **Larsson, P.-O., and K. Mosbach.** 1971. Preparation of a NAD(H)-polymer matrix showing coenzymic function of the bound pyridine nucleotide. Biotechnol. Bioeng. **13:**393–398.

27. **Lee, L. G., and G. M. Whitesides.** 1986. Preparation of optically-active 1,2-diols and α-hydroxy ketones using glycerol dehydrogenase as catalyst - limits to enzyme-catalyzed synthesis due to noncompetitive and mixed inhibition by product. J. Org. Chem. **51:**25–36.

28. **Li, G., N. Z. Ma, and Y. Wang.** 2005. A new handheld biosensor for monitoring blood ketones. Sens. Actuators, B **109:**285–290.

29. **Li, H., R. Li, R. M. Worden, and S. Calabrese Barton.** 2014. Facilitation of high-rate NADH electrocatalysis using electrochemically activated carbon materials. ACS Appl. Mater. Inter. **6:**6687–6696.

30. **Li, H., H. Wen, and S. Calabrese Barton.** 2012. NADH oxidation by electropolymerized azines on carbon nanotube modified electrodes. Electroan. **24:**398–406.

31. **Li, M., J. Wu, X. Liu, J. Lin, D. Wei, and H. Chen.** 2010. Enhanced production of dihydroxyacetone from glycerol by overexpression of glycerol dehydrogenase in an alcohol dehydrogenase-deficient mutant of *Gluconobacter oxydans*. Bioresour. Technol. **101:**8294–8299.

32. **Liepins, J., S. Kuorelahti, M. Penttila, and P. Richard.** 2006. Enzymes for the NADPH-dependent reduction of dihydroxyacetone and D-glyceraldehyde and L-glyceraldehyde in the mould *Hypocrea jecorina*. FEBS J. **273:**4229–4235.

33. **Lindberg, M., P. Larsson, and K. Mosbach.** 1973. A new immobilized NAD^+ analogue, its application in affinity chromatography and as a functioning coenzyme. Eur. J. Biochem. **40:**187–193.

34. **Liu, W., S. Zhang, and P. Wang.** 2009. Nanoparticle-supported multi-enzyme biocatalysis with in situ cofactor regeneration. J. Biotechnol. **139:**102–107.

35. **Lobo, M. J., A. J. Miranda, and P. Tuñón.** 1997. Amperometric biosensors based on NAD(P)-dependent dehydrogenase enzymes. Electroan. **9:**191–202.

36. **López-Gallego, F., L. Betancor, C. Mateo, A. Hidalgo, N. Alonso-Morales, G. Dellamora-Ortiz, J. M. Guisán, and R. Fernández-Lafuente.** 2005. Enzyme stabilization by glutaraldehyde crosslinking of adsorbed proteins on aminated supports. J. Biotechnol. **119:**70–75.

37. **Lowe, C. R.** 1978. Immobilised coenzymes. Trends Biochem. Sci. **3:**134–137.

38. **Lowe, C. R., and P. D. G. Dean.** 1971. Affinity chromatography of enzymes on insolubilized cofactors. FEBS Lett. **14:**313–316.

39. **Muramatsu, M., I. Urabe, Y. Yamada, and H. Okada.** 1977. Synthesis and kinetic properties of a new NAD^+ derivative carrying a vinyl group. Eur. J. Biochem. **80:**111–117.

40. **Noguer, T., D. Szydlowska, J.-L. Marty, and M. Trojanowicz.** 2004. Sol-gel immobilization of aldehyde dehydrogenase and NAD^+ on screen-printed electrodes for designing of amperometric acetaldehyde biosensor. Polish J. Chem. **78:**1679–1689.

41. **O'Flaherty, M., M. McMahon, and P. Mulcahy.** 1999. A kinetic locking-on strategy for bioaffinity purification: further studies with alcohol dehydrogenase. Protein Expr. Purif. **15:**127–145.

42. **Oakey, L., and P. Mulcahy.** 2004. Immobilized cofactor derivatives for kinetic-based enzyme capture strategies: direct coupling of $NAD(P)^+$. Anal. Biochem. **335:**316–325.

43. **Okuda, K., I. Urabe, and H. Okada.** 1985. Synthesis of poly(ethylene glycol)-bound NADP by selective modification at the 6-amino group of NADP. Eur. J. Biochem. **151:**33–38.

44. **Ottolina, G., G. Carrea, S. Riva, and A. Bückmann.** 1990. Coenzymatic properties of low molecular-weight and macromolecular N^6-derivatives of NAD^+ and $NADP^+$ with dehydrogenases of interest for organic synthesis. Enzyme Microb. Technol. **12:**596–602.

45. **Pagliaro, M., R. Ciriminna, H. Kimura, M. Rossi, and C. Della Pina.** 2007. From glycerol to value-added products. Angew. Chem., Int. Ed. **46:**4434–4440.

46. **Parellada, J., A. Narváez, M. A. López, E. Domínguez, J. J. Fernández, V. Pavlov, and I. Katakis.** 1998. Amperometric immunosensors and enzyme electrodes for environmental applications. Anal. Chim. Acta **362:**47–57.

47. **Parhi, S. S. L.** 1986. Substituted 2-mercapto-imidazoles and their preparation. United States Patent**:**4,584,383.

48. **Persson, B., J. Hedlund, and H. Jörnvall.** 2008. Medium- and short-chain dehydrogenase/reductase gene and protein families: The MDR superfamily. Cell. Mol. Life Sci. **65:**3879–3894.

49. **Radianingtyas, H., and P. C. Wright.** 2003. Alcohol dehydrogenases from thermophilic and hyperthermophilic archaea and bacteria. FEMS Microbiol. Rev. **27:**593–616.

50. **Reed, J. L., T. D. Vo, C. H. Schilling, and B. O. Palsson.** 2003. An expanded genome-scale model of *Escherichia coli* K-12 (iJR904 GSM/GPR). Genome Biol. **4:**R54.

51. **Rocha-Martin, J., A. Acosta, J. Berenguer, J. M. Guisan, and F. Lopez-Gallego.** 2014. Selective oxidation of glycerol to 1,3-dihydroxyacetone by covalently immobilized glycerol dehydrogenases with higher stability and lower product inhibition. Bioresour. Technol. **170:**445–453.

52. **Ruzheinikov, S. N., J. Burke, S. Sedelnikova, P. J. Baker, R. Taylor, P. A. Bullough, N. M. Muir, M. G. Gore, and D. W. Rice.** 2001. Glycerol dehydrogenase: Structure, specificity, and mechanism of a family III polyol dehydrogenase. Structure **9:**789–802.

53. **Samec, Z., W. T. Bresnahan, and P. J. Elving.** 1982. Theoretical analysis of eletrochemical reactions involving two successive one-electron transfers with dimerization of intermediate-applicaiton to NAD^+/NADH redox couple. J. Electroanal. Chem. **133:**1–23.

54. **Schmakel, C. O., K. S. V. Santhanam, and P. J. Elving.** 1975. Nicotinamide adenine dinucleotide (NAD^+) and related compounds. electrochemical redox pattern and allied chemical behavior. J. Am. Chem. Soc. **97:**5083–5092.

55. **Shaked, Z. e., and G. M. Whitesides.** 1980. Enzyme-catalyzed organic synthesis: NADH regeneration by using formate dehydrogenase. J. Am. Chem. Soc. **102:**7104–7105.

56. **Song, S. H., N. Ahluwalia, Y. Leduc, L. T. Delbaere, and C. Vieille.** 2008. *Thermotoga maritima* TM0298 is a highly thermostable mannitol dehydrogenase. Appl. Microbiol. Biotechnol. **81:**485–495.

57. **Spencer, P., K. J. Brown, M. D. Scawen, T. Atkinson, and M. G. Gore.** 1989. Isolation and characterization of the glycerol dehydrogenase from *Bacillus stearothermophilus*. Biochim. Biophys. Acta **994:**270-279.

58. **Srinivasan, V., K. S. Ma, M. W. W. Adams, M. G. Newton, J. P. Rose, and B. C. Wang.** 2002. Towards the crystal structure of glycerol dehydrogenase from *Thermotoga maritima*. Acta Crystallog. D. **D58:**867–869.

59. **Studer, M.** 2003. Production of optically active α-hydroxyacetals. United States Patent**:**6,660,890.

60. **Tang, C. T., F. E. Ruch, and E. C. C. Lin.** 1979. Purification and properties of a nicotinamide adenine dinucleotide-linked dehydrogenase that serves an *Escherichia coli* mutant for glycerol catabolism J. Bacteriol. **140:**182–187.

61. **Tishkov, V. I., and V. O. Popov.** 2006. Protein engineering of formate dehydrogenase. Biomol. Eng. **23:**89–110.

62. **Tynan, J., J. Forde, M. McMahon, and P. Mulcahy.** 2000. Synthesis of a highly substituted N^6-linked immobilized NAD^+ derivative using a rapid solid-phase modular approach: suitability for use with the kinetic locking-on tactic for bioaffinity purification of NAD^+-dependent dehydrogenases. Protein Expression Purif. **20:**421–434.

63. **van der Donk, W. A., and H. Zhao.** 2003. Recent developments in pyridine nucleotide regeneration. Curr. Opin. Biotechnol. **14:**421–426.

64. **Vieille, C., and G. J. Zeikus.** 2001. Hyperthermophilic enzymes: sources, uses and molecular mechanisms for thermostability. Microbiol. Mol. Biol. Rev. **65:**1–43.

65. **Vrtis, J. M., A. K. White, W. W. Metcalf, and W. A. van der Donk.** 2002. Phosphite dehydrogenase: a versatile cofactor-regeneration enzyme. Angew. Chem., Int. Ed. **41:**3257–3259.

66. **Wang, Z., M. Etienne, F. Quilès, G.-W. Kohring, and A. Walcarius.** 2012. Durable cofactor immobilization in sol-gel bio-composite thin films for reagentless biosensors and bioreactors using dehydrogenases. Biosens. Bioelectron. **32:**111–117.

67. **Weckbecker, A., H. Groger, and W. Hummel.** 2010. Regeneration of nicotinamide coenzymes: principles and applications for the synthesis of chiral compounds. Adv. Biochem. Engin./Biotechnol. **120:**195–242.

68. **Wichmann, R., and D. Vasic-Racki.** 2005. Cofactor regeneration at the lab scale. Adv. Biochem. Engin./Biotechnol. **92:**225–260.

69. **Wollenberger, U., R. Spricigo, S. Leimkühler, and K. Schröder.** 2008. Protein electrodes with direct electrochemical communication. Adv. Biochem. Engin./Biotechnol. **109:**19–64.

70. **Woodyer, R., W. A. van der Donk, and H. Zhao.** 2003. Relaxing the nicotinamide cofactor specificity of phosphite dehydrogenase by rational design. Biochemistry **42:**11604–11614.

71. **Wu, X., F. Zhao, J. R. Varcoe, A. E. Thumser, C. Avignone-Rossa, and R. C. T. Slade.** 2009. Direct electron transfer of glucose oxidase immobilized in an ionic liquid reconstituted cellulose-carbon nanotube matrix. Bioelectrochemistry **77:**64–68.

72. **Wykes, J. R., P. Dunnill, and M. D. Lilly.** 1972. The preparation of soluble high molecular weight NAD derivative active as a cofactor. Biochim. Biophys. Acta **286:**260–268.

73. **Yamada-Onodera, K., N. Kawahara, Y. Tani, and H. Yamamoto.** 2004. Synthesis of optically active diols by *Escherichia coli* transformant cells that express the glycerol dehydrogenase gene of *Hansenula polymorpha* DL-1. Engin. Life Sci. **4:**413–417.

74. **Yamada-Onodera, K., A. Nakajima, and Y. Tani.** 2006. Purification, characterization, and gene cloning of glycerol dehydrogenase from *Hansenula ofunaensis*, and its expression for production of optically active diol. J. Biosci. Bioengin. **102:**545–551.

75. **Yang, D., J. H. Zhang, M. K. Wong, Y. C. Yip, and M. W. Tang.** 1998. Process for catalytic epoxidation of olefinic compounds, novel cyclic ketone catalysts useful in said process. United States Patent**:**5,763,623.

76. **Zhang, M., C. Mullens, and W. Gorski.** 2007. Co-immobilization of dehydrogenases and their cofactors in electrochemical biosensors. Anal. Chem. **79:**2446–2450.

77. **Zou, Y., H. Zhang, J. S. Brunzelle, T. W. Johannes, R. Woodyer, J. E. Hung, N. Nair, W. A. van der Donk, H. Zhao, and S. K. Nair.** 2012. Crystal structures of phosphite dehydrogenase provide insights into nicotinamide cofactor regeneration. Biochemistry **51:**4263–4270.

CHAPTER 2. Characterization of *Thermotoga maritima* glycerol dehydrogenase for use in the production of dihydroxyacetone in a bioelectronics system

This work is previously published and is reprinted with permission: **Beauchamp, J., P. G. Gross, and C. Vieille.** 2014. Characterization of *Thermotoga maritima* glycerol dehydrogenase for the enzymatic production of dihydroxyacetone. Appl. Microbiol. Biotechnol. **98:**7039–7050.

2.1 ABSTRACT

NAD-dependent *Thermotoga maritima* glycerol dehydrogenase (TmGlyDH) converts glycerol into dihydroxyacetone (DHA), a valuable synthetic precursor and sunless tanning agent. In this work, recombinant TmGlyDH was characterized to determine if it can be used to catalyze DHA production. The pH optima for glycerol oxidation and DHA reduction at 50°C were 7.9 and 6.0, respectively. Under the conditions tested, TmGlyDH had a linear Arrhenius plot up to 80°C. TmGlyDH was more thermostable than other glycerol dehydrogenases, remaining over 50% active after 7 h at 50°C. TmGlyDH was active on racemic 1,2-propanediol, and produced (R)-1,2-propanediol from hydroxyacetone with an enantiomeric excess above 99%, suggesting that TmGlyDH can also be used for chiral synthesis. (R)-1,2-propanediol production from hydroxyacetone was demonstrated for the first time in a one-enzyme cycling reaction using glycerol as the second substrate. Negative cooperativity was observed with glycerol and DHA, but not with the cofactor. Apparent kinetic parameters for glycerol, DHA, and NAD(H) were determined over a broad pH range. TmGlyDH showed little activity with N^6-carboxymethyl-NAD^+ (N^6-CM-NAD), an NAD^+ analog modified for easy immobilization to amino groups, but the double mutation V44A/K157G increased catalytic efficiency with N^6-CM-NAD^+ ten-fold. Finally we showed for the first time that a GlyDH is active with immobilized N^6-CM-NAD^+, suggesting that N^6-CM-NAD^+ can be immobilized on an electrode to allow TmGlyDH activity in a system that reoxidizes the cofactor electrocatalytically.

2.1 INTRODUCTION

Dehydrogenases catalyze redox reactions that reversibly transfer an electron pair and a proton from a cofactor such as NADH to the substrate (42). These enzymes have potential as

catalysts for the production of many different compounds including chiral molecules and pharmaceutical precursors (40, 42). However, the fact that the cofactor must be supplied in stoichiometric amounts to the reaction or be regenerated (40, 42) strongly limits current applications of these enzymes. Several cofactor regeneration methods have been used to drive dehydrogenase-based reactions including using another enzyme reaction and a second substrate (40). The high cost associated with supplying a second substrate and enzyme has limited the use of dehydrogenases to the production of high-value specialty products. Electrochemical regeneration promises to be a low-cost NAD(H) regeneration method allowing broader use of dehydrogenases. In the past, electrochemical regeneration has been limited by the high overpotentials (1.09 V vs. reversible hydrogen electrode) required for activity, which results in side reactions and electrode fouling (20). Recently polyazines have been electropolymerized onto carbon nanotube-modified electrodes, reducing the overpotential required down to ca 28 mV vs SHE while increasing NADH oxidation activity, thus providing a lower cost NAD^+ regeneration method (20).

The next step in the development of a bioelectrocatalytic reactor is to select a useful enzyme and immobilize the enzyme and cofactor onto an electrode. Glycerol dehydrogenase (GlyDH, EC 1.1.1.6), which interconverts glycerol and dihydroxyacetone (DHA) using NAD(H) as the cofactor, could be a good enzyme for this purpose (Figure 2.1).

Figure 2.1: TmGlyDH interconverts glycerol and DHA with the NAD(H) cofactor.

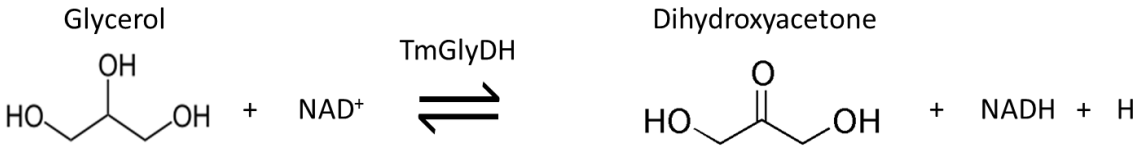

DHA is the only FDA-approved active ingredient used in sunless tanning creams (17), and it is used as a precursor to many valuable products (14). For example, DHA can be used to produce 1,2-propylene glycol, which is used in antifreeze and brake fluids, and to produce polyurethanes and polypropylene glycols (12). It is a precursor of anti-ulcer, antihypertensive, anti-inflammatory, analgesic (30), anti-ischemic, and α-2-adrenergic receptor agonist drugs (9). Many optically active epoxide-based drugs (44), pesticides (37), and sweeteners (3) also use DHA as a precursor.

DHA is currently produced by *Gluconobacter oxidans* grown on glycerol in a large stirred tank (14). Glycerol oxidation to DHA requires large quantities of oxygen, so high aeration levels must be maintained using oxygen-enriched air (14). An industrial strain of *G. oxidans* optimized to overcome DHA inhibition produced DHA at a rate of 3.6 g L^{-1} h^{-1} with 85% yield in a two-step fed-batch process (2). *G. oxidans* has been further optimized to produce DHA with a 96% yield at a rate ranging from 12 g L^{-1} h^{-1} (at 100 g/L glycerol) to 9.5 g L^{-1} h^{-1} (at 140 g/L glycerol). Productivity based on cell dry weight increased by 140% (21). Although optimization of the DHA production process has increased yields and production rates, the cost of DHA remains relatively high because of the fed-batch process, high aeration levels required, and downstream purification costs. An enzymatic catalytic system promises to be a good alternative to bacterial DHA production.

Escherichia coli GlyDH was recently characterized. DHA reduction activity was optimum at pH 8.0, while glycerol oxidation activity was optimum at pH 11 (31). The enzyme was fairly stable for a mesophilic enzyme, maintaining 100% glycerol oxidation activity after a 60-min incubation at pH 8.0 and 60°C, but it lost over 95% of its glycerol oxidation activity at pH 10.3, its optimum pH for glycerol oxidation. At pH 8.0, its glycerol oxidation activity was

also only about 10% of its maximum activity at pH 10.3. The lack of stability of *E. coli* GlyDH precludes its use in a biocatalytic system, and an enzyme is needed that is stable in conditions optimum for glycerol oxidation activity.

Enzymes originating from (hyper)thermophilic microbes are not only thermostable, but they often show increased resistance to other conditions such as high pressure, high salt concentrations, and high solvent concentrations (6, 32). Thus, they are likely to be more stable than enzymes from mesophiles in conditions required for biocatalysis. Thermostable dehydrogenases are being investigated to reduce costs associated with dehydrogenase-based catalysis and to optimize reaction conditions for industrial applications. Part of the cost reduction associated with thermostable enzymes comes from simple purification of overexpressed proteins via heat treatment (34). Thermostable enzymes typically have long shelf lives. They also allow higher operational temperatures for enzymatic processes than mesophilic enzymes do, thus reducing mass transfer limitations, reducing viscosity, increasing substrate and product solubility, and reducing the risk of microbial contamination (6, 39). Here we characterize the GlyDH from the hyperthermophilic bacterium *Thermotoga maritima* (TmGlyDH). Our rationale was that TmGlyDH should be more thermostable than the corresponding *E. coli* enzyme, allowing longer electrode life and higher operating temperatures. TmGlyDH was previously cloned, expressed, and crystallized, but only the zinc content of the enzyme and the specific activity of the enzyme for glycerol oxidation at pH 8.6 were reported (4, 36). Our studies aim to determine TmGlyDH's potential as a catalyst for DHA production. In this chapter, forward reaction refers to glycerol oxidation and reverse reaction refers to DHA reduction.

2.3 MATERIALS AND METHODS

2.3.1 Chemicals, bacterial strains, and culture conditions

All chemicals were purchased from Sigma-Aldrich (St. Louis, MO), unless stated otherwise. *T. maritima* strain MSB8 (ATCC 43589) was grown as described (34) and was the source of genomic DNA to clone *gldA*. *E. coli* strains DH5α (Invitrogen, Grand Island, NY), BL21(DE3) (EMD chemicals, Gibbstown, NJ), and XL2 Blue (Stratagene, La Jolla, CA) were used as cloning and plasmid propagation host, protein expression host, and transformation host after mutagenesis, respectively. *E. coli* strains were routinely grown in lysogeny broth (LB) in the presence of 25 μg/ml kanamycin when needed for plasmid maintenance.

2.3.2 Cloning of the gene encoding TmGlyDH

T. maritima's genomic DNA was extracted as described (34). The TmGlyDH-encoding gene, *gldA*, was amplified from *T. maritima* genomic DNA using primers *gldA*for and *gldA*rev (Table S2.1). The PCR product was cloned into the pCR2.1-TOPO vector (TOPO TA Cloning Kit, Invitrogen), sequenced, and subcloned into the *Nde*I and *Xho*I restriction sites of pET24a(+) (Novagen, Madison, WI), yielding plasmid pTmGlyDH. From this construct, TmGlyDH is expressed with a C-terminal His_6 tag. DNA manipulations followed standard protocols (1).

2.3.3 Expression and purification of TmGlyDH

TmGlyDH was purified from a 1-L culture of BL21(DE3)(pTmGlyDH). At an OD_{600} of 0.8, the culture was induced with 1.2 mM isopropyl-β-D-thiogalactopyranoside. After 4 h induction the cells were harvested by centrifugation (4,500 × *g*, 20 min) and stored at -80°C. The

pellet was resuspended in 40 mL of wash buffer (50 mM sodium phosphate buffer [pH 8.0], 0.5 M NaCl) containing 60 mg lysozyme, 1,000 units DNase I, and 1,000 units RNase, and incubated for 1 h at 25°C. The cells were sonicated on ice for six 10-s bursts on high power using a microtip (50% duty cycle, output control 4.5, Branson Sonifier 450). The cell debris were removed by centrifuging at 15,000 × *g* for 30 min. Non-thermostable proteins were removed by a 20-min heat treatment at 85°C followed by cooling on ice and centrifugation at 15,000 × *g* for 30 min. The lysate was added to a 7-mL nickel nitriloacetic acid agarose (Ni-NTA, Qiagen, Valencia, CA) column equilibrated with wash buffer. Unbound proteins were eluted with 20 column volumes (CV) of wash buffer followed by 10 CV of wash buffer containing 20 mM imidazole and 10 CV of wash buffer. TmGlyDH was eluted in nine 10-mL fractions with wash buffer containing 250 mM imidazole. The purified protein was concentrated by ultrafiltration and dialyzed 3 times against 20 mM Tris-HCl (pH 8.0) containing 250 mM NaCl and 5 mM β-mercaptoethanol. Because the enzyme lost over 90% of its activity after dialysis into Tris buffer as compared to the eluted protein in wash buffer containing 250 mM imidazole, the enzyme was dialyzed three times against 50 mM sodium phosphate buffer (pH 8.0) containing 250 mM NaCl. Protein concentrations were determined using the Bio-Rad protein assay kit (Bio-Rad, Richmond, CA), with bovine serum albumin as the standard.

2.3.4 TmGlyDH activity assays

All activity assays were performed in triplicate in 1-mL volumes in a Varian Cary 300 UV/Vis spectrophotometer (Palo Alto, CA) equipped with a Peltier heating system. Standard glycerol oxidation assays were performed at 80°C with 100 mM buffer (either phosphate or 2-[cyclohexylamino]ethanesulfonic acid [CHES]) adjusted to the desired pH, 678 mM glycerol,

500 μM NAD^+, and 6.7 μg TmGlyDH. Activity assays with alternative substrates were performed in 50 mM phosphate buffer (pH 7.4) containing 300 μM NAD^+, 33.5 μg enzyme, and 500 mM glycerol, 1,2-propanediol, 1,2-butanediol, ethylene glycol, isopropanol, 1,3-propanediol, 1-propanol, or glycolic acid. For all assays, water, buffer, and substrate were heated in the cuvette at 80°C for 15 min, the cofactor was added, and the initial absorbance was monitored at 340 nm for 20 s. The reaction was started by adding 10 μL enzyme. The reaction was monitored for 20 s, and initial velocity was calculated using the initial linear portion of the slope. The extinction coefficient for NADH (6,220 M^{-1} cm^{-1} at 340 nm) was used to calculate activity.

The effect of temperature on TmGlyDH kinetic stability was determined by incubating 6.7 μg TmGlyDH in 50 mM phosphate buffer (pH 7.4) for increasing amounts of time at 50°C and 80°C, and measuring the remaining activity at 50°C by adding 200 mM DHA and 300 μM NADH. The samples heated at 80°C were cooled on ice for at least 30 min, then preheated at 50°C for 15 min before measuring remaining activity at 50°C. The effect of DHA on TmGlyDH stability was measured similarly by adding 200 mM DHA to the incubation solution. The effect of temperature on activity was determined by measuring TmGlyDH activity at temperatures ranging from 30°C to 90°C with 200 mM DHA, 200 μM NADH, and 3.35 μg TmGlyDH. The effect of KCl and NH_4Cl on DHA reduction was measured at 50°C by adding increasing concentrations of KCl or 100 mM NH_4Cl to the assay mixture. The effect of KCl and NH_4Cl on glycerol oxidation was measured by adding 100 mM of either salt to the assay mixture.

2.3.5 Determination of TmGlyDH's apparent kinetic parameters

Apparent kinetics of TmGlyDH for NAD^+ were measured at 50°C to provide kinetic data at a temperature likely to be used to operate a bioelectronic reactor. Reaction mixtures contained 50 mM phosphate buffer (pH 6.0–7.9), 678 mM glycerol, 3.35 μg TmGlyDH, and 5 μM to 300 μM NAD^+. Apparent kinetics of TmGlyDH for NADH were measured as described for NAD^+, except that 200 mM DHA and 5 μM to 200 μM NADH were substituted for glycerol and NAD^+, respectively, and that 50 mM phosphate (pH 6.0-7.9) or CHES buffer (pH 8.0-9.0) was used. TmGlyDH's apparent kinetic parameters for DHA were measured with 50 mM phosphate or CHES buffer, 200 μM NADH, 3.35 μg TmGlyDH, and 0.05 mM to 300 mM DHA. TmGlyDH apparent kinetic parameters for glycerol were measured with 50 mM phosphate or CHES buffer, 300 μM NAD^+, 3.35 μg TmGlyDH, and 10 mM to 810 mM glycerol. Apparent kinetic parameters for NAD^+ and NADH were calculated using a non-linear fit of the Michaelis-Menten equation in Origin 8.0 (Originlab, Northampton, MA). Apparent kinetic parameters for DHA and glycerol were calculated using a non-linear fit to the Hill equation (equation 2.1). The Hill equation adequately describes cooperative kinetics, and it allows the determination of V_{max} and $K_{0.5}$. ($K_{0.5}$ is similar to the K_m, expressing the concentration of substrate required to produce half of the V_{max}.) The Hill coefficient, n, describes the degree of cooperativity. A value of n above 1 indicates positive cooperativity, whereas n below 1 indicates negative cooperativity. Michaelis-Menten kinetics apply when n=1 (8). Apparent kinetics of TmGlyDH for N^6-carboxymethyl-NAD^+ (N^6-CM-NAD^+) were measured with 50 mM phosphate buffer (pH 7.4), 810 mM glycerol, 33.5 μg TmGlyDH, and 40 μM to 2,000 μM N^6-CM-NAD^+.

Eq. 2.1

$$V = \frac{V_{max} * (S)^n}{K_{0.5}^n + (S)^n}$$

2.3.6 N^6-CM-NAD^+ synthesis and purification

N^6-CM-NAD^+ was synthesized from 1 g NAD^+ as described (11, 22) with the following modifications: (i) N^1-CM-NAD^+ was filtered on Whatman #1 filter paper and washed twice each time with cold acetone and ether; (ii) in the N^1-CM-NAD^+ reduction step, the solution was deaerated with N_2 gas for 5 min instead of 2 min; and (iii) precipitated N^6-CM-NAD^+ was washed twice each with cold acetone and ether. N^1-CM-NAD^+ was found to be unstable when stored dissolved in water. Molar yield and molecular weight were calculated using the extinction coefficient 19,000 M^{-1} cm^{-1} (22) for N^6-CM-NAD^+ and the measured mass.

N^6-CM-NAD^+ was dissolved in water and one third of the volume was loaded onto a Dowex 1X2 Cl-form column (2.5 cm × 35 cm) that had been washed with 2 CV of 3 M HCl followed by deionized water until the pH was above 4.0. The column loaded with N^6-CM-NAD^+ was washed with 2 CV of H_2O, and then 2 CV of 5 mM $CaCl_2$ (pH 2.7). N^6-CM-NAD^+ was eluted with a linear 5 mM (pH 2.7) to 100 mM (pH 2.0) $CaCl_2$ gradient over 13 CV. The fractions containing N^6-CM-NAD^+ as measured by OD_{266} were lyophilized, dissolved in a minimum amount of H_2O, desalted in 2-mL batches on a sephadex G10 column (2.5 cm × 23 cm), lyophilized again, and stored at -20°C.

2.3.7 Site-directed mutagenesis of TmGlyDH

Point mutations were introduced in *T. maritima gldA* with plasmid pTmGlyDH as the template using the QuikChange® (Stratagene, La Jolla, CA) protocol. Single mutations V44A, I154A, K157N, and K157G as well as double mutations I154A/K157N, V44A/K157G, V44A/K157N, V44A/I154A, and I154A/K157G, plus the triple mutation V44A/I154A/K157G were created with the primers listed in Table S2.1. PCR reactions were transformed into electrocompetent XL2 Blue. Mutated genes were sequenced, and the mutated plasmids were transformed into BL21(DE3) for protein expression as described above.

2.3.8 Determination of 1,2-propanediol enantiomeric excess

Twenty mM hydroxyacetone was converted to (R)-1,2-propanediol at 50°C with NADH recycling in a 10-mL reaction containing 50 mM phosphate buffer (pH 7.4), 600 mM glycerol, 200 μM NADH, and 0.0153 mg/mL TmGlyDH. A 20 mM racemic mixture of (R) and (S) 1,2-propanediol was resolved by removing (R)-1,2-propanediol with NAD^+ recycling at 50°C in a 10-mL reaction containing 400 mM DHA, 50 mM phosphate buffer (pH 7.4), 200 μM NADH, and 0.0153 mg/mL TmGlyDH. Reaction samples were diluted 1:10 in acetonitrile, incubated on ice for 20 min, centrifuged at 15,000 × *g* for 10 min, and analyzed using an Agilent GC-MS (6890N GC coupled to a 5973 Inert Mass Selective Detector) equipped with a CP-Chirasil-Dex CB column (25 m, 0.25 mm inner diameter) as described (43). The enantiomeric excess (ee) was calculated using the peak areas of the enantiomers. If no peak was observed, the amount present was assumed to be equal to the limit of detection for the GC-MS, which was determined as described (41).

2.3.9 DHA stability assays

DHA stability was assayed in 50 mM phosphate buffer at 50°C for up to 6 h at pH 6.4, 7.4, and 7.9. Samples collected every 90 min were analyzed on a Breeze high-performance liquid chromatograph (HPLC, Waters, Milford, MA) equipped with an Aminex-87C carbohydrate analysis column (Bio-Rad, Hercules, CA). The molecules were separated at 80°C using water as the mobile phase. DHA and glyceraldehyde were detected with a Waters 2478 Dual λ Absorbance UV detector at 210 nm.

2.3.10 Activity assays with N^6-CM-NAD^+ immobilized on Sepharose beads

N^6-CM-NAD^+ was immobilized on cyanogen bromide-activated Sepharose 4b as described (38) using bis(3-aminopropyl)amine (B3APA) as the linker, yielding NAD-CM-B3APA-Sepharose. B3APA loading on the Sepharose was quantified using 2,4,6-trinitrobenzene sulfonic acid using the G-Biosciences protocol (Cat # BC86). N^6-CM-NAD^+ binding to B3APA-Sepharose was quantified by phosphorus analysis after digestion with H_2SO_4 and H_2O_2 (26). The enzyme cycling reaction was performed in 50 mM sodium phosphate (pH 7.4) containing 200 mM glycerol, 100 mM hydroxyacetone, 37–41 mg wet NAD-CM-B3APA-Sepharose, and 0.345 mg TmGlyDH in 10-mL. Ethylene diamine (ED) and diethylene triamine (DETA) were also used as linkers following the above protocols. The amounts of NAD-ED-Sepharose and NAD-DETA-Sepharose used in cycling reactions were calculated to give the same NAD concentration as that present in the NAD-B3APA-Sepharose reactions. DHA and 1,2-propanediol produced were quantified by GC-MS as described above. Glycerol and hydroxyacetone consumed were quantified on a HPLC as described above except that analytes were detected with a Waters 410 refractive index detector.

2.4 RESULTS

2.4.1 Expression, purification, and characterization of TmGlyDH

TmGlyDH purified using a Tris buffer system gave high yields of pure enzyme (72 mg/L) with very low glycerol oxidation activity (3 ± 2 μmol min^{-1} mg^{-1} at 80°C, pH 7.9), compared to the enzyme assayed in N-(2-hydroxyethyl)piperazine-N-(3-propanesulfonic acid) (96 μmol min^{-1} mg^{-1} at pH 8.6) (36). Dialyzing TmGlyDH against phosphate buffer increased activity to 45 ± 4 μmol min^{-1} mg^{-1} at 80°C (pH 7.9). TmGlyDH inhibition by Tris was likely due to the structural similarity of Tris to glycerol. Tris is a four-carbon molecule with a primary amine on the second carbon. Its three alcohol groups (Figure S2.1) make its structure look very similar to that of glycerol and likely allow it to act as a competitive inhibitor of GlyDH. Bicine and glycine buffers also inhibited enzyme activity (Table S2.2). GlyDH from *Schizosaccharomyces pombe* is also reported to be inhibited by Tris (24). TmGlyDH showed 45 ± 2 μmol min^{-1} mg^{-1} glycerol oxidation activity (80°C, pH 7.4) when all purification steps were performed in phosphate buffer.

Because GlyDHs from other organisms are activated by KCl and NH_4Cl (24, 25, 27, 31), TmGlyDH activity in the presence of those salts was tested. DHA reduction activity was partially inhibited by KCl, with 60% activity retained in the presence of 40 mM KCl and 70% activity at KCl concentrations above 100 mM (Figure S2.2). DHA reduction activity was also inhibited by NH_4Cl, decreasing by 27% in 100 mM NH_4Cl. Glycerol oxidation activity increased by 39% and 18% in the presence of 100 mM NH_4Cl and 100 mM KCl, respectively. In DHA reduction assays performed in the presence of NH_4Cl, the background rate shifted from a negative slope due to autoxidation of NADH to a positive slope 3.4-fold higher in magnitude. A study of DHA stability found DHA to be more stable near neutral pH (pH 6.4 and 7.4) than at pH

7.9 (Figure S2.3). During these studies DHA degradation corresponded with an increase in absorbance at 280 nm with a broad shoulder overlapping 340 nm (not shown). The rate of OD_{280} increase when 50 mM DHA was incubated in 50 mM phosphate buffer (pH 7.4) at 50°C was 3-fold higher in the presence of 100 mM NH_4Cl than in its absence (not shown). Thus, we concluded that NH_4Cl likely increases the degradation rate of DHA. For this reason, no further studies with NH_4Cl were performed because its presence would reduce DHA yields in a catalytic reactor.

Table 2.1: TmGlyDH's oxidizing activity on glycerol-related substrates at 80°C, pH 7.4. Results shown are the average ± standard deviation of three independent experiments.

Substrate	Specific activity ($\mu mol\ min^{-1}\ mg^{-1}$)	Activity (%)
Glycerol	49 ± 2	100
rac-1,2-propanediol	23 ± 1	47
rac-1,2-butanediol	17 ± 3	35
Ethylene glycol	3.5 ± 0.1	7
Isopropanol	0.29 ± 0.05	0.6
1,3-propanediol	0.22 ± 0.03	0.4
1-propanol	0.0	0

While TmGlyDH exhibited significant activity on 1,2-propanediol and 1,2-butanediol, it was less active on ethylene glycol, and barely active to completely inactive on the other substrates tested (Table 2.1). Since enzymes typically are only active on one enantiomer of a racemate, batch reactions were set up to determine which 1,2-propanediol enantiomer is

preferred. TmGlyDH converted 20 mM hydroxyacetone to 5.9 ± 0.3 mM (*R*)-1,2-propanediol in 180 min with ee greater than 99%. A 20 mM racemic mixture of (*R* and *S*) 1,2-propanediol was resolved leaving the (*S*)-1,2-propanediol with an ee of 46% after 360 min.

2.4.2 Effect of temperature on TmGlyDH stability and activity

TmGlyDH was stable when stored at -80°C, maintaining 97% of its activity after at least three months at -80°C. When incubated at 50°C, TmGlyDH linearly lost 42% of its activity over 7 h (R^2 = 0.9731, Figure 2.2). At 80°C, TmGlyDH inactivation appeared to follow bi-exponential decay (Figure 2.2). The enzyme lost 66% of its activity after 20 min and 80% of its activity after 120 min. At 50°C TmGlyDH was initially more stable in the presence of DHA than in its absence, maintaining 100% activity over 120 min, but it quickly inactivated after 120 min, losing over 84% of its activity in the next 5 h (Figure 2.2). The effect of temperature on TmGlyDH's DHA reduction activity is shown in Figure 2.3. The Arrhenius plot (Figure 2.3 inset) was linear between 30°C and 80°C (R^2 = 0.999) with an apparent activation energy of 45.7 ± 0.7 kJ/mol.

Figure 2.2: Inactivation of TmGlyDH at 50°C (A) and 80°C (B). Open circles: inactivation in the absence of DHA; Closed circles and dashed lines: inactivation in the presence of 200 mM DHA. The linear regression is shown for TmGlyDH inactivation at 50°C in the absence of DHA, starting at 1 h. In panel B, the best fit for enzyme inactivation was to the biexponential decay equation y = 0.44e-0.0067x + 0.56e-0.133x, with R^2 = 0.985. Results shown are the average ± standard deviation of three independent experiments.

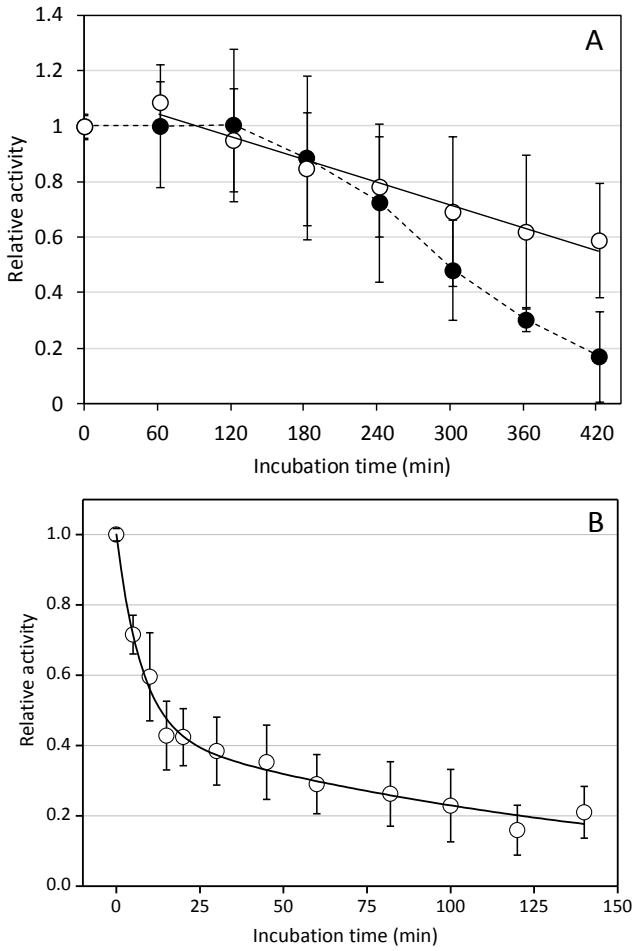

Figure 2.3: Effect of temperature on TmGlyDH's DHA reduction activity at pH 7.4. Inset: Arrhenius plot. Results shown are the average ± standard deviation of three independent experiments.

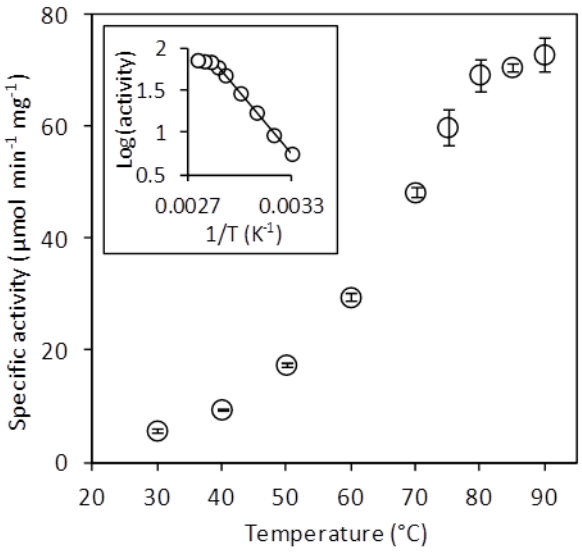

2.4.3 TmGlyDH apparent kinetic parameters

The V_{max} of TmGlyDH was larger for NAD+ in the glycerol oxidation reaction than for NADH in the DHA reduction sequence at pH 7.9 (Table 2.2). The K_m however, was 2–4 times higher for NAD^+ than NADH at all pH values. The initial rate velocities of TmGlyDH for DHA and glycerol did not fit the Michaelis-Menten equation well (not shown). Because the crystal structure shows TmGlyDH to be a tetramer (36), and because the non-linear shapes of the Hofstee plots (Figure 2.4C and 2.4F) are characteristic of cooperative behavior, a cooperative model was used instead. The data fit the Hill equation well (Figure 2.4). The largest V_{max} for DHA reduction was at pH 6.0, while that for glycerol oxidation was at pH 7.9 (Table 2.3). The apparent V_{max} for glycerol oxidation was 1.8-fold higher than the apparent V_{max} for DHA reduction at their respective pH optima. The $K_{0.5}$ for glycerol was significantly higher than the $K_{0.5}$ for DHA at all the pH values tested. At pH 7.9, the V_{max} for DHA reduction was half the

V_{max} for glycerol oxidation and the $K_{0.5}$ for glycerol was twice the $K_{0.5}$ for DHA (Table 2.3). Because an initial screen of apparent V_{max} values vs pH for NAD^+ indicated that the pH optimum was pH 7.4, all other experiments performed at a single pH value were performed at pH 7.4.

Table 2.2: Apparent kinetic parameters of TmGlyDH for NADH and NAD^+ at 50°C.

pH	6.0[a]	6.4[a]	6.9[a]	7.4[a]	7.9[a]	8.5[b]	9.0[b]
NADH							
V_{max} (μmol min^{-1} mg^{-1})	ND	11.3 ± 0.3	13.1 ± 0.5	12.2 ± 0.3	13.4 ± 0.6	11.9 ± 0.6	9.8 ± 0.3
K_m (μM)	ND	14 ± 2	18 ± 2	17 ± 2	20 ± 3	41 ± 7	49 ± 4
NAD^+							
V_{max} (μmol min^{-1} mg^{-1})	2.5 ± 0.3	4.1 ± 0.2	7.3 ± 0.3	11.4 ± 0.3	29.8 ± 0.9	6.5 ± 0.2	ND
K_m (μM)	80 ± 20	62 ± 10	59 ± 7	31 ± 3	51 ± 5	78 ± 7	ND

[a] Phosphate buffer

[b] CHES buffer

ND: Not determined

Table 2.3: Apparent kinetic parameters of TmGlyDH for DHA and glycerol at 50°C based on the Hill equation (Eq. 1).

pH	6.0[a]	6.4[a]	6.9[a]	7.4[a]	7.9[a]	8.5[b]	9.0[b]
DHA							
V_{max} (μmol min^{-1} mg^{-1})	13.4 ± 0.7	10.2 ± 0.4	9.7 ± 0.5	11.4 ± 0.8	11 ± 1	7.7 ± 0.9	7.4 ± 0.8
$K_{0.5}$ (mM)	30 ± 5	13 ± 2	12 ± 2	11 ± 3	19 ± 8	19 ± 9	12 ± 5
n	0.81 ± 0.06	0.85 ± 0.08	0.71 ± 0.07	0.59 ± 0.07	0.55 ± 0.07	0.56 ± 0.08	0.7 ± 0.2
Glycerol							
V_{max} (μmol min^{-1} mg^{-1})	3.0 ± 0.8	7.7 ± 1.58	7.0 ± 1.9	10.8 ± 1.2	24.0 ± 1.4	6.0 ± 0.3	ND
$K_{0.5}$ (mM)	393 ± 250	611 ± 315	204 ± 161	51 ± 22	39 ± 7	87 ± 14	ND
n	0.88 ± 0.16	0.76 ± 0.07	0.71 ± 0.14	0.58 ± 0.09	0.86 ± 0.13	0.63 ± 0.04	ND

[a] Phosphate buffer

[b] CHES buffer

Figure 2.4: TmGlyDH's glycerol oxidizing activity (A, B and C) and DHA reducing activity (D, E and F) at 50°C, pH 7.4. (A and D) Initial velocity fitted to the Hill equation. (B and E) Residuals of curve fit in A and C. (C and F) Hofstee plots of v vs. v/[glycerol] (C) and of v vs. v/[DHA] (F). Data from triplicate experiments are shown in A, B, D, and E. Averages are shown in C and F.

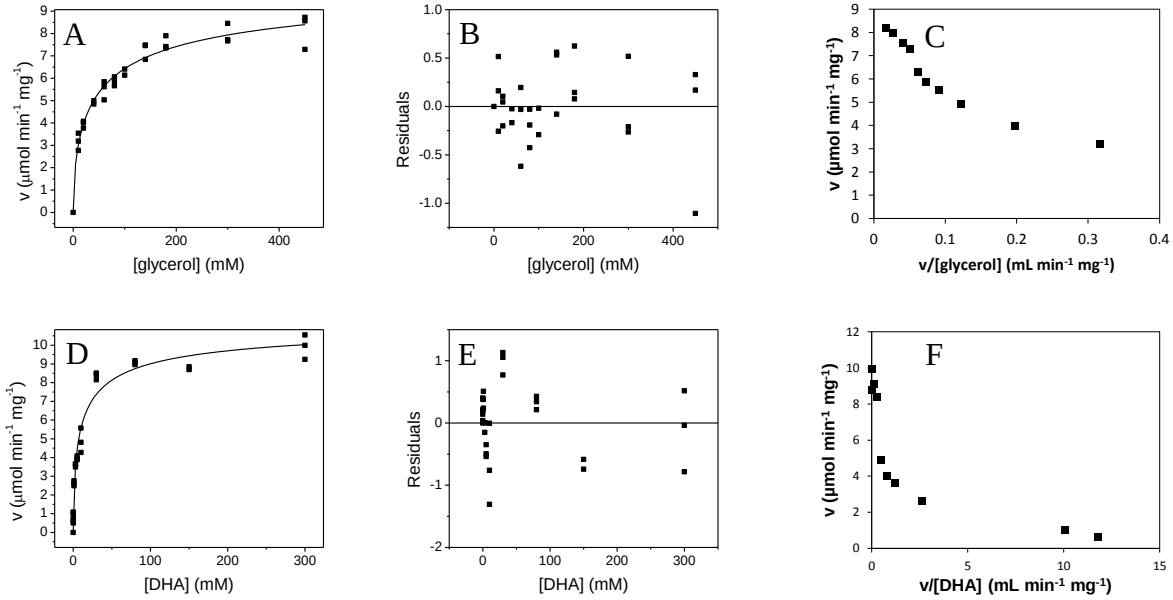

2.4.4 Introduction of NAD^+ into the 3D structure of TmGlyDH

In an electrochemical reactor the cofactor would ideally be bound to the surface of the electrode. N^6, S^6, 8'-Azo, and direct coupling are published methods for immobilizing NAD (11, 22, 28, 29, 38). Direct coupling gives binding at a mixture of the phosphate backbone and the N^6 locations (29). The N^6 position was selected because studies of affinity chromatography matrices demonstrated that N^6-linked NAD could capture a wider variety of NAD-dependent enzymes than NAD immobilized using the other methods mentioned here (11). N^6-CM-NAD^+ can be linked to amino-terminal linker molecules attached onto an electrode surface through a simple procedure of amide bond formation, and several dehydrogenases have been shown to be active with N^6-CM-NAD^+ in solution (22). We introduced NAD^+ into the 3D structure of TmGlyDH to

predict how active the enzyme would be with N^6-CM-NAD^+. The crystal structure of TmGlyDH does not contain NAD^+ (4, 36). TmGlyDH shares 48% sequence identity (with 1% gaps) with BsGlyDH (protein sequences were aligned using Clustal Omega at http://www.ebi.ac.uk/Tools/msa/clustalo/) (13, 33), and the crystal structure of BsGlyDH is available in complex with NAD^+. After superposing the two proteins structures in PyMol, the calculated RMSD for the backbone atoms was 1.03 Å. When the active site zinc and the 27 amino acids with atoms within 4 Å of NAD were used to align the structures, the all-atom RMSD between the two active sites was 0.70 Å, indicating that the alignment was suitable for importing NAD^+ into the TmGlyDH structure. Minimization of the TmGlyDH•NAD complex further improved the conformation of TmGlyDH-bound NAD (Figure 2.5A). The N^6 amine group in the TmGlyDH•NAD^+ complex appeared only slightly solvent accessible (Figure 2.5B), thus we do not expect TmGlyDH to be highly active on N^6 amine-modified analogs.

2.4.5 Kinetics of TmGlyDH on N^6-CM-NAD^+

N^6-CM-NAD^+ was synthesized from NAD^+ with a purified molar yield of 13.7% and a molecular weight of 1,114 g/mol (expected molecular weight 725 g/mol), indicating the presence of H_2O or $CaCl_2$. TmGlyDH's V_{max} with N^6-CM-NAD^+ was 2% of that with NAD^+, and its K_m for N^6-CM-NAD^+ was 15-fold higher than for NAD^+ (Table 2.4). By modeling the carboxymethyl group onto TmGlyDH-bound NAD^+ with PyMol, three residues (V44, I154, and K157) were identified that were very close to the carboxymethyl group and potentially caused steric clashes with the NAD^+ analog. Single, double, and triple mutants of V44, I154, and K157 were produced to reduce steric hindrance. Several of the TmGlyDH mutants showed increased V_{max} and lower K_m values for N^6-CM-NAD^+ compared to the wild-type enzyme (Table 2.4).

Compared to TmGlyDH, the V44A/I154A mutant had a 5-fold higher V_{max}, but its K_m increased 8-fold; the K157G mutant had a 5-fold lower K_m, but its V_{max} decreased 25%. The V44A/K157G mutant had the best catalytic efficiency (V_{max}/K_m) with a 4-fold higher V_{max} and a 32% lower K_m than TmGlyDH.

Figure 2.5: (A) Ribbon representation of alignment of BsGlyDH (Blue) and minimized TmGlyDH (green), (B) active site residues around NAD. The red NAD is the conformation from BsGlyDH, the yellow NAD is the conformation from minimization of TmGlyDH. The crystal structure of TmGlyDH (Protein Data Bank [PDB] entry 1KQ3) was structurally aligned with 27 residues within 4 Å of NAD and the active site zinc in the 3D structure of *Bacillus stearothermophilus* GlyDH (BsGlyDH, PDB entry 1JQ5) using the PyMOL Molecular Graphics System, Version 1.5.0.4 (Schrödinger, LLC), allowing NAD^+, which is present in the BsGlyDH structure, to be imported into the TmGlyDH binding pocket. The structure of the TmGlyDH•NAD^+ complex was solvated and the energy minimized at 100 K for 2,000 steps using CHARMM, version c38a2 (5).

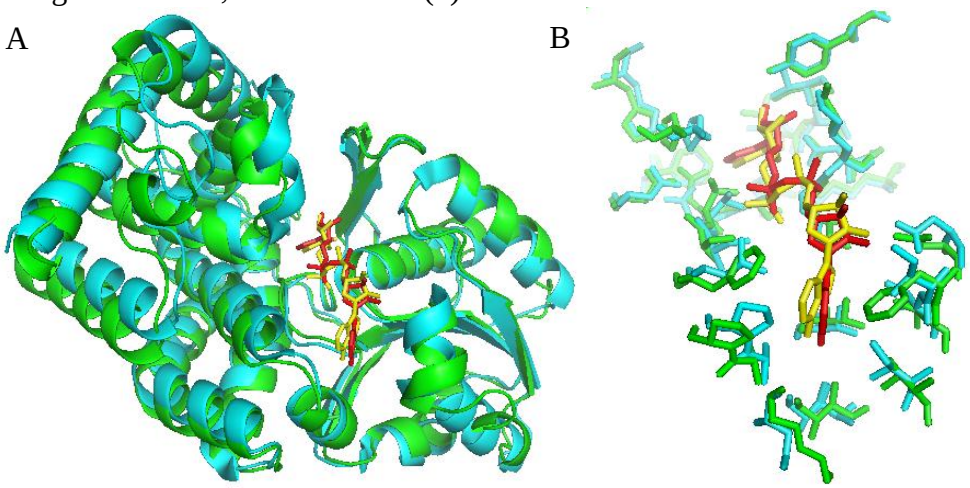

Table 2.4: Apparent kinetic parameters of TmGlyDH (WT) and its mutant derivatives on NAD^+ and N^6-CM-NAD^+. Assays were performed in phosphate buffer (pH 7.4) at 50°C

Enzyme	WT	K157N	K157G	V44A	I154A	V44A/ K157N	V44A/ I154A	V44A/K157G
NAD^+								
V_{max} (μmol min^{-1} mg^{-1})	12.2 ± 0.8	6.9 ± 0.3	19.0 ± 0.7	20.2 ± 0.7	36 ± 2	17.4 ± 0.5	16.6 ± 0.8	3.6 ± 0.1
K_m (μM)	24 ± 5	25 ± 4	31 ± 3	70 ± 6	88 ± 9	39 ± 3	351 ± 25	21 ± 2
V_{max}/K_m (L min^{-1} mg^{-1})	0.5 ± 0.1	0.28 ± 0.05	0.61 ± 0.06	0.29 ± 0.03	0.41 ± 0.05	0.45 ± 0.04	0.047 ± 0.004	0.17 ± 0.02
N^6-CM-NAD^+								
Approx. V_{max} (μmol min^{-1} mg^{-1})	0.28 ± 0.02	0.21 ± 0.04	0.208 ± 0.007	0.61 ± 0.03	0.48 ± 0.03	0.41 ± 0.01	1.4 ± 0.2	1.11 ± 0.2
Approx. K_m (μM)	370 ± 50	360 ± 120	80 ± 10	150 ± 30	730 ± 80	186 ± 14	2,900 ± 500	250 ± 20
V_{max}/K_m ($x10^{-3}$) (L min^{-1} mg^{-1})	0.8 ± 0.1	0.6 ± 0.2	2.6 ± 0.3	4.1 ± 0.8	0.66 ± 0.08	2.2 ± 0.2	0.5 ± 0.1	4.4 ± 0.9

Table 2.4 (cont'd)

Enzyme	I154A/K157G	V44A/I154A/K157G
NAD^+		
V_{max} (μmol min^{-1} mg^{-1})	31.6 ± 0.8	22 ± 2
K_m (μM)	108 ± 6	600 ± 100
V_{max}/K_m (L min^{-1} mg^{-1})	0.29 ± 0.02	0.037 ± 0.007
N^6-CM-NAD^+		
Approx. V_{max} (μmol min^{-1} mg^{-1})	0.40 ± 0.07	0.5 ± 0.2
Approx. K_m (μM)	1,500 ± 350	2,300 ± 1200
V_{max}/K_m ($x10^{-3}$) (L min^{-1} mg^{-1})	0.027 ± 0.008	0.02 ± 0.01

2.4.6 Activity of TmGlyDH with N^6-CM-NAD^+ immobilized on Sepharose beads

As a proof of concept that TmGlyDH is active with immobilized N^6-CM-NAD^+, TmGlyDH activity was measured with N^6-CM-NAD^+ immobilized on Sepharose beads. Loading of the linker B3APA on Sepharose was 4.3 ± 0.9 μmol/g wet Sepharose. Loading of N^6-CM-NAD^+ on B3APA-Sepharose was 1.3 ± 0.2 μmol/g wet Sepharose, occupying approximately one in four linker molecules. TmGlyDH activity was measured by cycling NAD-CM-B3APA-Sepharose in two reactions catalyzed by the enzyme: glycerol oxidation to DHA and hydroxyacetone reduction to (R)-1,2-propanediol. 13.6 ± 1.0 mM glycerol and 16.5 ± 0.9 mM hydroxyacetone were consumed and 7.3 ± 0.2 mM DHA and 11.5 ± 0.5 mM (R)-1,2-propanediol were produced after 22.3 h (Figure 2.6). Some of the DHA produced could have reacted with the free amines on B3APA-Sepharose, explaining why less DHA was detected than (R)-1,2-propanediol. Cycling reactions using N^6-CM-NAD^+ immobilized with the shorter DETA and ED linkers produced 11.2 ± 0.1 mM and 10.72 ± 0.01 mM (R)-1,2-propanediol, respectively, indicating that the length of the linker had no effect on catalysis. TmGlyDH mutant derivatives V44A/K157G, V44A, and K157G tested with NAD-CM-ED-Sepharose produced 1.5 ± 0.2 mM, 6.3 ± 0.7 mM, and 10.8 ± 0.7 mM of (R)-1,2-propanediol, respectively, after 22.5 h.

2.5 DISCUSSION

TmGlyDH was expressed at high levels in *E. coli* and purified to high purity. TmGlyDH's glycerol oxidation activity compared well to that of other characterized GlyDHs. In the absence of added cations, TmGlyDH showed higher glycerol oxidizing specific activity at 80°C (49 ± 2 μmol min^{-1} mg^{-1}) than the GlyDHs from *S. pombe* at 24°C (V_{max} = 4.8 μmol min^{-1} mg^{-1}) (24), *K. pneumoniae* at 27°C (V_{max} = 13.5 μmol min^{-1} mg^{-1}) (25), *B. stearothermophilus* at

30°C (specific activity = 25 µmol min^{-1} mg^{-1}) (35), and *E. coli* at 30°C (V_{max} = 33 µmol min^{-1} mg^{-1}) (31). TmGlyDH glycerol oxidation activity increased moderately in the presence of NH_4Cl, but the added salt increased the rate of DHA degradation and was deemed unsuitable for a reactor process producing DHA from glycerol.

Figure 2.6: Activity of TmGlyDH with N^6-CM-NAD^+ immobilized on B3APA-Sepharose. (■): glycerol; (●): hydroxyacetone; (□): DHA; (○): R-1,2-propanediol.

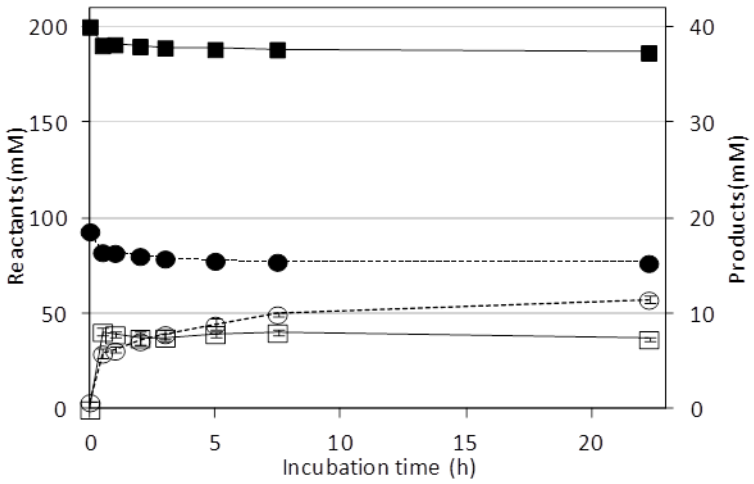

TmGlyDH's high glycerol oxidation activity levels, its independence from the presence of activating cations, together with its high thermostability and its optimum activity near neutral pH, make this enzyme an excellent candidate for DHA production. Another benefit of using TmGlyDH is the similar pH optima for glycerol oxidation and DHA stability (Figure S2.3). In a bioreactor, the pH could be held near pH 7 to maximize DHA stability without sacrificing much enzymatic activity.

High activity on 1,2-propanediol and high enantiomeric excess observed when producing (R)-1,2-propanediol from hydroxyacetone indicate that TmGlyDH could also be a useful catalyst for producing optically active products. Synthesis of optically active 1,2-propanediol from

hydroxyacetone has been reported using resting *E. coli* cells expressing GlyDH and glucose dehydrogenase with glucose in the reaction mixture to recycle NAD^+ (43). Here we have demonstrated for the first time a one-enzyme, cell-free system for the production of (R)-1,2-propanediol using glycerol (a cheap byproduct of biodiesel production) as the recycling substrate. In optimized reaction conditions, TmGlyDH could also be a useful catalyst for resolving a racemic mixture of 1,2-propanediol leaving the (S)-enantiomer. Similar enantiomer preference is expected for 1,2-butanediol.

All characterized GlyDHs have pH optima near 8–12 and 4–8 for the forward and reverse directions, respectively (Table S2.3) (24, 25, 27, 31, 35). Which makes sense because the oxidation of glycerol releases a proton to solution. TmGlyDH was similar to other GlyDHs in its pH requirements for DHA reduction, but it required a lower pH than other GlyDHs for optimal glycerol oxidation (Table S2.3). All the residues located within 10 Å (approximately 3-fold the length of a hydrogen bond) of the TmGlyDH active site Zn^{2+} were identical or chemically conserved (not shown) in the sequences of the *B. stearothermophilus*, *E. coli*, *K. pneumoniae***,** and *S. pombe* enzymes, suggesting that the p$K_A$values of the catalytic residues are in similar ranges in all these enzymes. Note that TmGlyDH differs kinetically from other GlyDHs. At around 30 μM, TmGlyDH's K_m for NAD^+ was over 25-fold lower than those of the *E. coli* and *K. pneumoniae* enzymes (around 800 μM) (25, 31).

The cooperative behavior of TmGlyDH can be explained by the fact that the enzyme is a homotetramer. The *E. coli* enzyme is an octameric enzyme, also showing negative cooperativity for DHA, but no cooperativity for glycerol, NAD^+, or NADH, except that it shows positive cooperativity for NADH in the presence of KCl (31). Cooperativity has also been observed in other enzymes involved in glycerol metabolism such as glyceraldehyde-3-phosphate

dehydrogenase and 1,3-propanediol dehydrogenase (15, 23). Cooperativity arises when substrate binding to one subunit affects the affinity of the other subunits for that substrate. It can also be the result of an enzyme following a bi bi sequential random kinetic mechanism. The steady state-derived kinetic equation for the random mechanism contains squared terms (not shown) that, in themselves, can lead to apparent cooperative behavior (10, 16). Cooperative behavior is widespread with about 25% of all multi-subunit enzymes showing cooperativity, and approximately half of those showing negative cooperativity (19). Although not well understood, negative cooperativity is thought to help regulate homeostasis. Negatively cooperative enzymes have been found to correlate with branch-point enzymes, and simulations have demonstrated that metabolic pathways can be better regulated by cooperative enzymes (7, 19). Cooperativity makes kinetic characterization more difficult because the enzymes do not follow Michaelis-Menten kinetics. To allow comparison to Michaelis-Menten parameters of other enzymes, TmGlyDH's apparent kinetic parameters were determined from the Hill equation. Although the Hill equation is purely empirical, the parameters given provide information similar to the Michaelis-Menten equation. Mathematical modeling of a reactor system that includes NADH regeneration on the electrode, TmGlyDH's kinetic mechanism and corresponding parameters, as well as diffusion parameters (18) is in progress (Li et al., in progress).

A bioelectrocatalytic reactor will require specific conditions for optimal performance. The properties of TmGlyDH determined here will allow reactor conditions to be selected for optimal enzyme activity as well as for optimizing cofactor and enzyme immobilization conditions. The broad, near-neutral pH range for glycerol oxidation activity is beneficial because it allows the pH conditions to be more broadly determined by other reactor constraints such as electron transfer to the cofactor, DHA stability, or the immobilization interface stability. Ideally,

the cofactor and enzyme will be immobilized on the electrode of a bioelectrocatalytic system. The cofactor should be immobilized on the electrode first, and the enzyme would then be immobilized by affinity for the cofactor. The entire complex could be immobilized by crosslinking. TmGlyDH had similar K_m values for NAD^+ and NADH (Table 2.2), indicating that either cofactor form would be suitable for immobilizing the enzyme on an electrode.

Liver alcohol dehydrogenase, lactate dehydrogenase (beef heart, type III), and malate dehydrogenase (pig heart) have been shown to have 55%, 65%, and 75% activity, respectively, with soluble N^6-CM-NAD^+ compared to their activity with NAD^+, and immobilized NAD^+ analogs have been shown to be reducible by yeast alcohol and aldehyde dehydrogenases, suggesting that N^6-immobilized NAD^+ can be used with a number of different dehydrogenases (22, 38). TmGlyDH had very low activity with N^6-CM-NAD^+, but mutant V44A/K157G's catalytic efficiency on the NAD^+ analog was 10-fold higher. The next step towards building a bioelectrocatalytic system will be to immobilize N^6-CM-NAD^+ on an electrode in a manner that allows enzyme binding and activity. Our proof-of-concept immobilization experiments indicate that TmGlyDH is active with N^6-CM-NAD^+ immobilized on B3APA-, ED-, and DETA-Sepharose. The yields of DHA and (R)-1,2-propanediol were low in these first experiments, but improving the interface by optimizing the chemical properties (e.g., hydrophobicity) of the linker and optimizing N^6-CM-NAD^+ loading on the linker are beyond the scope of this study. An unexpected result was that the V44A/K157G and V44A mutants were less active with the immobilized cofactor than the wild-type enzyme. These results suggest that, although convenient, screening mutants with NAD^+ or NAD^+ analogs in solution is not necessarily a good predictor of activity with the immobilized cofactor.

TmGlyDH is a promising catalyst for the production of DHA from glycerol. It is as active and more stable than other known GlyDHs. The broad, near neutral, pH range for TmGlyDH activity will be useful for optimizing other reactor constraints. TmGlyDH double mutant V44A/K157G had a ten-fold increased catalytic efficiency with N^6-CM-NAD^+. Finally we showed for the first time that a GlyDH is active with immobilized N^6-CM-NAD^+.

2.6 ACKNOWLEDGEMENTS

We thank Dr. Hanzi Li for providing expertise in the use of the IGOR program. We thank the Michigan State University Mass Spectrometry Core facility for providing the GC-MS, helping with experimental design and instrument specific training. We thank Dr. Michael Feig for helping with the energy minimization of the TmGlyDH*NAD complex, and we thank Drs. Scott Calabrese Barton and R. Mark Worden for constructive discussions. This work was supported by grants from the National Science Foundation grant (no. CBET 0756703) and the United States Department of Agriculture **Cooperative State Research, Education, and Extension Service** National Research Initiative (no. 2008-35504-04611), and by Michigan State University start up funds.

2.7 SUPLEMENTARY MATERIALS

Table S2.1: Primers used for Chapter 2.

Primer	Sequence (5' to 3')
*gldA*for	GCCATATGATAACAACCACCATATTTCC (*Nde*I site underlined)
*gldA*rev	GCCTCGAGAGTGAGGTTTTTTCTCATCC (*Xho*I site underlined)
V44Afor	GATTTTGTGGACAAAAACGCGCTAGGAGAAAATTTCTTCAGC
V44Arev	GCTGAAGAAATTTTCTCCTAGCGCGTTTTTGTCCACAAAATC
I154Afor	CTGGTAGACACGGAGGCTGTGGCGAAAGCCCCC
I154Arev	GGGGGCTTTCGCCACAGCCTCCGTGTCTACCAG
K157Nfor	CGGAGATTGTGGCGAATGCCCCCGCGAGGTTTC
K157Nrev	GAAACCTCGCGGGGGCATTCGCCACAATCTCCG
K157Gfor	CGGAGATTGTGGCGGGAGCCCCCGCGAGGTTTC
K157Grev	GAAACCTCGCGGGGGCTCCCGCCACAATCTCCG
I154A/K157Nfor	CTGGTAGACACGGAGGCTGTGGCGAATGCCCCC
I154A/K157Nrev	GGGGGCATTCGCCACAGCCTCCGTGTCTACCAG
I154A/K157Gfor	CTGGTAGACACGGAGGCTGTGGCGGGAGCCCCC
I154A/K157Grev	GGGGGCTCCCGCCACAGCCTCCGTGTCTACCAG

Table S2.2: Relative effects of different buffers on TmGlyDH activity.

Buffer	Activity (%)
Phosphate	100
Tris	4
Bicine	71
Glycine	49

Table S2.3: pH optima for different glycerol dehydrogenases.

Species	DHA reduction	Glycerol oxidation	Reference
T. maritima	6.0	7.9	This study
E. coli	7–8	10–11	(31)
K. pneumoniae	4–8	8–9	(25)
S. pombe	6	10–12	(24)
Cellulomonas sp. NT3060	6	9	(27)

Figure S2.1: Structure of glycerol and Tris

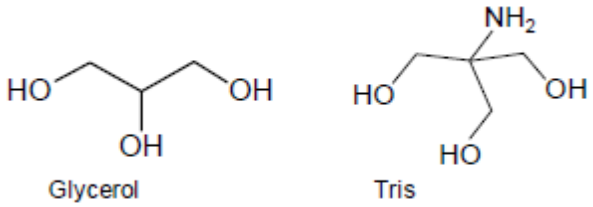

Figures S2.2: TmGlyDH activity for DHA reduction in the presence of increasing KCl concentrations. Results shown are the average ± standard deviation of three independent experiments.

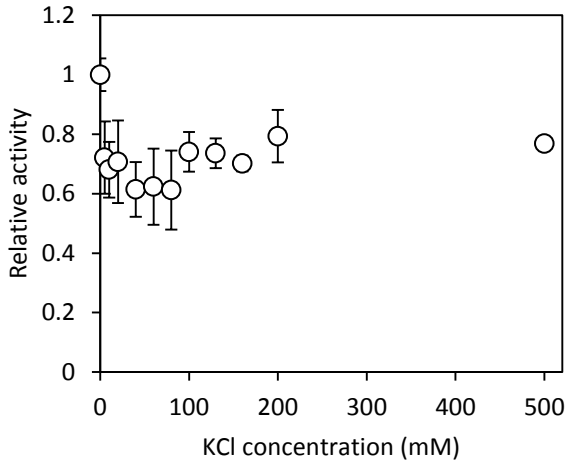

Figure S2.3: DHA stability at 50°C in phosphate buffer. Circles and uninterrupted lines: pH 6.4; squares and dashed lines: pH 7.4; triangles and dotted lines, pH 7.9; Open symbols: DHA; white-filled symbols: glyceraldehyde; and gray-filled symbols: other DHA degradation products. At time t, other degradation products are calculated as [DHA]initial – [DHA]t – [glyceraldehyde]t. Results shown are the average ± standard deviation of three independent experiments.

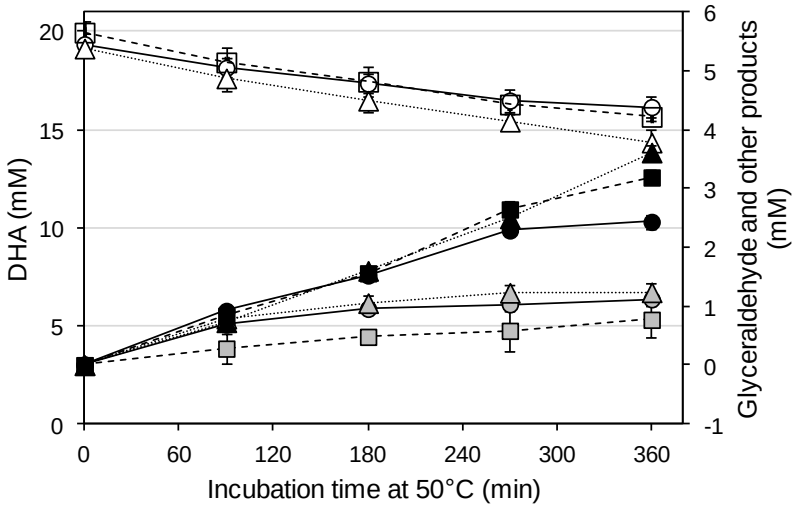

2.8 PERMISSIONS

SPRINGER LICENSE

TERMS AND CONDITIONS

Apr 10, 2015

This is a License Agreement between Justin L Beauchamp ("You") and Springer ("Springer") provided by Copyright Clearance Center ("CCC"). The license consists of your order details, the terms and conditions provided by Springer, and the payment terms and conditions.

All payments must be made in full to CCC. For payment instructions, please see information listed at the bottom of this form.

License Number	3600491122584
License date	Apr 01, 2015
Order Content Publisher	Springer
Order Content Publication	Applied Microbiology and Biotechnology
Order Content Title	Characterization of Thermotoga maritima glycerol dehydrogenase for the enzymatic production of dihydroxyacetone
Order Content Author	Justin Beauchamp
Order Content Date	Jan 1, 2014
Volume number	98
Issue number	16
Type of Use	Thesis/Dissertation
Portion	Full text
Number of copies	6
Author of this Springer article	Yes and you are the sole author of the new work
Order reference number	None
Title of your thesis / dissertation	Thermotoga Maritima Glycerol Dehydrogenase as a Catalyst for Dihydroxyacetone Production: Enzyme Characterization, engineering and Cofactor Immobilization.
Expected completion date	May 2015
Estimated size(pages)	100
Total	0.00 USD

Terms and Conditions

Introduction

The publisher for this copyrighted material is Springer Science + Business Media. By clicking "accept" in connection with completing this licensing transaction, you agree that the following terms and conditions apply to this transaction (along with the Billing and Payment terms and

conditions established by Copyright Clearance Center, Inc. ("CCC"), at the time that you opened your Rightslink account and that are available at any time at http://myaccount.copyright.com).

Limited License
With reference to your request to reprint in your thesis material on which Springer Science and Business Media control the copyright, permission is granted, free of charge, for the use indicated in your enquiry.

Licenses are for one-time use only with a maximum distribution equal to the number that you identified in the licensing process.

This License includes use in an electronic form, provided its password protected or on the university's intranet or repository, including UMI (according to the definition at the Sherpa website: http://www.sherpa.ac.uk/romeo/). For any other electronic use, please contact Springer at (permissions.dordrecht@springer.com or permissions.heidelberg@springer.com).

The material can only be used for the purpose of defending your thesis limited to university-use only. If the thesis is going to be published, permission needs to be re-obtained (selecting "book/textbook" as the type of use).

Although Springer holds copyright to the material and is entitled to negotiate on rights, this license is only valid, subject to a courtesy information to the author (address is given with the article/chapter) and provided it concerns original material which does not carry references to other sources (if material in question appears with credit to another source, authorization from that source is required as well).

Permission free of charge on this occasion does not prejudice any rights we might have to charge for reproduction of our copyrighted material in the future.

Altering/Modifying Material: Not Permitted
You may not alter or modify the material in any manner. Abbreviations, additions, deletions and/or any other alterations shall be made only with prior written authorization of the author(s) and/or Springer Science + Business Media. (Please contact Springer at (permissions.dordrecht@springer.com or permissions.heidelberg@springer.com)

Reservation of Rights
Springer Science + Business Media reserves all rights not specifically granted in the combination of (i) the license details provided by you and accepted in the course of this licensing transaction, (ii) these terms and conditions and (iii) CCC's Billing and Payment terms and conditions.

Copyright Notice:Disclaimer
You must include the following copyright and permission notice in connection with any reproduction of the licensed material: "Springer and the original publisher /journal title, volume, year of publication, page, chapter/article title, name(s) of author(s), figure number(s), original copyright notice) is given to the publication in which the material was originally published, by

adding; with kind permission from Springer Science and Business Media"

Warranties: None

Example 1: Springer Science + Business Media makes no representations or warranties with respect to the licensed material.

Example 2: Springer Science + Business Media makes no representations or warranties with respect to the licensed material and adopts on its own behalf the limitations and disclaimers established by CCC on its behalf in its Billing and Payment terms and conditions for this licensing transaction.

Indemnity
You hereby indemnify and agree to hold harmless Springer Science + Business Media and CCC, and their respective officers, directors, employees and agents, from and against any and all claims arising out of your use of the licensed material other than as specifically authorized pursuant to this license.

No Transfer of License
This license is personal to you and may not be sublicensed, assigned, or transferred by you to any other person without Springer Science + Business Media's written permission.

No Amendment Except in Writing
This license may not be amended except in a writing signed by both parties (or, in the case of Springer Science + Business Media, by CCC on Springer Science + Business Media's behalf).

Objection to Contrary Terms
Springer Science + Business Media hereby objects to any terms contained in any purchase order, acknowledgment, check endorsement or other writing prepared by you, which terms are inconsistent with these terms and conditions or CCC's Billing and Payment terms and conditions. These terms and conditions, together with CCC's Billing and Payment terms and conditions (which are incorporated herein), comprise the entire agreement between you and Springer Science + Business Media (and CCC) concerning this licensing transaction. In the event of any conflict between your obligations established by these terms and conditions and those established by CCC's Billing and Payment terms and conditions, these terms and conditions shall control.

Jurisdiction
All disputes that may arise in connection with this present License, or the breach thereof, shall be settled exclusively by arbitration, to be held in The Netherlands, in accordance with Dutch law, and to be conducted under the Rules of the 'Netherlands Arbitrage Instituut' (Netherlands Institute of Arbitration).***OR:***

All disputes that may arise in connection with this present License, or the breach thereof, shall be settled exclusively by arbitration, to be held in the Federal Republic of Germany,

in accordance with German law.

Other terms and conditions:

v1.3

Questions? customercare@copyright.com or +1-855-239-3415 (toll free in the US) or +1-978-646-2777.

Gratis licenses (referencing $0 in the Total field) are free. Please retain this printable license for your reference. No payment is required.

.SPRINGER LICENSE

TERMS AND CONDITIONS

May 04, 2015

This is a License Agreement between Justin L Beauchamp ("You") and Springer ("Springer") provided by Copyright Clearance Center ("CCC"). The license consists of your order details, the terms and conditions provided by Springer, and the payment terms and conditions.

All payments must be made in full to CCC. For payment instructions, please see information listed at the bottom of this form.

License Number	3600500361357
License date	Apr 01, 2015
Order Content Publisher	Springer
Order Content Publication	Applied Microbiology and Biotechnology
Order Content Title	Characterization of Thermotoga maritima glycerol dehydrogenase for the enzymatic production of dihydroxyacetone

Order Content Author	Justin Beauchamp
Order Content Date	Jan 1, 2014
Volume number	98
Issue number	16
Type of Use	Book/Textbook
Requestor type	Publisher
Publisher	ProQuest
Portion	Full text
Format	Print and Electronic
Will you be translating?	No
Print run	6
Author of this Springer article	Yes and you are the sole author of the new work
Order reference number	None
Title of new book	Thermotoga Maritima Glycerol Dehydrogenase as a Catalyst for Dihydroxyacetone Production: Enzyme Characterization, engineering and Cofactor Immobilization.
Author of new book	Justin L Beauchamp
Expected publication date of new book	May 2015
Estimated size of new book (pages)	100
Total	0.00 USD

Terms and Conditions

Introduction

The publisher for this copyrighted material is Springer Science + Business Media. By clicking "accept" in connection with completing this licensing transaction, you agree that the following terms and conditions apply to this transaction (along with the Billing and Payment terms and conditions established by Copyright Clearance Center, Inc. ("CCC"), at the time that you opened your Rightslink account and that are available at any time at http://myaccount.copyright.com).

Limited License

Springer Science + Business Media hereby grants to you a non-exclusive license to use this material, for the use as indicated in your inquiry. Licenses are for one-time use only with a maximum distribution equal to the number that you identified in the licensing process.

This License includes use in an electronic form, provided it's password protected, on intranet, or CD-Rom/E-book. For any other electronic use, please contact Springer at permissions.dordrecht@springer.com or permissions.heidelberg@springer.com

Although Springer holds copyright to the material and is entitled to negotiate on rights, this

license is only valid, provided permission is also obtained from the author (address is given with the article/chapter) and provided it concerns original material which does not carry references to other sources (if material in question appears with credit to another source, authorization from that source is required as well).

Geographic Rights: Scope
Licenses may be exercised anywhere in the world.

Altering/Modifying Material: Not Permitted
However figures and illustrations may be altered minimally to serve your work. Any other abbreviations, additions, deletions and/or any other alterations shall be made only with prior written authorization of the author(s) and/or Springer Science + Business Media. (Please contact Springer at permissions.dordrecht@springer.com or permissions.heidelberg@springer.com)

Reservation of Rights
Springer Science + Business Media reserves all rights not specifically granted in the combination of (i) the license details provided by you and accepted in the course of this licensing transaction, (ii) these terms and conditions and (iii) CCC's Billing and Payment terms and conditions.

License Contingent on Payment
While you may exercise the rights licensed immediately upon issuance of the license at the end of the licensing process for the transaction, provided that you have disclosed complete and accurate details of your proposed use, no license is finally effective unless and until full payment is received from you (either by Springer Science + Business Media or by CCC) as provided in CCC's Billing and Payment terms and conditions. If full payment is not received by Due Date, then any license preliminarily granted shall be deemed automatically revoked and shall be void as if never granted. Further, in the event that you breach any of these terms and conditions or any of CCC's Billing and Payment terms and conditions, the license is automatically revoked and shall be void as if never granted. Use of materials as described in a revoked license, as well as any use of the materials beyond the scope of an unrevoked license, may constitute copyright infringement and Springer Science + Business Media reserves the right to take any and all action to protect its copyright in the materials.

Copyright Notice:
Please include the following copyright citation referencing the publication in which the material was originally published. Where wording is within brackets, please include verbatim.

"With kind permission from Springer Science+Business Media: <book/journal title, chapter/article title, volume, year of publication, page, name(s) of author(s), figure number(s), and any original (first) copyright notice displayed with material>."

Warranties
Springer Science + Business Media makes no representations or warranties with respect to the licensed material.

Indemnity
You hereby indemnify and agree to hold harmless Springer Science + Business Media and CCC, and their respective officers, directors, employees and agents, from and against any and

all claims arising out of your use of the licensed material other than as specifically authorized pursuant to this license.

No Transfer of License
This license is personal to you and may not be sublicensed, assigned, or transferred by you to any other person without Springer Science + Business Media's written permission.

No Amendment Except in Writing
This license may not be amended except in a writing signed by both parties (or, in the case of Springer Science + Business Media, by CCC on Springer Science + Business Media's behalf).

Objection to Contrary Terms
Springer Science + Business Media hereby objects to any terms contained in any purchase order, acknowledgment, check endorsement or other writing prepared by you, which terms are inconsistent with these terms and conditions or CCC's Billing and Payment terms and conditions. These terms and conditions, together with CCC's Billing and Payment terms and conditions (which are incorporated herein), comprise the entire agreement between you and Springer Science + Business Media (and CCC) concerning this licensing transaction. In the event of any conflict between your obligations established by these terms and conditions and those established by CCC's Billing and Payment terms and conditions, these terms and conditions shall control.

Jurisdiction
All disputes that may arise in connection with this present License, or the breach thereof, shall be settled exclusively by the country's law in which the work was originally published.

Other terms and conditions:

v1.3

Questions? customercare@copyright.com or +1-855-239-3415 (toll free in the US) or +1-978-646-2777.

Gratis licenses (referencing $0 in the Total field) are free. Please retain this printable license for your reference. No payment is required.

REFERENCES

REFERENCES

1. **Ausubel, F. M., R. Brent, R. E. Kingston, D. D. Moore, J. G. Seidman, J. A. Smith, and K. Struhl (ed.).** 1993. Current Protocols in Molecular Biology, vol. Greene Publishing & Wiley-Interscience, New York.

2. **Bauer, R., N. Katsikis, S. Varga, and D. Hekmat.** 2005. Study of the inhibitory effect of the product dihydroxyacetone on *Gluconobacter oxydans* in a semi-continuous two-stage repeated-fed-batch process. Bioprocess Biosys. Engin. **28:**37–43.

3. **Bliznak, J. B., and R. E. Harcarufka.** 1981. Sweetener and flavoring compositions and method of producing same. United States Patent**:**4,277,511.

4. **Brinen, L. S., J. M. Canaves, X. Dai, A. M. Deacon, M. A. Elsliger, S. Eshaghi, R. Floyd, A. Godzik, C. Grittini, S. K. Grzechnik, C. Guda, L. Jaroszewski, C. Karlak, H. E. Klock, E. Koesema, J. S. Kovarik, A. Kreusch, P. Kuhn, S. A. Lesley, D. McMullan, T. M. McPhillips, M. A. Miller, M. D. Miller, A. Morse, K. Moy, J. Ouyang, A. Robb, K. Rodrigues, T. L. Selby, G. Spraggon, R. C. Stevens, H. v. d. Bedem, J. Velasquez, J. Vincent, X. Wang, B. West, G. Wolf, S. S. Taylor, K. O. Hodgson, J. Wooley, and I. A. Wilson.** 2003. Crystal structure of a zinc-containing glycerol dehydrogenase (TM0423) from *Thermotoga maritima* at 1.5 Å resolution. Proteins: Struct., Funct., and Bioinf. **50:**371–374.

5. **Brooks, B. R., C. L. Brooks, A. D. Mackerell, L. Nilsson, R. J. Petrella, B. Roux, Y. Won, G. Archontis, C. Bartels, S. Boresch, A. Caflisch, L. Caves, Q. Cui, A. R. Dinner, M. Feig, S. Fischer, J. Gao, M. Hodoscek, W. Im, K. Kuczera, T. Lazaridis, J. Ma, V. Ovchinnikov, E. Paci, R. W. Pastor, C. B. Post, J. Z. Pu, M. Schaefer, B. Tidor, R. M. Venable, H. L. Woodcock, X. Wu, W. Yang, D. M. York, and M. Karplus.** 2009. CHARMM: The biomolecular simulation program. J. Comput. Chem. **30:**1545–1614.

6. **Bruins, M. E., A. E. M. Janssen, and R. M. Boom.** 2001. Thermozymes and their applications. Appl. Biochem. Biotechnol. **90:**155–186.

7. **Bush, E. C., A. E. Clark, C. M. Deboever, L. E. Haynes, S. Hussain, S. Ma, M. M. McDermott, A. M. Novak, and J. S. Wentworth.** 2012. Modeling the role of negative cooperativity in metabolic regulation and homeostasis. PLOS ONE **7:**e48920.

8. **Cornish-Bowden, A.** 1995. Fundamentals of enzyme kinetics, vol. Portland Press Ltd., London.

9. **Cossement, E., J. P. Geerts, J. Gobert, P. Michel, and E. Wulfert.** 1990. Substituted 1-(1H-imidazol-4-yl)alkyl-benzamides as anti-ischemics and as α-2-adrenergic receptor agonists. United States Patent**:**4,923,865

10. **Ferdinand, W.** 1966. The interpretation of non-hyperbolic rate curves for two-substrate enzymes. Biochem. J. **98:**278–283.

11. **Forde, J., L. Oakey, L. Jennings, and P. Mulchahy.** 2005. Fundamental differences in bioaffinity of amino acid dehydrogenases for N^6- and S^6-linked immobilized cofactors using kinetic-based enzyme capture strategies. Anal. Biochem. **338:**102–112.

12. **Gehrer, E., and H. Wolfgang.** 1994. Manufacture of 1,2-propylene glycol. United States Patent**:**5,306,847.

13. **Goujon, M., H. McWilliam, W. Z. Li, F. Valentin, S. Squizzato, J. Paern, and R. Lopez.** 2010. A new bioinformatics analysis tools framework at EMBL-EBI. Nucl. Acids Res. **38:**W695–W699.

14. **Hekmat, D., R. Bauer, and J. Fricke.** 2003. Optimization of the microbial synthesis of dihydroxyacetone from glycerol with *Gluconobacter oxydans*. Bioprocess Biosys. Engin. **26:**109–116.

15. **Henis, Y. I., and A. Levitzki.** 1980. Mechanism of negative cooperativity in glyceraldehyde-3-phosphate dehydrogenase deduced from ligand competition experiments. Proc. Natl. Acad. Sci. USA **77:**5055–5059.

16. **Ivanetich, K. M., R. D. Goold, and C. N. Sikakana.** 1990. Explanation of the non-hyperbolic kinetics of the glutathione s-transferases by the simplest steady-state random sequential bi bi mechanism. Biochem. Pharmicol. **39:**1999–2004.

17. **Johnson, J. A., and R. M. Fusaro.** 1994. Alteration of skin surface protein with dihydroxyacetone: A useful application of the Maillard browning reaction, p. 114–119. *In* T. P. Labuza, G. A. Reineccius, V. M. Monnier, J. O'Brien, and J. W. Baynes (ed.), Maillard Reactions in Chemistry, Food, and Health. The Royal Society of Chemistry, Cambridge.

18. **Kar, P., H. Wen, H. Li, S. D. Minteer, and S. Calabrese Barton.** 2011. Simulation of multistep enzyme-catalyzed methanol oxidation in biofuel cells. J. Electrochem. Soc. **158:**B580–B586.

19. **Koshland, D. E., and K. Hamadani.** 2002. Proteomics and models for enzyme cooperativity. J. Biol. Chem. **277:**46841–46844.

20. **Li, H., H. Wen, and S. Calabrese Barton.** 2012. NADH oxidation by electropolymerized azines on carbon nanotube modified electrodes. Electroan. **24:**398–406.

21. **Li, M., J. Wu, X. Liu, J. Lin, D. Wei, and H. Chen.** 2010. Enhanced production of dihydroxyacetone from glycerol by overexpression of glycerol dehydrogenase in an alcohol dehydrogenase-deficient mutant of *Gluconobacter oxydans*. Bioresour. Technol. **101:**8294-8299.

22. **Lindberg, M., P. Larsson, and K. Mosbach.** 1973. A new immobilized NAD^+ analogue, its application in affinity chromatography and as a functioning coenzyme. Eur. J. Biochem. **40:**187–193.

23. **Marçal, D., A. T. Rego, M. A. Carrondo, and F. J. Enguita.** 2009. 1,3-Propanediol dehydrogenase from *Klebsiella pneumoniae*: Decameric quaternary structure and possible subunit cooperativity. J. Bacteriol. **191:**1143–1151.

24. **Marshall, J. H., J. W. May, and J. Sloan.** 1985. Purification and properties of glycerol:NAD^+ 2-oxidoreductase (glycerol dehydrogenase) from *Schizosaccharomyces pombe*. J. Gen. Microbiol. **131:**1581–1588.

25. **McGregor, W. G., J. E. Phillips, and C. H. Suelter.** 1974. Purification and kinetic characterization of a monovalent cation-activated glycerol dehydrogenase from *Aerobacter aerogenes*. J. Biol. Chem. **249:**3132–3139.

26. **Mosbach, K.** 1974. AMP and NAD as general ligands, p. 229–242. Meth. Enzymol., vol. 34. Academic Press.

27. **Nishise, H., A. Nagao, Y. Tani, and H. Yamada.** 1984. Further characterization of glycerol dehydrogenase from *Cellulomonas* sp. NT3060. Agric. Biol. Chem. **48:**1603–1609.

28. **O'Flaherty, M., M. McMahon, and P. Mulcahy.** 1999. A kinetic locking-on strategy for bioaffinity purification: further studies with alcohol dehydrogenase. Protein Expr. Purif. **15:**127–145.

29. **Oakey, L., and P. Mulcahy.** 2004. Immobilized cofactor derivatives for kinetic-based enzyme capture strategies: direct coupling of $NAD(P)^+$. Anal. Biochem. **335:**316–325.

30. **Parhi, S. S. L.** 1986. Substituted 2-mercapto-imidazoles and their preparation. United States Patent**:**4,584,383.

31. **Piattoni, C. V., C. M. Figueroa, M. D. A. Diez, I. L. Parcerisa, S. Antuna, R. A. Comelli, S. A. Guerrero, A. J. Beccaria, and A. A. Iglesias.** 2013. Production and characterization of *Escherichia coli* glycerol dehydrogenase as a tool for glycerol recycling. Process Biochem. **48:**406–412.

32. **Sellek, G. A., and J. B. Chaudhuri.** 1999. Biocatalysis in organic media using enzymes from extremophiles. Enzyme Microbial Technol. **25:**471–482.

33. **Sievers, F., A. Wilm, D. Dineen, T. J. Gibson, K. Karplus, W. Z. Li, R. Lopez, H. McWilliam, M. Remmert, J. Soding, J. D. Thompson, and D. G. Higgins.** 2011. Fast, scalable generation of high-quality protein multiple sequence alignments using Clustal Omega. Mol. Syst. Biol. **7**.

34. **Song, S. H., N. Ahluwalia, L. Yvonne, L. T. J. Delbaere, and C. Vieille.** 2008. *Thermotoga maritima* TM0298 is a highly thermostable mannitol dehydrogenase. Appl. Microbiol. Biotechnol. **81:**485-495.

35. **Spencer, P., K. J. Brown, M. D. Scawen, T. Atkinson, and M. G. Gore.** 1989. Isolation and characterization of the glycerol dehydrogenase from *Bacillus stearothermophilus*. Biochim. Biophys. Acta **994:**270–279.

36. **Srinivasan, V., K. S. Ma, M. W. W. Adams, M. G. Newton, J. P. Rose, and B. C. Wang.** 2002. Towards the crystal structure of glycerol dehydrogenase from *Thermotoga maritima*. Acta Crystallog. D. **D58:**867–869.

37. **Studer, M.** 2003. Production of optically active α-hydroxyacetals. United States Patent**:**6,660,890.

38. **Tynan, J., J. Forde, M. McMahon, and P. Mulcahy.** 2000. Synthesis of a highly substituted N^6-linked immobilized NAD^+ derivative using a rapid solid-phase modular approach: Suitability for use with the kinetic locking-on tactic for bioaffinity purification of NAD^+-dependent dehydrogenases. Protein Express. Purif. **20:**421–434.

39. **Vieille, C., and J. G. Zeikus.** 2001. Hyperthermophilic enzymes: sources, uses, and molecular mechanisms for thermostability. Microbiol. Mol. Biol. Rev. **65:**1–43.

40. **Weckbecker, A., H. Groger, and W. Hummel.** 2010. Regeneration of nicotinamide coenzymes: principles and applications for the synthesis of chiral compounds. Adv. Biochem. Engin./Biotechnol. **120:**195–242.

41. **Wells, G., H. Prest, and C. W. Russ IV.** 2011. Signal, noise, and detection limits in mass spectrometry. Agilent Technologies. Technical note:5990-7651EN.

42. **Wichmann, R., and D. Vasic-Racki.** 2005. Cofactor regeneration at the lab scale. Adv. Biochem. Engin./Biotechnol. **92:**225–260.

43. **Yamada-Onodera, K., N. Kawahara, Y. Tani, and H. Yamamoto.** 2004. Synthesis of optically active diols by *Escherichia coli* transformant cells that express the glycerol dehydrogenase gene of *Hansenula polymorpha* DL-1. Engin. Life Sciences **4:**413–417.

44. **Yang, D., J. H. Zhang, M. K. Wong, Y. C. Yip, and M. W. Tang.** 1998. Process for catalytic epoxidation of olefinic compounds, novel cyclic ketone catalysts useful in said process. United States Patent**:**5,763,623.

CHAPTER 3. Activity of select dehydrogenases with sepharose-immobilized N^6-CM-NAD

3.1 ABSTRACT

N^6-carboxymethyl-NAD (N^6-CM-NAD) can be used to immobilize NAD onto a substrate containing terminal primary amines. We previously immobilized N^6-CM-NAD onto sepharose beads and showed that *Thermotoga maritima* glycerol dehydrogenase could use and recycle the immobilized cofactor. We now show that *Saccharomyces cerevisiae* alcohol dehydrogenase, rabbit muscle L-lactate dehydrogenase (type XI), bovine liver L-glutamic dehydrogenase (type III), *Leuconostoc mesenteroides* glucose-6-phosphate dehydrogenase, and *Thermotoga maritima* mannitol dehydrogenase are active with soluble N^6-CM-NAD. The products of all enzymes except 6-phospho-D-glucono-1,5-lactone were formed when sepharose-immobilized N^6-CM-NAD was recycled by *T. maritima* glycerol dehydrogenase, indicating that N^6-immobilized NAD is suitable for use by a variety of different dehydrogenases. Observations of the enzyme active sites suggest that steric hindrance plays a greater role in limiting or allowing activity with the modified cofactor than do polarity and charge of the residues surrounding the N^6-amine group on NAD.

3.2 INTRODUCTION

NAD(P)-dependent dehydrogenases participate in a wide variety of metabolic pathways. They catalyze over 12% of all metabolic reactions in *Escherichia coli* (8). The requirement that the cofactor be provided in stoichiometric amounts is the greatest limitation to using dehydrogenases as catalysts. Widespread industrial use will require regeneration of the cofactor. Immobilization of the cofactor allows it to be retained in a reaction vessel or recovered more easily, allowing the same cofactor to be used for many cycles. As a proof of concept, we previously synthesized the NAD analog N^6-carboxymethyl-NAD (N^6-CM-NAD), in which the

N^6 primary amine in the adenine moiety is now –NH-CH_2-COO^-, and we immobilized it on sepharose beads using a diamino linker. The immobilized cofactor was tested with *Thermotoga maritima* glycerol dehydrogenase (TmGlyDH) in two simultaneous reactions: glycerol oxidation to dihydroxyacetone (DHA), and hydroxyacetone reduction to (R)-1,2-propanediol. TmGlyDH could use and recycle the immobilized cofactor for more than 1,800 turnovers to allow measurable product accumulation (2).

Ottolina and colleagues (1990) used a similar N^6 linkage to modify NAD (6). They studied the effects of strong cationic and anionic substituents as well as that of a large polymer (PEG, 20 kDa) on the properties of the cofactor . The eleven enzymes tested generally showed increased K_m and decreased V_{max} with the modified NADs. Enzyme activity with PEG-NAD varied from as high as 66% of the activity with native NAD to undetectably low. A strong anionic substituent led to a stronger reduction in activity (8-43% of native NAD) than a strong cationic substituent (4-93% of native NAD). The large differences in activity of the various enzymes with the NAD analogs were likely caused by the different shapes and chemistries of these enzymes' NAD binding sites.

NAD(P)-dependent dehydrogenases share a common NAD-binding domain and Rossman fold (7). However, the nature and positioning of residues around the NAD binding site can vary significantly from one enzyme to the next, causing variations in enzymes' affinity for the cofactor, determining whether NADP or NAD is the preferred cofactor, and changing which areas of the cofactor are solvent-accessible. Here we test five NAD-dependent dehydrogenases for activity with Sepharose-bead immobilized N^6-CM-NAD to address two questions. Is our immobilization method suitable for use with a broad set of enzymes? And can structural information on the NAD-binding site and cofactor solvent accessibility be used to predict

activity with immobilized N^6-CM-NAD? We selected four commercially available NAD-dependent dehydrogenases whose crystal structure in complex with NAD is known, as well as *T. maritima* mannitol dehydrogenase (TmMtDH), which we had studied previously (11).

Table 3.1: Enzymes used in this study.

Enzyme	Reaction catalyzed	Protein Data Bank code for enzyme• NAD complex
TmGlyDH	Glycerol + $NAD^+ \rightleftharpoons$ Dihydroxyacetone + NADH	1KQ3[a]
TmMtDH	Mannitol + $NAD^+ \rightleftharpoons$ Fructose + NADH	None
Saccharomyces cerevisiae alcohol dehydrogenase (yADH)	Ethanol + $NAD^+ \rightleftharpoons$ Acetaldehyde + NADH	2HCY
Rabbit muscle type XI L-lactate dehydrogenase (rLDH)	L-Lactate + $NAD^+ \rightleftharpoons$ Pyruvate + NADH	3H3F
Bovine liver type III L-glutamate dehydrogenase (bGDH)	L-Glutamate + H_2O + $NAD^+ \rightleftharpoons$ 2-Oxoglutarate + NH_3 + NADH	3MW9
Leuconostoc mesenteroides glucose-6-phosphate dehydrogenase (LmG6PDH)	D-Glucose 6-phosphate + $NAD^+ \rightleftharpoons$ 6-Phospho-D-glucono-1,5-lactone + NADH	1H94

[a] Structure without NAD. NAD was imported into the structure as described (2).

3.3 RESULTS AND DISCUSSION

The Sigma-Aldrich website was searched for commercially available dehydrogenases and NAD-dependent oxidoreductases. The list of enzymes generated was then cross-referenced against the

Protein Data Bank (PDB). Of the ten enzymes that had a crystal structure in complex with NAD, four (Table 3.1) were selected and purchased from Sigma-Aldrich for our study. TmMtDH was added to the study because it was already available as a purified, recombinant enzyme in our laboratory (11). To allow comparison of its active site, we built a 3D model of TmMtDH in complex with NAD (Figure 3.1).

The adenine moiety binding portion of the NAD binding pocket of the five enzymes and of TmGlyDH was visualized (Figure 3.1). The residues and pocket structure around the adenine varied greatly among the enzymes. The configuration of NAD is similar in TmMtDH, yADH, rLDH, bGDH, and LmG6PDH, with the adenine's N^6-amine pointing toward the solvent. In TmGlyDH, NAD's adenine moiety is flipped, with the N^6-amine pointing towards the enzyme's surface. Since NAD's N^6-amine is less solvent exposed in TmGlyDH than in the other enzymes, we expected TmGlyDH to have the lowest activity with N^6-CM-NAD. The specific activity of the mesophilic enzymes with NAD and N^6-CM-NAD and the V_{max} values with the cofactor and analog of TmGlyDH and TmMtDH were compared (Table 3.2). TmMtDH's V_{max} with N^6-CM-NAD was almost 70% of that with NAD and the K_m increased only 1.8 fold. In contrast, TmGlyDH's V_{max} with N^6-CM-NAD was only 2% of that with NAD and the K_m increased 15 fold. With the exception of LmG6PDH, the N^6-amine solvent-accessible area (Table 3.2) correlated well ($R^2 = 0.95$ for linear regression, not shown) with the percent activity with N^6-CM-NAD (Table 2) ($R^2 = 0.61$when LmG6PDH is included). In contrast, the type of residues (i.e., charged, polar, or non-polar) surrounding the N^6-amine (Table 3.2) showed no relationship to activity with N^6-CM-NAD (Table 3.2).

Figure 3.1: Zoom view of enzyme-bound NAD (8-iodo-NAD for yADH). A. TmMtDH, B. TmGlyDH, C. yADH, D. LmG6PDH, E. rLDH, F. bGDH. PDB numbers are listed in Table 1. Several 3D models of TmMtDH were generated using Modeller software8 and the online homology modeling server I-TASSER.9-11. The different modeling approaches used single and multiple templates that each showed over 25% identity and below 10% gaps in alignments with TmMtDH. Models were analyzed using the scoring methods DOPE, DFIRE, and OPUS.12-14 The best model was produced by I-TASSER using the structures of the silverleaf whitefly sorbitol dehydrogenase (PDB # 1E3J), human sorbitol dehydrogenase (PDB # 1PL8), *Sulfolobus solfataricus* glucose dehydrogenase (PDB # 2CDC), *Thermus thermophilus* threonine 3-dehydrogenase (PDB # 2DQ4), and mouse class II alcohol dehydrogenase (PDB # 1E3I) as templates. The structure was minimized using the CHARMM force field15 and NAD was imported into TmMtDH's active site using the coordinates of NAD in human sorbitol dehydrogenase. Enzyme surfaces were visualized using The PyMOL Molecular Graphics System, Version 1.3 Schrödinger, LLC.

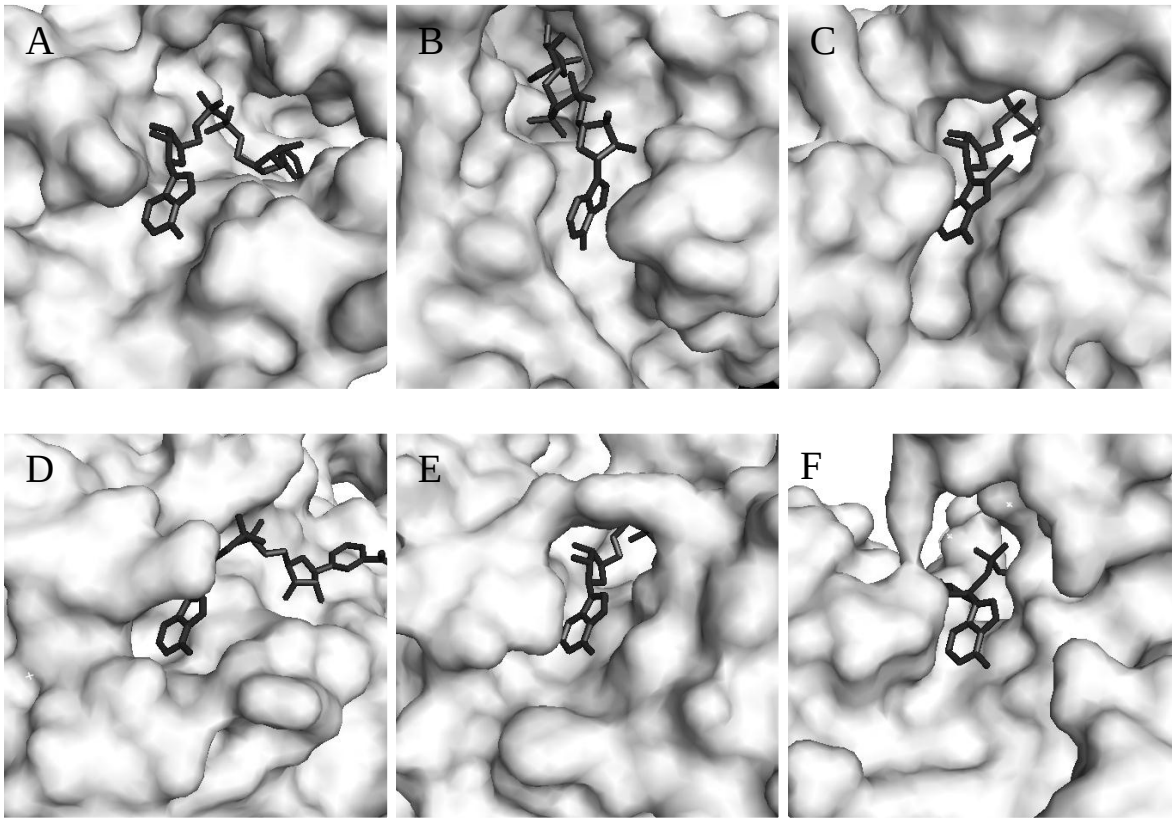

Table 3.2: Specific activity of the selected enzymes with 100 μM NAD and N^6-CM-NAD and enzyme ranking by polarity/charge and openness of the area surrounding NAD's N^6-amine. Specific activities were tested at 25°C by following the increase in A340nm in quartz cuvettes containing 100 mM substrate (L-lactate, glucose-6-phosphate, L-glutamate, or ethanol), 100 μM NAD or N^6-CM-NAD in 50 mM sodium phosphate (pH 7.5). Reactions were started by adding 1.25 μg (rLDH), 1.08 μg (yADH) 0.201 μg (LmG6PDH), or 4.22 μg (bGDH) enzyme. Using the crystal structures or 3D models of the enzymes visualized in PyMOL, amino acid side-chains and backbone groups within 5 Å of the N^6-amine were assessed for polarity and charge. The N^6-amine solvent-accessible area was calculated using PyMOL.

Enzyme	NAD (μmol min^{-1} mg^{-1})	N^6-CM-NAD (μmol min^{-1} mg^{-1})	% activity	Polar groups near the N^6-amine	N^6-amine solvent-accessible area ($Å^2$)
TmMtDH	2.2 ± 0.1[a]	1.5 ± 0.5[a]	68	1 Polar, 1 negative charge	49.9
bGDH	1.42 ± 0.05	0.81 ± 0.24	57	2 Polar, 1 non-polar	43.9
LmG6PDH	260 ± 40	46 ± 4	18	1 Negative charge, 2 non-polar	41.7
yADH	38 ± 2	15.5 ± 0.9	41	1 Polar, 2 non-polar	28.8
rLDH	10 ± 1	2.5 ± 0.4	25	3 Non-polar	24.8
TmGlyDH	12.2 ± 0.8[b]	0.28 ± 0.2[b]	2	2 Polar	16.2

a -V_{max} values for TmMtDH were measured at 50°C as described for TmGlyDH except that mannitol was substituted for glycerol (2).
b-V_{max} values at 50°C previously measured (2).

To test enzyme activity with Sepharose-bound N^6-CM-NAD, we initially tested bGDH as the cofactor-recycling enzyme in recycling reactions between rLDH and bGDH and between LmG6PDH and bGDH. In these recycling reactions, rLDH and LmG6DH were set to reduce the cofactor, and bGDH to oxidize it. Neither of the two reactions yielded any product. We could not tell whether none of the enzymes used the immobilized N^6-CM-NAD, or if the recycling enzyme (bGDH) was causing the problem. Note that bGDH showed very low specific activity with NAD in the conditions tested (Table 3.2). For these reasons, we repeated the recycling reactions with TmGlyDH as the cofactor-recycling enzyme. Even though TmGlyDH is poorly active at 25°C, we knew it to be active with Sepharose-bound N^6-CM-NAD (2). Recycling reactions were set

between TmGlyDH and each of yADH, rLDH, bGDH, and TmMtDH, where yADH, rLDH, bGDH, and TmMtDH oxidized the cofactor and TmGlyDH reduced it while oxidizing glycerol to DHA. Reaction progress was monitored by measuring DHA accumulation with high-performance liquid chromatography. Because LmG6PDH's only commercially available substrate is glucose-6-phosphate, the recycling reaction between LmG6PDH and TmGlyDH was set with TmGlyDH producing NAD^+ during DHA reduction to glycerol, and reaction progress was monitored by measuring glycerol accumulation by high-performance liquid chromatography. No product accumulation was observed in the LmG6PDH-TmGlyDH reaction (not shown). Even though LmG6PDH has the highest specific activity with soluble N^6-CM-NAD of the six enzymes tested (Table 3.2), LmG6PDH could be inactive with immobilized N^6-CM-NAD. Because TmGlyDH is inhibited by its products (not shown), glycerol added as part of the LmG6PDH suspension (initial glycerol concentration in the reaction estimated at 138 mM) could also have inhibited glycerol production by TmGlyDH, preventing cofactor recycling. Product accumulation was observed for the recycling reactions involving yADH, rLDH, bGDH, and TmMtDH (Figure 3.2). Although the solvent-accessible area of the N^6-amine correlated well with activity for soluble N^6-CM-NAD (Table 3.2), no such relationship was apparent after immobilization on Sepharose, with only small differences in DHA accumulation observed between the different reactions. Regardless, our results indicate that many different enzymes can use Sepharose-immobilized N^6-CM-NAD as their cofactor.

Note that we used TmGlyDH, the enzyme with the least activity with soluble N^6-CM-NAD (Table 3.2), as the cofactor-recycling enzyme because it was previously shown to be active with the immobilized cofactor. TmMtDH, bGDH, and yADH showed the highest relative activities with soluble N^6-CM-NAD (Table 3.2). bGDH used in combination with TmMtDH as the

cofactor-recycling enzyme produced 2.6 times more product than in combination with TmGlyDH (data not shown), suggesting that poor activity of TmGlyDH with immobilized N^6-CM-NAD could have limited product accumulation. In contrast, the yADH/TmMtDH combination produced only 20% as much product as the yADH/TmGlyDH combination. The reason behind this poor yield is unknown, since the two enzymes were not inhibited by each other's substrate (data not shown).

3.4 CONCLUSION

Our work demonstrates that N^6-CM-NAD immobilized onto a large particle, such as Sepharose, can be used by a variety of enzymes. NAD's N^6-amine solvent-accessible area in an enzyme•NAD complex is a good indicator of whether that enzyme will be active with N^6-CM-NAD. The possibility of one enzyme's substrate inhibiting the enzyme used in combination highlights the need for an alternative cofactor regeneration method. Electrochemical regeneration could be a good alternative but requires efficient methods for cofactor and enzyme immobilization on electrodes. N^6-CM-NAD could be used to create a bioelectronics linkage similar to that previously developed by Hassler and Worden (4). They developed a renewable bioelectronics interface with the enzyme and cofactor immobilized on an electrode surface. The immobilization method used relied on a boronate linkage to NADP's *cis*-diol. The main limitation of the boronate linkage was that this linkage is relatively weak with a dissociation constant (K_d) of 5.9×10^{-3}, and boronate shows high affinity for other *cis*-diols found on the substrates of many dehydrogenases (1). The enzyme substrates would displace the cofactor from the electrode surface. The N^6-immobilized NAD tested here would allow a new linkage to be produced that is stable in the presence of the enzyme substrates and products.

3.5 ACKNOWLEDGEMENTS

We thank Phillip G. Gross for contributing to the kinetic studies of TmGlyDH. We thank Dr. Srinivasa Gopal for helping with CHARMM minimization and DOPE, DFIRE and OPUS analysis of the TmMtDH model, and Dr. Kaillathe Padmanabhan for his help with PyMOL and solvent-accessible area determination. This work was supported by grant # CBET 0756703 from the National Science Foundation, grant # 2008-35504-04611 from the United States Department of Agriculture **Cooperative State Research, Education, and Extension Service** National Research Initiative, grant # 2010-04061 from the United States Department of Agriculture National Institute for Food and Agriculture's Sustainable Bioenergy Research Program, and by Michigan State University start up funds.

REFERENCES

REFERENCES

1. **Bailon, P., G. K. Ehrlich, W.-J. Fung, and W. Berthold (ed.).** 2000. Methods in molecular biology: affinity chromatography methods and protocols, vol. 147. Humana Press Inc, Totowa NJ.

2. **Beauchamp, J., P. G. Gross, and C. Vieille.** 2014. Characterization of *Thermotoga maritima* glycerol dehydrogenase for the enzymatic production of dihydroxyacetone. Appl Microbiol Biotechnol **98:**7039–7050.

3. **Brooks, B. R., C. L. Brooks, A. D. Mackerell, L. Nilsson, R. J. Petrella, B. Roux, Y. Won, G. Archontis, C. Bartels, S. Boresch, A. Caflisch, L. Caves, Q. Cui, A. R. Dinner, M. Feig, S. Fischer, J. Gao, M. Hodoscek, W. Im, K. Kuczera, T. Lazaridis, J. Ma, V. Ovchinnikov, E. Paci, R. W. Pastor, C. B. Post, J. Z. Pu, M. Schaefer, B. Tidor, R. M. Venable, H. L. Woodcock, X. Wu, W. Yang, D. M. York, and M. Karplus.** 2009. CHARMM: The biomolecular simulation program. J. Comput. Chem. **30:**1545–1614.

4. **Hassler, B. L., N. Kohli, J. G. Zeikus, I. Lee, and R. M. Worden.** 2007. Renewable dehydrogenase-based interfaces for bioelectronic applications. Langmuir **23:**7127–7133.

5. **Lu, M., A. D. Dousis, and J. Ma.** 2008. OPUS-PSP: an orientation-dependent statistical all-atom potential derived from side-chain packing. J. Mol. Biol. **376:**288–301.

6. **Ottolina, G., G. Carrea, S. Riva, and A. Bückmann.** 1990. Coenzymatic properties of low molecular-weight and macromolecular N6-derivatives of NAD^+ and $NADP^+$ with dehydrogenases of interest for organic synthesis. Enzyme Microb. Technol. **12:**596–602.

7. **Rao, S. T., and M. G. Rossmann.** 1973. Comparison of super-secondary structures in proteins. J. Mol. Biol. **76:**241–256.

8. **Reed, J. L., T. D. Vo, C. H. Schilling, and B. O. Palsson.** 2003. An expanded genome-scale model of *Escherichia coli* K-12 (iJR904 GSM/GPR). Genome Biol. **4:**R54.

9. **Sali, A., and T. L. Blundell.** 1993. Comparative protein modeling by satisfaction of spatial restraints. J. Mol. Biol. **234:**779–815.

10. **Shen, M. Y., and A. Sali.** 2006. Statistical potential for assessment and prediction of protein structures. Protein Sci **15:**2507–2524.

11. **Song, S. H., N. Ahluwalia, Y. Leduc, L. T. Delbaere, and C. Vieille.** 2008. *Thermotoga maritima* TM0298 is a highly thermostable mannitol dehydrogenase. Appl. Microbiol. Biotechnol. **81:**485–495.

12. **Wu, S., J. Skolnick, and Y. Zhang.** 2007. Ab initio modeling of small proteins by iterative TASSER simulations. BMC Biol. **5:**17.

13. **Zhang, Y.** 2008. I-TASSER server for protein 3D structure prediction. BMC Bioinf. **9:**40.

14. **Zhang, Y.** 2007. Template-based modeling and free modeling by I-TASSER in CASP7. Proteins **69 Suppl 8:**108–117.

15. **Zhou, H., and Y. Zhou.** 2002. Distance-scaled, finite ideal-gas reference state improves structure-derived potentials of mean force for structure selection and stability prediction. Protein Sci. **11:**2714–2726.

CHAPTER 4. Inactivation of *Thermotoga maritima* glycerol dehydrogenase by its product, dihydroxyacetone

4.1 ABSTRACT

Thermotoga maritima glycerol dehydrogenase (TmGlyDH), which oxidizes glycerol into dihydroxyacetone (DHA) in an NAD-dependent reaction, is susceptible to inactivation by DHA. DHA reacts readily with primary amines on the enzyme surface through Maillard reactions. TmGlyDH's Arg and Lys residues modified by DHA were identified in tryptic and chymotryptic digests of TmGlyDH by mass spectrometry. To make TmGlyDH a better catalyst, the residues susceptible to modification by DHA were systematically mutagenized, and the mutant enzymes were screened for increased stability in the presence of DHA. Wild-type TmGlyDH lost all activity after 4 h in the presence of DHA at 50°C, but mutants K104Q and K361Q showed increased stability, maintaining 90% of activity after 5 h in DHA at 50°C.

4.2 INTRODUCTION

We previously characterized recombinant *Thermotoga maritima* glycerol dehydrogenase (TmGlyDH) (2). TmGlyDH is a multimeric enzyme whose crystal structure was solved as part of a structural proteomics project (3, 15), but its activity and stability properties had not been studied. Only the coordinates of one TmGlyDH monomer are deposited in the PDB by the authors of the crystal structure (3), so it is unclear whether the native enzyme is a tetramer as reported after the first crystallization (15), or an octamer as predicted by Pisa software and deposited in the PDB (7). The homologous glycerol dehydrogenase from *Bacillus stearothermophilus* shares 48% sequence identity with TmGlyDH and was reported to be a homooctamer (13). TmGlyDH has the potential to be used as a catalyst for dihydroxyacetone (DHA) production from glycerol or to produce R-1,2-propanediol at high enantiomeric excess from hydroxyacetone. While characterizing the enzyme, we observed that TmGlyDH was

inactivated by its product dihydroxyacetone (2). Dihydroxyacetone is the only FDA-approved sunless tanning reagent. It is able to turn skin brown through Maillard reactions with the primary amines in the Lys and Arg residues in proteins on the surface of the skin (Figure 4.1) (6).

Figure 4.1: Maillard reaction scheme.

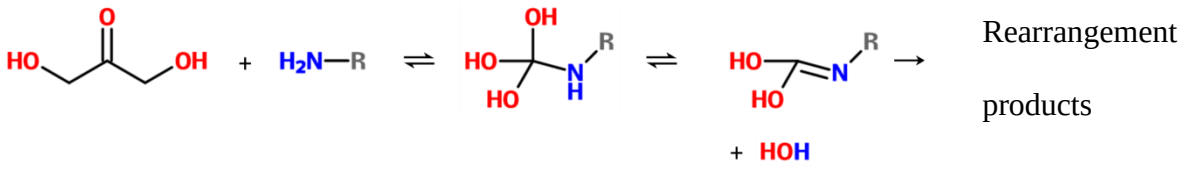

Protein glycation has been primarily studied because it leads to the formation of advanced glycation endproducts that are involved in the aging process as well as diabetes and diabetes related diseases (11, 12). DHA has also been observed to glycate human serum albumin (14). The extent of glycation by DHA increased with temperature (5 sites at 23°C, 9 at 37°C, and 14 at 41°C; at 30 mM DHA and pH 7.4), pH (5 sites at pH 5, 9 at pH 7.4, and 20 at pH 8.0; at 30 mM DHA and 37°C), and substrate concentration (14).

Glycation has also been observed to inactivate enzymes. The K_{cat}/K_m ratio of the rat liver aldehyde reductase decreased by 32% after glycation (16). During the enzymatic production of biologically active oligosaccharides, glycation was shown to inactivate *Penicillium citrinum* 1,2-α-mannosidase and almond α-mannosidase, and higher molecular weight enzyme species formed by glycation were observed using Matrix-assisted laser desorption/ionization-time of flight mass spectrometry (MALDI-TOF) (10). After a two-week reaction at 55°C, 40-60% of enzyme activity was lost. In reactions containing Maillard reaction inhibitors, the yield increased 27-53% compared to the control (10). However, adding inhibitors to synthetic reactions increases reaction costs and may also increase downstream purification costs.

Since TmGlyDH is inactivated by its product DHA, and DHA is known to readily react with amino groups through Maillard reactions (6), we expect that the main contributor to enzyme inactivation is glycation by DHA. We determined which Lys and Arg residues are susceptible to modification by DHA. These residues were targeted for mutagenesis to increase TmGlyDH's resistance to inactivation by DHA.

4.3 MATERIALS AND METHODS

4.3.1 Materials

TmGlyDH was purified, enzyme activity assays were performed, and mutants were constructed as described (2). Sequencing-grade trypsin and chymotrypsin were purchased from Promega (Madison, WI). DHA, iodoacetamide (IAA), and trifluoroacetic acid (TFA) were purchased from Sigma-Aldrich (St. Louis, MO). Monosodium and disodium phosphate were from J.T Baker (Avantor Performance Materials, Inc., Center Valley, PA). Ultrapure urea was from Invitrogen (Carlsbad, CA). 190 proof pure ethanol was from Koptec (King of Prussia, PA). Ammonium bicarbonate was from Jade scientific (Canton, MI).

4.3.2 Enzyme activity assays

Enzyme activity was measured at 50°C and 80°C by monitoring the absorbance of NADH at 340 nm (ε_{340} = 6,220 M^{-1} cm^{-1}) with a Varian Cary 300 UV/Vis spectrophotometer (Palo Alto, CA) equipped with a Peltier heating system. The final assay mixture typically contained 6.7 μg enzyme, 200 mM DHA, 200 μM NADH, and 50 mM sodium phosphate buffer (pH 7.45 at 50°C and pH 7.4 at 80°C). The reaction was started by adding 20 μL of 10 mM

NADH to 980 μL of the other components or adding 40 μL of enzyme (0.168 mg/mL) to 960 μL of other components in a heated quartz cuvette. All activity measurements at 50°C were performed in triplicate, and all activity measurements at 80°C were performed in quadruplicate.

4.3.3 Two-hour enzyme inactivation assays

For 2-h heat inactivations at 50°C, 44 μL of a 0.168 mg/mL solution (7.39 μg) of enzyme (wild-type or mutant) was added to 814 μL of 65 mM sodium phosphate buffer (pH 7.45), and incubated in an Eppendorf tube at 50°C for 2 h. The remaining activity was measured by adding 200 μL of pre-warmed 1 M DHA to the 780-μl enzyme solution, and starting the reaction by adding 20 μL of 10 mM NADH.

For 2-h inactivations by DHA at 50°C, 44 μL of a 0.168 mg/mL solution of enzyme was added to 1,034 μL of 50 mM sodium phosphate buffer (pH 7.45) containing 200 mM DHA, and incubated in an Eppendorf tube at 50°C for 2 h. Activity was measured after transferring 980 μL of the enzyme-DHA solution to a heated cuvette, and the reaction was started by adding 20 μL of 10 mM NADH. A two tailed student's t-test was used to determine if results were significant.

4.3.4 Time course enzyme inactivation assays

For time course heat inactivation assays at 50°C, TmGlyDH (58.6 μg) was incubated at 50°C for 7 h in 6.8 mL of 65 mM sodium phosphate buffer (pH 7.45 at 50°C) in a polypropylene tube. At each time point, 780 μL of the enzyme solution was added to 200 μL of 1 M DHA preheated at 50°C in a quartz cuvette, and the reaction was started by adding 20 μL of 10 mM

NADH. Non-linear curve fitting of all inactivation time courses was performed using Origin 8.0 (Originlab, Northampton, MA).

For time course inactivations by DHA at 50°C, TmGlyDH (58.6 μg) was incubated at 50°C for 7 h in 8.3 mL of 51 mM sodium phosphate buffer (pH 7.45 at 50°C) containing 200 mM DHA in a polypropylene tube. At each time point, 980 μL of the enzyme solution was added to a quartz cuvette preheated at 50°C, and the reaction was started by adding 20 μL of 10 mM NADH.

For time course heat inactivation assays at 80°C, TmGlyDH (6.7 μg) was incubated at 80°C for 0, 4, 8, 12, 16, and 20 min in 780 μL of a preheated solution of 64 mM sodium phosphate buffer (pH 7.4 at 80°C) in a quartz cuvette. After incubation, 20 μL of 10 mM NADH was added, and the reaction was started by adding 200 μL of preheated (80°C) 1 M DHA.

Time course inactivations by DHA at 80°C were set up as described for the time course heat inactivation assays at 80°C, except that the preheated DHA solution was added at the same time as the enzyme, and after incubation the reaction was started by adding NADH.

4.3.5 Trypsin and chymotrysin digests of TmGlyDH

Prior to digesting the enzyme, 1 nmol TmGlyDH was added to 300 μL of water. TmGlyDH was precipitated by diluting 5-fold with -20°C acetone and cooled at -20°C for 60 min. After centrifugation at 13,000 × *g* for 10 min at room temperature, the supernatant was decanted and the pellet was air dried for 30 min at room temperature. The pellet was dissolved in 100 μL of 8 M urea containing 400 mM ammonium bicarbonate, and incubated at 50°C for 30 min. The solution was cooled to room temperature and 12 μL of 100 mM iodoacetamide (IAA) was added. The solution was incubated at room temperature for 20 min in the dark, and diluted 8-fold with

50 mM ammonium bicarbonate. The digestion was started by adding 1 μg trypsin per nmol of TmGlyDH. The digestion was incubated overnight at 37°C, and stopped by adding trifluoroacetic acid (TFA) to a final concentration of 0.5% w/w. The digestion by chymotrypsin was as described above for trypsin. For the chymotrypsin/trypsin double digest, trypsin was added after the chymotrypsin digestion and incubated overnight at 37°C; the reaction was stopped by the addition of TFA. To ensure that hydrophobic peptides were not sticking to the sides of the Eppendorf tube, another set of digestions was performed followed by rinsing the tubes used for the digestion with ethanol. After the acetone precipitation step, the reaction was prepared using half the amount of all reagents (500 μL total). After the digestion, the tube was rinsed with 500 mL ethanol.

4.3.6 Identification of peptides by electrospray ionization time-of-flight mass spectrometry (ESI)-TOF

Immediately following digestion, peptides were separated by HPLC (Waters Corporation, Milford MA) using a C18 column (Beta basic-18, particle size 5 μm, dimensions 100 mm × 2.1 mm, Thermo scientific, Waltham, MA) at 0.25 mL/min at 30°C using a gradient from 98% A (0.1% formic acid) to 98% B (acetonitrile or methanol) over 10 min (acetonitrile) or 23 min (methanol) followed by a constant flow at 98% B for 2 min. Peptide masses were analyzed using ESI-TOF (Q-tof ultima, Waters Corporation, Milford MA). The molecular masses of all expected peptides, as well as those of the peptides modified by TCA or IAA, were calculated and searched for in the mass spectrum.

4.3.7 Identification of the TmGlyDH residues modified by DHA

To identify which residues were modified by DHA, TmGlyDH was incubated with DHA prior to being digested with trypsin and chymotrypsin. Five nmol of TmGlyDH (207 μg) were added to 300 μL of 200 μM DHA and incubated at 50°C for 5, 15, and 60 min. After acetone precipitation, the enzyme was digested as described above. Peptides were identified by ESI-TOF as described above. The previously observed peptides were searched for with and without the addition of the molecular mass of DHA. The Arg and Lys residues susceptible to modification by DHA were located in the TmGlyDH protein structure (PDB no. 1KQ3) and visualized using the PyMOL Molecular Graphics System, Version 1.3 (Schrödinger, LLC). The macromolecular assembly generated by Pisa software (7) was downloaded from the PDB and used to visualize TmGlyDH as an octamer in PylMol.

4.4 RESULTS

4.4.1 TmGlyDH inactivation by DHA at 50°C

During the previously reported kinetic characterization of TmGlyDH, we observed that TmDlyDH becomes inactivated by DHA (2). We set up a time course inactivation experiment to determine how much faster the enzyme inactivates in the presence of DHA (Figure 4.2). TmGlyDH quickly lost activity in the presence of DHA at 50°C, losing almost all activity after 4 h. In the absence of DHA, the enzyme retained over 90% activity after 7 h at 50°C. To engineer TmGlyDH for increased resistance to inactivation by DHA, the next step was to determine which residues get modified by DHA.

Figure 4.2: Time course of TmGlyDH inactivation at 50°C with and without DHA. (■): heat inactivation, exponential fit (—); (○): Inactivation by DHA, exponential fit (---)

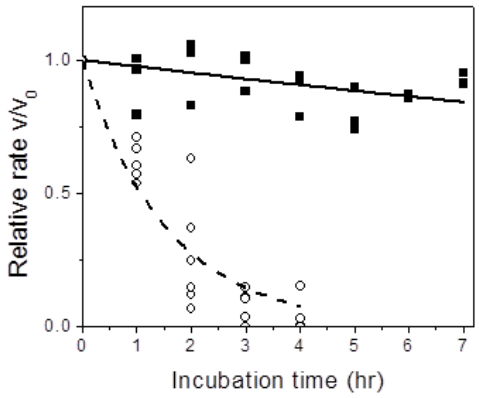

4.4.2 Identification of the TmGlyDH residues modified by DHA

To identify the amino acids susceptible to modification by DHA, we needed to observe all the TmGlyDH Arg and Lys residues represented in the TmGlyDH fragments after digestion with trypsin. The peptides were analyzed using HPLC electrospray ionization time of flight (HPLC-ESI-TOF) mass spectrometry. To facilitate observing large hydrophobic peptides, a second set of digestions was prepared including an ethanol rinsing step to recover the most hydrophobic fragments. Because not all Arg and Lys residues were represented in the peptides identified in tryptic digests, the enzyme was also digested with chymotrypsin and a combination of trypsin plus chymotrypsin.

Peptides corresponding to 23 of the 40 total Lys + Arg residues were identified in the trypsin digest. Adding the ethanol wash after the trypsin digestion yielded peptides for ten of the 40 total Lys + Arg residues, one of them not seen in the trypsin-only digest. Peptides corresponding to 26 of the 40 total Lys + Arg residues were identified in the chymotrypsin digest, eleven of them not found in the trypsin-only and trypsin-ethanol treatments. The chymotrypsin-ethanol treatment yielded peptides for 29 of the 40 total Lys + Arg residues, two

of them not found previously. The chymotrypsin/trypsin double digest yielded fragments corresponding to only four of the 40 total Lys + Arg residues, but three of them had not been found in the single digests. Combining results from all of the digests, peptides corresponding to every Lys and Arg residue were observed (Table S4.1).

The digestions and analysis were repeated after preincubating the enzyme with DHA for 5, 15, and 60 min at 50°C. Fifteen different Lys and Arg residues were found to be modified by DHA (Table 4.1). The residues modified by DHA were clustered together in five different regions on the surface of the protein (Figure 4.3). Five of the 15 total Arg and ten of the 25 total Lys residues become modified by DHA. Of the seven Arg and four Lys residues at subunit interfaces, only two (R143 and R217) become modified by DHA. Of the remaining, solvent-exposed 21 Lys and 7 Arg residues, 10 Lys and 3 Arg become modified by DHA.

Table 4.1: TmGlyDH residues found to be modified by DHA. Redundant information from different digestion conditions is not shown. Negative sign indicates no modification, positive sign indicates modification, asterisk indicates the peak disappeared, implying modification.

Residue	**Experimental conditions**	**Incubation Time (min)**		
		5	15	60
K60	Trypsin	-	*	*
K104	Trypsin	-	+	+
K106	Chymotrypsin-Ethanol	-	+	+
K107	Chymotrypsin-Ethanol	-	+	+
R143	Chymotrypsin-Ethanol	+	+	-
K157	Chymotrypsin-Ethanol	+	+	-
R161	Chymotrypsin-Ethanol	+	+	-
K181	Chymotrypsin-Ethanol	-	*	*
K183	Chymotrypsin-Ethanol	-	*	*
K216	Chymotrypsin	+	+	+
R217	Chymotrypsin	+	+	+
K222	Chymotrypsin	+	+	+
R358	Chymotrypsin-Ethanol	+	+	+
R360	Chymotrypsin-Ethanol	+	+	+
K361	Chymotrypsin-Ethanol	+	+	+

Figure 4.3: Crystal structure of TmGlyDH showing the residues modified by DHA. Left panel – ribbon diagram of one monomer showing the residues modified by DHA in stick representation. Right panel – ribbon diagram of one monomer and surfaces of surrounding subunits. All Lys and Arg residues of one monomer are shown in stick representation. Cyan – ribbon structure of TmGlyDH, Yellow – Lys and Arg residues modified by DHA, Red – all other Lys and Arg residues, Orange – active site Zn, Gray – surfaces of surrounding subunits.

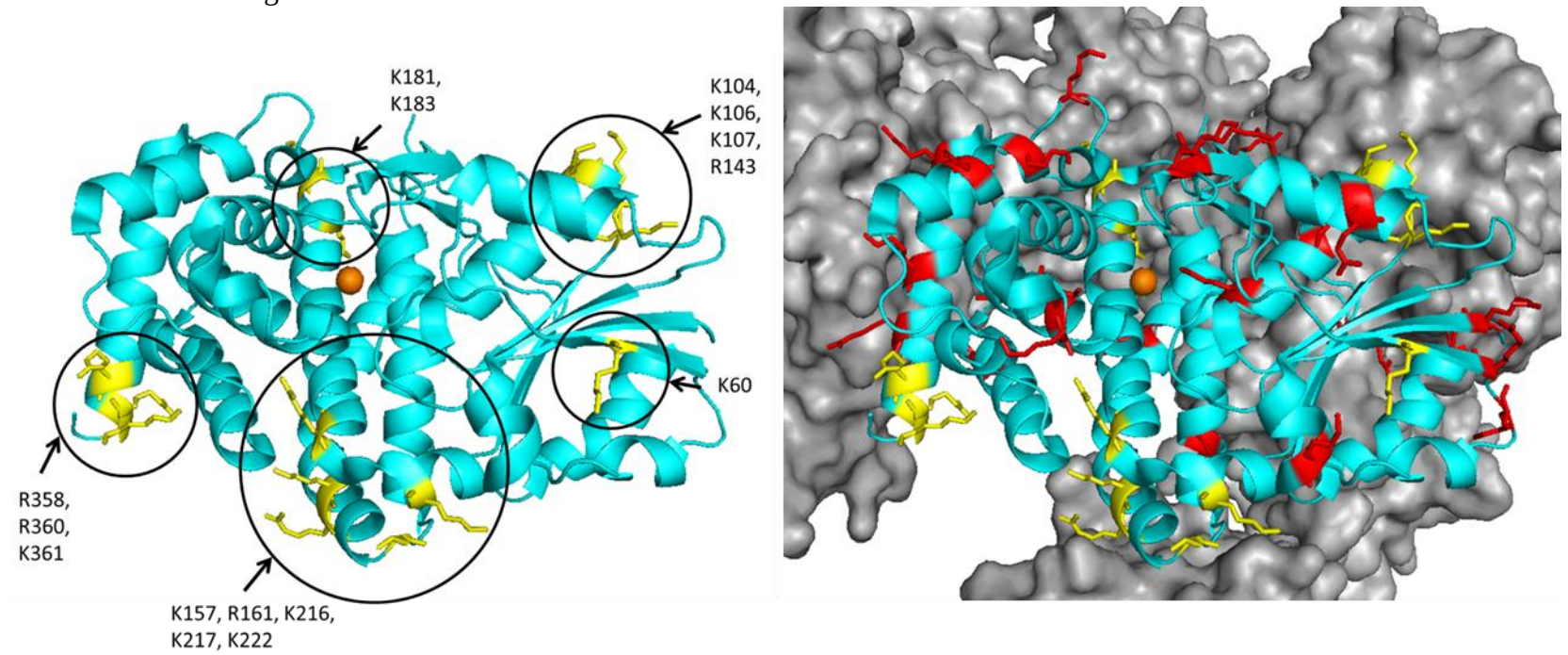

4.4.3 Screening TmGlyDH mutants for increased stability to DHA

Based on the hypothesis that modification by DHA of several of the 15 Arg and Lys identified leads to enzyme inactivation, mutations of these residues should make the enzyme less susceptible to inactivation by DHA. To test this premise, 14 of these 15 Lys and Arg residues were mutated individually to Gln. We chose Gln for the substitution because Gln is the amino acid most similar in size and hydrophilicity to Lys and it is able to form hydrogen bonds. K157 had previously been mutated to Gly in previous work (2). All the mutants maintained more than 60% of the wild type activity, except R143 and K183Q which only had 39% and 46% of the wild-type activity respectively.

Figure 4.4: Screening of TmGlyDH mutants for increased resistance to inactivation by DHA at 50°C. (■): Initial activity at 50°C; (▨): residual activity after a 2-h incubation at 50°C; (□): residual activity after a 2-h incubation with 200 mM DHA at 50°C; *: Statistically different from the wild-type enzyme's thermostability at 50°C ($p \leq 0.05$); **: Statistically different from the wild-type enzyme's stability in the presence of DHA at 50°C ($p \leq 0.05$).

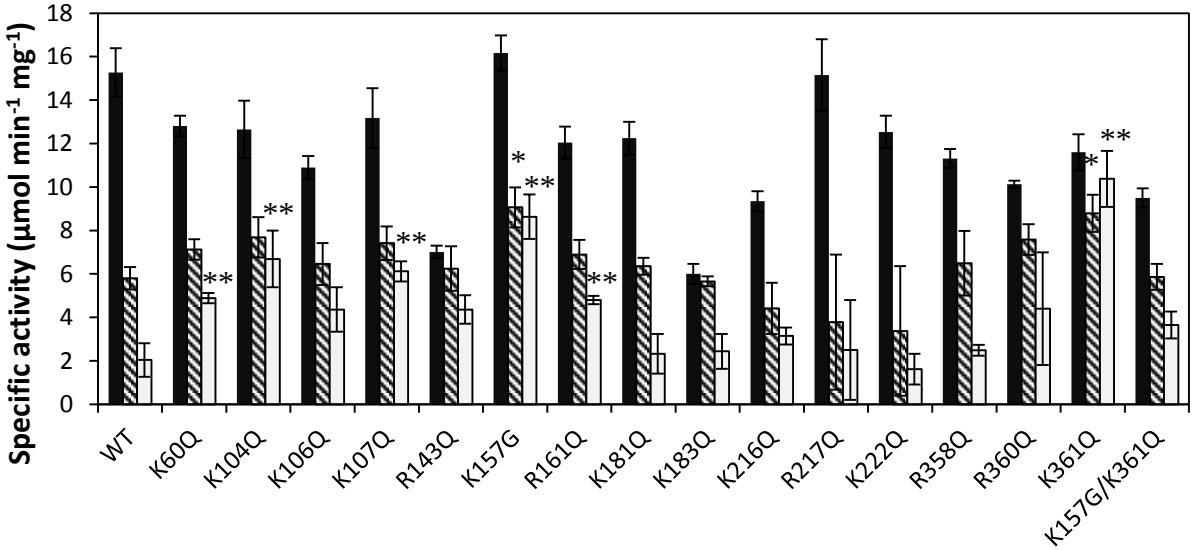

Mutant enzymes were first screened for stability to DHA by testing activity remaining after a 2-h incubation with DHA at 50°C (Figure 4.4). Stability in the absence of DHA was also

measured to highlight any change in thermostability. Six of the mutant enzymes (K60Q, K104Q, K107Q, K157G, R161Q, and R361Q) showed significantly ($p \leq 0.05$) increased stability compared to wild-type TmGlyDH in the presence of DHA.

Because temperature can have a large impact on enzyme inactivation, mutant enzymes that were significantly more stable than wild-type TmGlyDH at 50°C with DHA were also screened for increased resistance to inactivation by DHA at 80°C. In contrast to the 50°C results, mutants K104Q and K107Q were not significantly more stable than wild-type TmGlyDH with DHA at 80°C. Mutant K157G was the most stable, instead of K361Q. (Figure 4.5).

Figure 4.5: Residual activity of TmGlyDH and its mutants after a 16-min incubation with DHA at 80°C. (■): Initial activity at 80°C; (▨): residual activity after a 16-min incubation at 80°C; (□): residual activity after a 16-min incubation with 200 mM DHA at 80°C; *: Statistically different from the wild-type enzyme's thermostability at 80°C ($p \leq 0.05$); **: Statistically different from the wild-type enzyme's stability in the presence of DHA at 80°C ($p \leq 0.05$).

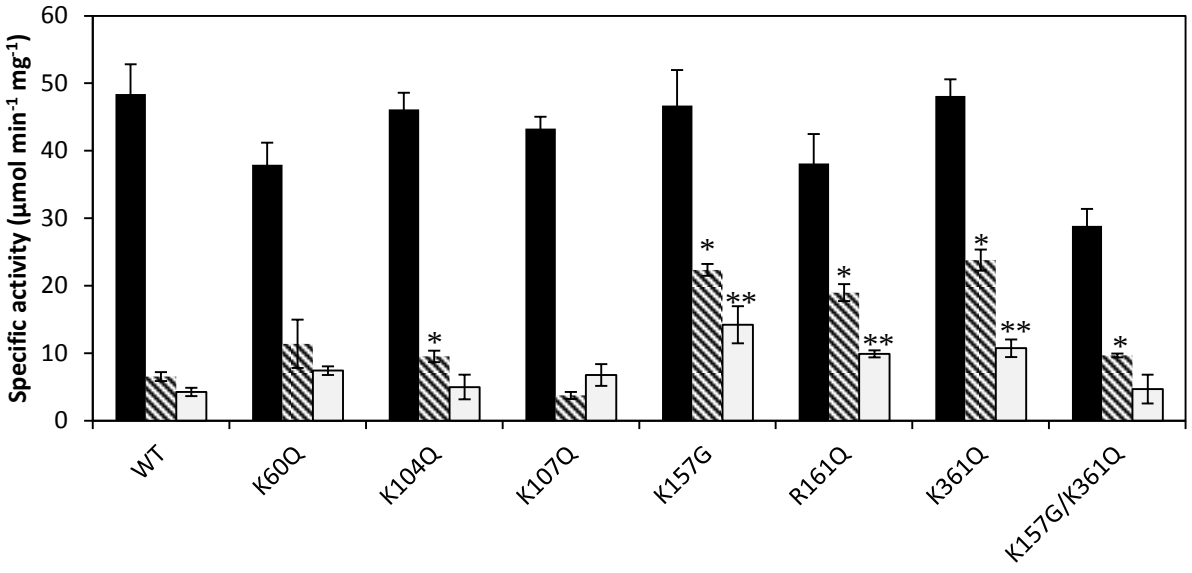

4.4.4 Time course analysis of mutants' stability to DHA

The three mutant enzymes showing the most increased resistance to inactivation by DHA at 50°C (K104G, K157G, and K361Q) and two of the most stable mutants at 80°C (K157G and R161Q) were further tested in a 7-h time course inactivation assay at 50°C. Data points were fit to an exponential decay model (eq. 1), but the fit was generally poor, so decay constants could not be calculated (Figure 4.6).

Equation 4.1

$$\frac{v}{v_0} = e^{-kt}$$

In general, the mutant enzymes were less thermostable than wild-type TmGlyDH, but K104Q and K361Q TmGlyDHs were stabilized by the presence of DHA. In the presence of DHA, wild-type TmGlyDH lost half of its activity between 1 and 2 h. Mutant K104Q was less thermostable than wild-type TmGlyDH, but DHA temporarily prevented its thermoinactivation, and its activity was only reduced by half after 7 h. The K157G and R161Q mutants were less thermostable than wild-type TmGlyDH, and both lost half of their activity after less than an hour in the presence of DHA. Mutant K361Q was less thermostable than wild-type TmGlyDH, but was the most resistant to inactivation by DHA; it remained almost 100% active after 5 h in the presence of DHA, and lost less than half its activity over the 7-h inactivation time course.

The four mutant TmGlyDHs that showed increased stability to DHA at both 80°C and 50°C were selected for a time course inactivation study at 80°C. Enzymes were incubated with and without DHA at 80°C, and activity was tested after 0, 4, 8, 12, 16, and 20 min of incubation. The inactivation time course data points were fit to an exponential decay model (eq. 1) where relative activity was plotted against incubation time and the exponential decay constant K was

calculated. The fits to the inactivation time courses at 80°C (Figure 4.7) (adjusted R^2 ranged from 0.66 to 0.98) were much better than the fits to the 50°C time course data, so decay constants are reported in Figure 4.8. The R161Q mutant had the smallest decay constant in the presence of DHA at 80°C, but the K157G mutant retained higher activity after 16 min of incubation with DHA at 80°C.

Figure 4.6: Time courses of TmGlyDH and mutants' inactivations at 50°C with and without DHA. (■): heat inactivation, exponential fit (—); (○): Inactivation by DHA, exponential fit (---).

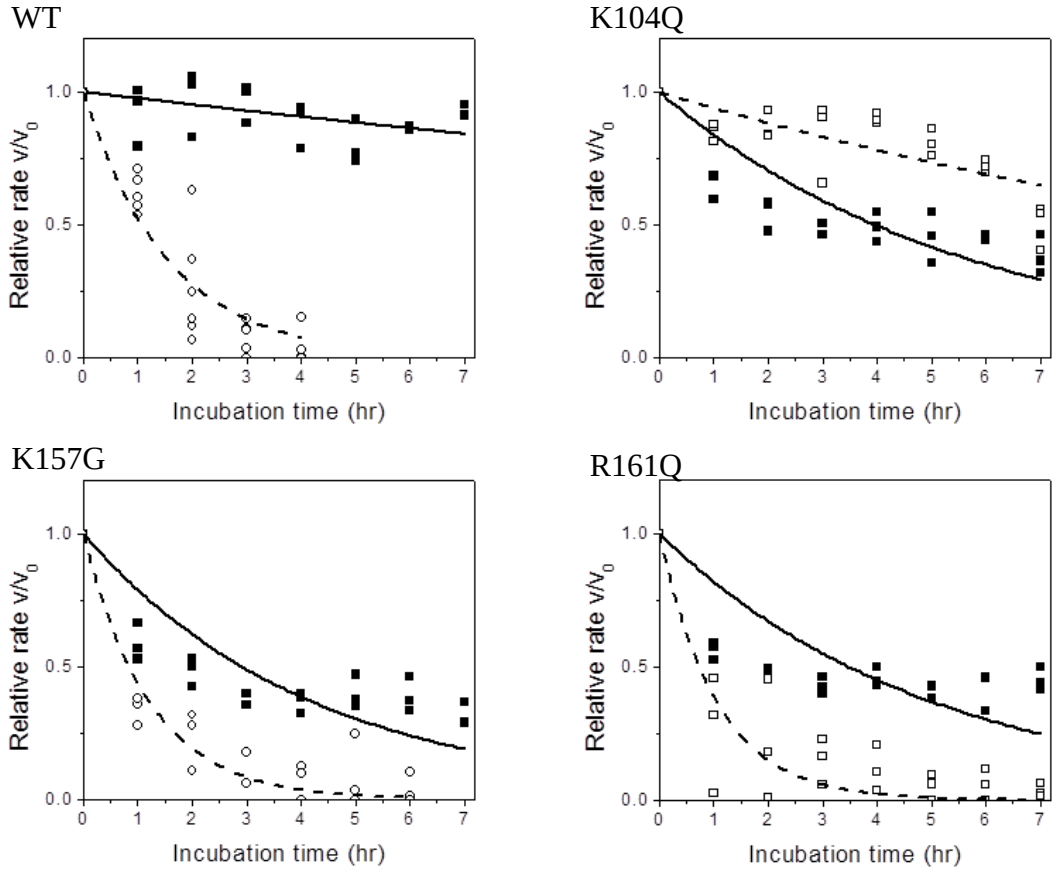

Figure 4.6 (cont'd)

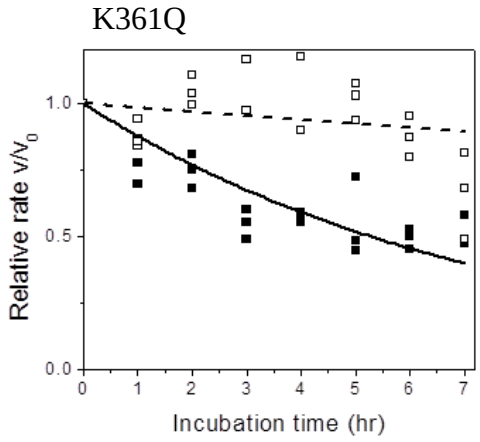

Figure 4.7: Inactivation time courses of TmGlyDH and its mutants at 80°C with and without DHA. (■): heat inactivation, exponential fit (—); (○): Inactivation by DHA, exponential fit (---). (A) Wild-type TmGlyDH; (B) TmGlyDH K60Q, (C) TmGlyDH K157G, (D) TmGlyDH R161Q, (E) TmGlyDH K361Q, (F) TmGlyDH K157G/K361Q, (G) TmGlyDH K157G/R161Q.

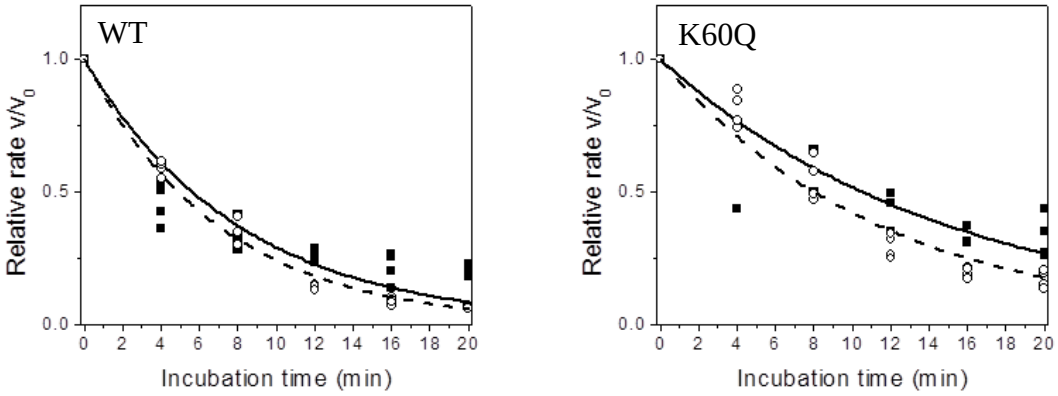

Figure 4.7 (cont'd)

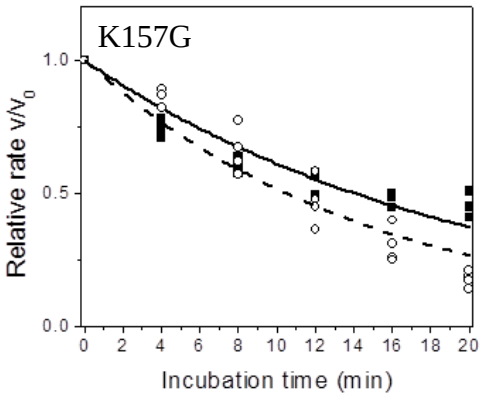

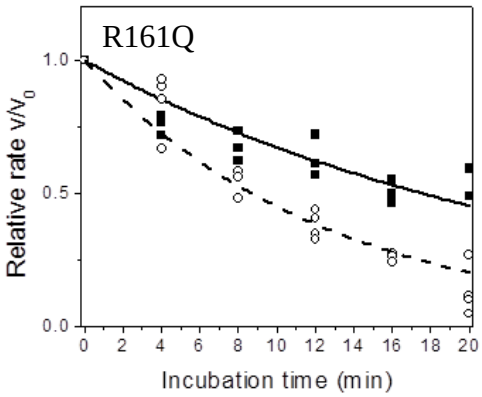

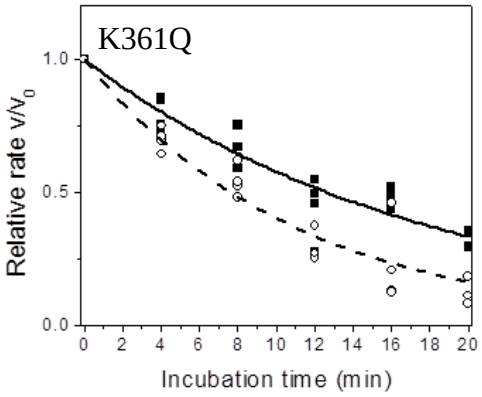

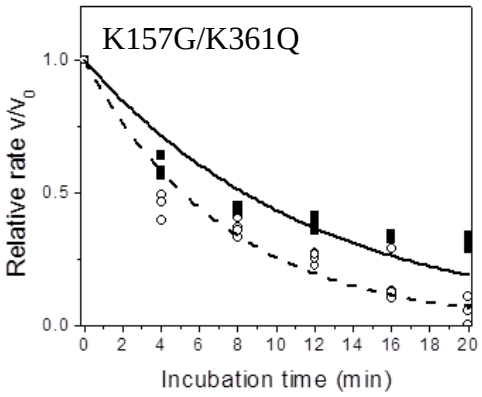

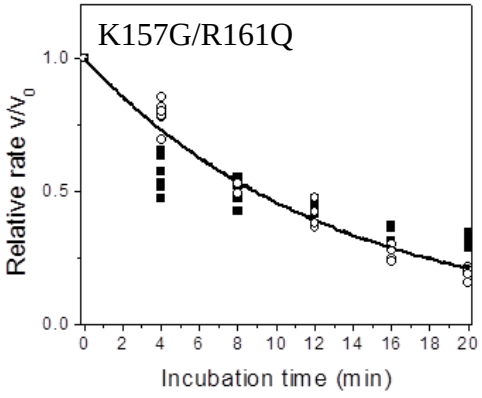

Figure 4.8: Specific activities and decay constants of wild-type TmGlyDH and its mutants at 80°C with and without DHA. Decay constants with standard error of TmGlyDH mutants incubated with DHA (dark gray) or in buffer only (light gray) at 80°C; specific activity at 80°C (Δ). *: Statistically different from the wild-type enzyme's thermostability at 80°C ($p \leq 0.05$), **: Statistically different from the wild-type enzyme's stability with DHA at 80°C ($p \leq 0.05$).

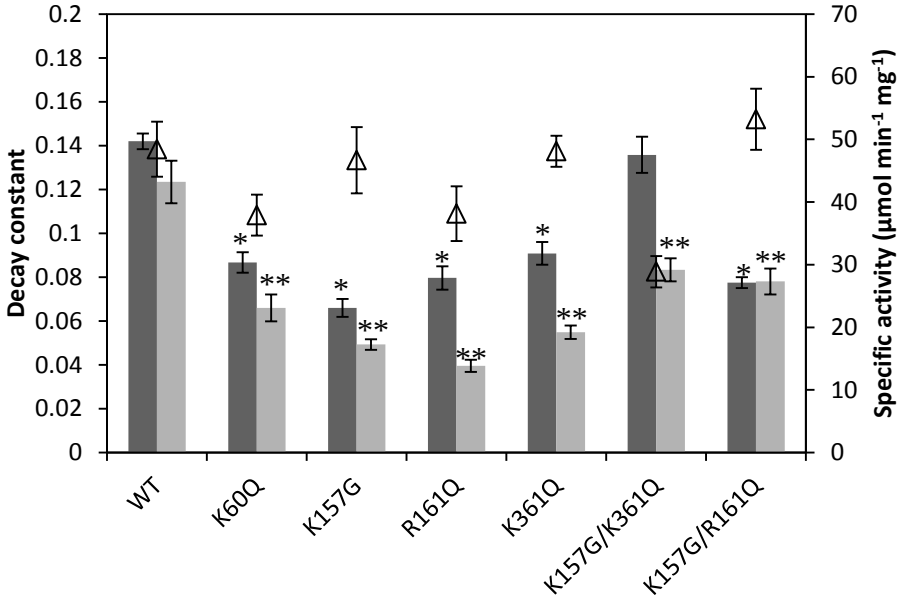

The mechanisms of inactivation by DHA at 50°C and 80°C appear to be different as evidenced by the different patterns of the time course inactivations. Surprisingly, the K104Q and K107Q mutants that were more resistant to inactivation by DHA at 50°C, were not particularly so at 80°C. We prepared a K157G/K361Q double mutant and tested it in both screens at 50°C and 80°C and in a time course inactivation at 80°C. The double mutant was less stable than the individual mutants at 80°C (Figures 4.7 and 4.8), and it was not significantly different from wild-type TmGlyDH at 50°C (Figure 4.5).

4.5 DISCUSSION

4.5.1 The importance of TmGlyDH stability

TmGlyDH has been previously characterized to determine if it is suitable for use in a catalytic reactor to produce DHA from glycerol (2). To use glycerol dehydrogenase as a catalyst, NAD^+ must be supplied to the reaction in stoichiometric amounts or it must be regenerated. Glutamate dehydrogenase and NADH oxidase have been used to regenerate oxidized cofactor, but their use is limited to the production of high value products because of the cost associated with using two enzymes for one reaction (17). Recent advances in electrochemical oxidation of NADH could make electrochemical regeneration of oxidized cofactors a lower cost alternative to enzymatic regeneration (9). Apart from supplying the cofactor to the reaction, the other main cost of enzymatic catalysis is the cost of producing and purifying the enzyme. Optimally the enzyme will be usable for many batch reactions, or for use in a flow-through reactor for many turnovers. In this study, we show that wild-type TmGlyDH is unstable in the presence of DHA, and therefore, wild-type TmGlyDH would need to be replaced often if used in a catalytic reactor. Reducing TmGlyDH inactivation by DHA will help address this issue.

4.5.2 TmGlyDH inactivation by DHA is a complex process

Our inactivation results have not been highly reproducible. For example, in the 2-h DHA inactivation screen, the K157G mutant retained more than 50% of its activity, but only showed about 25% of its activity after 2 h in the time course inactivation by DHA at 50°C. The variation between experiments could be explained by the complexity of the inactivation process. DHA could react with any of the 15 Lys and Arg residues accessible to modification in any order and at different rates. Not all modifications by DHA lead to inactivation, but for the ones that do, the kinetics of inactivation of each residue and the order in which the different residues get modified

in each experiment will affect the inactivation course. We might observe reproducible stabilization results only once enough residues are mutagenized to remove this stochasticity.

There are a number of different pathways to inactivation. When DHA modifies a given residue, neighboring residues may be more likely to get modified. And DHA reacting at some sites may have no effect on the enzyme at all. Also, modification at different specific sites could have a synergistic inactivating effect. DHA modification in one subunit may also change the inactivation process of adjacent subunits. Note that TmGlyDH has been shown to behave cooperatively in its kinetics for glycerol and dihydroxyacetone, where substrate binding in one subunit changes the substrate affinity of the other subunits (2). Also as the protein unfolds, it can start aggregation processes that can destabilize neighboring subunits in the multimer (8). The order of modification and effect on the enzyme could vary greatly between inactivation time courses. Mutating all the Lys and Arg residues that, once modified by DHA, inactivate the enzyme should make the kinetic data more consistent. In general, we trust the inactivation time course data more than the 2-h screening at 50°C and 16-min at 80°C data points because of the context of the surrounding time points.

4.5.3 DHA modification sites

The residues modified by DHA are localized in five general regions (Figure 4.3). Because the DHA modification sites seemed to cluster together at specific locations in the enzyme, it is possible that modification at one of the residues in each cluster leads to partial local unfolding, allowing nearby Lys and Arg residues to be modified by DHA as well. Similar proportions of Arg and Lys (33% and 40%, respectively) were modified by DHA, suggesting that both types of residues are equally susceptible to modification. The mutations that increased

stability to DHA (K104Q, and K361Q) at 50°C targeted residues that are solvent-exposed on the multimeric enzyme and are relatively far from the active site. At 50°C, the K361Q mutant is the enzyme most resistant to DHA, followed by the K104Q mutant. Both K361 and K104 form salt bridges (with E309 and E73, respectively). Mutations to Gln would disrupt these salt bridges, which may destabilize the protein at high temperatures and allow the heat inactivation processes to take place faster. But the effect of breaking the salt bridge may be small at 50°C because salt bridges are more stabilizing at higher temperatures than at moderate temperatures (4). Surprisingly, the addition of DHA actually stabilized these two mutant enzymes, allowing them to maintain their activity for several hours in DHA at 50°C. This effect could be because the substrate helps the enzyme retain its active conformation, modifications at other Lys or Arg residues offset the effect of breaking the salt bridges, or the substrate allows the enzyme to form an active oligomer different from the starting multimer (see below).

Because TmGlyDH is a multimer and the most stabilizing mutations are far from the active site, we checked whether these mutations are at subunit interfaces. Neither K104 nor K361 are. Of the 15 amino acids modified by DHA, only R143 and R217 are at a subunit interface, but neither mutant was more stable than the wild-type enzyme in the 2-h inactivation screen. In general, the Lys and Arg residues located at subunit interfaces are protected from modification by DHA: only 18% were modified versus 46% of solvent-exposed Lys and Arg residues. Of the two least active mutants, the R143Q mutant could have lower activity than wild-type TmGlyDH because of disruptions in the subunit interface. There was no clear reason for the K183Q mutant to have substantially reduced activity. K183 forms hydrogen bonds with the main chain oxygens of H335 and E337, but modeling of the K183Q mutation in TmGlyDH with PyMol suggests that Gln could maintain those hydrogen bonds (not shown).

4.5.4 Stability and biphasic behavior in 50°C inactivation time-courses

The inactivation time courses at 50°C with and without DHA did not follow first-order kinetics. As reported for urease and luciferase, non-first-order kinetics comes about when the different reactions that lead to inactivation are interacting with each other (8). Biphasic inactivation results from a combination of denaturation, aggregation, and coagulation. In most models of inactivation, the initial drop in activity results from denaturation of the oligomer reaching equilibrium, and the second phase is a result of coagulation and aggregation processes (5, 8). (Aggregation is the formation of non-native oligomers of the folded monomer, coagulation is the coalescence of unfolded monomers.) When peptide denaturation and multimer denaturation are at equilibrium, inactivation becomes directly proportional to aggregation and coagulation (8). For most of the mutants, inactivation in the absence of DHA at 50°C showed a biphasic pattern. For the K361Q and K104Q mutants, stability to DHA at 50°C appeared to have a period of stability, followed by inactivation. A so called grace period or induction period in inactivation time courses has been adequately described by changes in the multimeric species (1, 8). Particularly, multimeric enzymes that dissociate into active oligomers show a grace period in their inactivation kinetics (1, 8). The grace period is a result of the formation of active intermediates that subsequently form inactive aggregates, and the kinetics of this process is such that at higher temperatures, the inactivation will look more like first-order inactivation (1, 5, 8). Because the grace period was only observed in the presence of DHA, the enzyme-substrate complex may be able to form alternative active oligomers or DHA reacting at certain residues forms active intermediates, while the enzyme alone is unable to do so. Although we previously observed a brief grace period during inactivation of wild-type TmGlyDH by DHA at 50°C (2),

the enzyme had been cooled on ice after inactivation and then reheated to 50°C for 15 min prior to measuring residual activity. Here we tested activity directly after inactivation.

At higher temperatures, the acceleration of the inactivation process can make the multistep process appear to follow first-order kinetics (5, 8), which could explain why we observed better fits to the first-order inactivation equation at 80°C. At 80°C, inactivation processes that do not involve DHA will take place faster, reducing the relative effect of DHA on the enzymes' stability. The effect of modification by DHA is much more apparent at 50°C than at 80°C, as illustrated by the larger difference between the inactivation time courses with and without DHA at 50°C than at 80°C, indicating that thermal denaturation is the dominant process at 80°C. At 80°C, the K157G mutant is the most stable followed by the R161Q mutant. The most stabilizing mutations at 80°C are in (K157G) or near (R161Q) the NAD binding pocket. Modification of the wild-type enzyme by DHA at these sites could reduce affinity for the cofactor, thus reducing the apparent activity. If true, we would expect this effect to be small, though, because we used concentrations of NAD nearly 10-fold the K_m. If cofactor affinity is playing a role in the inactivation, testing activity with higher concentrations of NAD would eliminate the reduction in activity. It is possible that mutations K157G and R161Q both act through the same mechanism to increase stability, because the K157G/R161Q double mutant was not more stable than either of the individual mutants. The kinetics of modification at each site may be different at 50°C and 80°C, leading to different inactivation pathways. Determining the rate of modification at the two different temperatures could clarify the difference in inactivation mechanism. For our purposes, the increase in stability of TmGlyDH mutants with DHA at 50°C is more important because our proposed catalytic reactor will operate at 50°C and DHA will accumulate during operation.

4.6 CONCLUSION

TmGlyDH becomes inactivated by its product DHA by DHA reacting with different Lys and Arg residues. We identified 15 different amino acids susceptible to modification by DHA, located in five regions of the protein. The two sites that destabilize the enzyme most in DHA at 50°C are Lys361 and Lys104. Mutating these residues to Gln stabilized TmGlyDH in the presence of DHA at 50°C. Although the stability increased substantially, the enzyme still lost substantial activity after 7 h at 50°C. Combining multiple mutations may lead to increased stability of the enzyme.

4.7 SUPPLEMENTARY MATERIALS

Table S4.1: Conditions used to detect peptides containing all Lys and Arg residues. •: Peptide detected prior to incubation with DHA, and not modified by DHA. º: Peptide detected prior to incubation with DHA and susceptible to modification by DHA. *: peptide detected prior to incubation with DHA, but disappearing after incubation with DHA.

			Trypsin digest		Chymotrypsin digest		Chymotrypsin then trypsin
	Residue		Normal	With ethanol	Normal	With ethanol	Normal
1	R	10	•	•	•		
2	R	27	•	•	•	•	
3	R	31					•
4	K	42	•		•	•	
5	K	55	•		•		
6	R	57			•		
7	K	60	*		•		
8	R	74			•		
9	K	93	•		•		
10	K	99			•	•	
11	K	104	º			º	
12	K	106				º	
13	K	107				º	
14	K	136			•	•	
15	R	137			•	•	
16	R	143	•	•		º	
17	K	157	•	•	•	º	
18	R	161	•		•	º	
19	K	181			•	*	
20	K	183			•	*	
21	R	191	•	•	•	•	
22	R	202	•			•	
23	K	216			º	º	
24	R	217	*		º	º	
25	K	222	•		º	º	
26	K	230	•	•		•	
27	K	266			•	•	
28	K	272			•	•	
29	K	286	•		•	•	
30	R	288	•		•	•	
31	K	289			•	•	
32	K	322					•
33	K	326		•			
34	K	330	•	•			•
35	K	344					•
36	K	351	•	•	•	•	
37	R	355	•		•	•	
38	R	358	•	•		º	
39	R	360	•			º	
40	K	361	•			º	

REFERENCES

REFERENCES

1. **Atyaksheva, L. F., O. S. Pilipenko, E. S. Chukhrai, and O. M. Poltorak.** 2008. Similarity of and differences between the mechanisms of thermal inactivation of β-galactosidases of different origins. Russ. J. Phys. Chem. A **82:**864–869.

2. **Beauchamp, J., P. G. Gross, and C. Vieille.** 2014. Characterization of *Thermotoga maritima* glycerol dehydrogenase for the enzymatic production of dihydroxyacetone. Appl Microbiol Biotechnol **98:**7039–7050.

3. **Brinen, L. S., J. M. Canaves, X. Dai, A. M. Deacon, M. A. Elsliger, S. Eshaghi, R. Floyd, A. Godzik, C. Grittini, S. K. Grzechnik, C. Guda, L. Jaroszewski, C. Karlak, H. E. Klock, E. Koesema, J. S. Kovarik, A. Kreusch, P. Kuhn, S. A. Lesley, D. McMullan, T. M. McPhillips, M. A. Miller, M. D. Miller, A. Morse, K. Moy, J. Ouyang, A. Robb, K. Rodrigues, T. L. Selby, G. Spraggon, R. C. Stevens, H. v. d. Bedem, J. Velasquez, J. Vincent, X. Wang, B. West, G. Wolf, S. S. Taylor, K. O. Hodgson, J. Wooley, and I. A. Wilson.** 2003. Crystal structure of a zinc-containing glycerol dehydrogenase (TM0423) from *Thermotoga maritima* at 1.5 Å resolution. Proteins: Struct., Funct., Bioinf. **50:**371–374.

4. **Elcock, A. H.** 1998. The stability of salt bridges at high temperatures: implications for hyperthermophilic proteins. J. Mol. Biol. **284:**489–502.

5. **Illeová, V., M. Polakovič, V. r. Štefuca, P. Ačai, and M. Juma.** 2003. Experimental modelling of thermal inactivation of urease. J. Biotechnol. **105:**235–243.

6. **Johnson, J. A., and R. M. Fusaro.** 1994. Alteration of skin surface protein with dihydroxyacetone: a useful application of the Maillard browning reaction, p. 114–119. *In* T. P. Labuza, G. A. Reineccius, V. M. Monnier, J. O'Brien, and J. W. Baynes (ed.), Maillard Reactions in Chemistry, Food, and Health. The Royal Society of Chemistry, Cambridge.

7. **Krissinel, E., and K. Henrick.** 2007. Inference of macromolecular assemblies from crystalline state. J. Mol. Biol. **372:**774–797.

8. **Lencki, R. W., J. Arul, and R. J. Neufeld.** 1992. Effect of subunit dissociation, denaturation, aggregation, coagulation, and decomposition on enzyme inactivation kinetics: II. Biphasic and grace period behavior. Biotechnol. Bioeng. **40:**1427–1434.

9. **Li, H., R. Li, R. M. Worden, and S. Calabrese Barton.** 2014. Facilitation of high-rate NADH electrocatalysis using electrochemically activated carbon materials. ACS Appl. Mater. Inter. **6:**6687–6696.

10. **Maitin, V., and R. A. Rastall.** 2004. Enzyme glycation influences product yields during oligosaccharide synthesis by reverse hydrolysis. J. Mol. Catal. B: Enzym. **30:**195–202.

11. **Nowotny, K., T. Jung, A. Höhn, D. Weber, and T. Grune.** 2015. Advanced glycation end products and oxidative stress in type 2 diabetes mellitus. Biomolecules **5:**194–222.

12. **Prasad, C., V. Imrhan, F. Marotta, S. Juma, and P. Vijayagopal.** 2014. Lifestyle and advanced gycation end products (AGEs) burden: its relevance to healthy aging. Aging Dis. **5:**212–217.

13. **Ruzheinikov, S. N., J. Burke, S. Sedelnikova, P. J. Baker, R. Taylor, P. A. Bullough, N. M. Muir, M. G. Gore, and D. W. Rice.** 2001. Glycerol dehydrogenase: structure, specificity, and mechanism of a family III polyol dehydrogenase. Structure **9:**789–802.

14. **Seneviratne, C., G. W. Dombi, W. Liu, and J. A. Dain.** 2012. In vitro glycation of human serum albumin by dihydroxyacetone and dihydroxyacetone phosphate. Biochem. Biophys. Res. Commun. **417:**817–823.

15. **Srinivasan, V., K. S. Ma, M. W. W. Adams, M. G. Newton, J. P. Rose, and B. C. Wang.** 2002. Towards the crystal structure of glycerol dehydrogenase from *Thermotoga maritima*. Acta Crystallog. D. **D58:**867–869.

16. **Takahashi, M., Y.-b. Lu, T. Myint, J. Fujii, Y. Wada, and N. Taniguchi.** 1995. In vivo glycation of aldehyde reductase, a major 3-deoxyglucosone reducing enzyme: identification of glycation sites. Biochemistry **34:**1433–1438.

17. **van der Donk, W. A., and H. Zhao.** 2003. Recent developments in pyridine nucleotide regeneration. Curr. Opin. Biotechnol. **14:**421–426.

CHAPTER 5. Conclusions and future work

5.1 REVIEW OF PROJECT

Dehydrogenases are potential catalysts for the production of many different compounds, including chiral compounds and pharmaceutical precursors (17, 18). Catalytic use of dehydrogenases has been limited due to the need to supply NAD to the reaction in stoichiometric amounts or regenerate the cofactor. A limited number of high-value chemicals are produced by dehydrogenases with a cofactor regeneration method. Typically the cofactor is regenerated by a second dehydrogenase working in the opposite direction. The extra cost associated with cofactor regeneration is the main limitation for industrial applications. Electrochemical cofactor regeneration could be a lower cost alternative to enzyme coupled regeneration. The efficiency of NADH electro-oxidation has been substantially increased recently, making electrochemical regeneration a suitable alternative for reactions that require NAD^+ (10, 11). Immobilizing the enzyme and cofactor onto the electrode surface will allow reuse of the electrode for many catalytic cycles. The goal of the collaboration project of the Vieille, Worden, and Calabrese Barton laboratories is to develop a bioelectronic catalytic reactor that uses dehydrogenases to catalyze chemical reactions. The long-term goal is to produce DHA from glycerol using TmGlyDH in an electrochemical reactor. For my part of that project, I characterized and engineered TmGlyDH. I also immobilized NAD while maintaining its coenzymic activity.

5.1.1 Review of TmGlyDH characterization

To determine appropriate reactor operating conditions and enzyme immobilization conditions, TmGlyDH's apparent kinetic parameters were determined for glycerol, DHA, and NAD(H) at different pH values at 50°C. The Michaelis-Menten equation was not a good fit to the kinetics data for glycerol and DHA because of apparent negative cooperativity. Thus kinetic

data for these substrates were fit to the Hill equation. The optimum pH for glycerol oxidation was 7.9 with apparent V_{max}, $K_{0.5}$ for glycerol, and n of 24 ± 1.4 μmol min^{-1} mg^{-1}, 39 ± 7 mM, and 0.86 ± 0.13, respectively, where n indicates the cooperativity level. TmGlyDH activity with N^6-CM-NAD^+ was only 2% of the activity with NAD^+. Single and double mutations and a triple mutant in the enzyme's active site were produced to increase activity with the soluble NAD analogue; the activity of the best mutant with N^6-CM-NAD^+ increased over 10-fold. However, the activity of the TmGlyDH mutants with sepharose-immobilized N^6-CM-NAD was the same or lower than that of the wild-type enzyme.

In a catalytic system, the longevity of the catalyst is critical because renewing the catalyst is costly. We observed that TmGlyDH becomes inactivated by its product, DHA. TmGlyDH inactivation by DHA is a result of the enzyme being modified by Maillard reactions between the Lys and Arg residues and DHA. In Chapter 4, I used mass spectrometry to identify which amino acids are being modified by DHA and mutated those amino acids to improve TmGlyDH stability in the presence of DHA. The mutants' stability to DHA was not consistent at 50°C and 80°C. The mutant most stable to DHA at 50°C was K361Q while the mutant most stable to DHA at 80°C was K157G. Combining the K157G and K361Q mutations together did not improve stability to DHA at 50°C or at 80°C significantly. Overall, the best mutant (K361Q) retained initial activity and maintained activity twice as long as the wild-type enzyme in the presence of DHA at 50°C.

5.1.2 Suitability of TmGlyDH for use in bioelectrocatalytic system

TmGlyDH promises to be a useful catalyst for the production of DHA using a regenerated cofactor, but there are several reasons for which using TmGlyDH as a model system

for a bioelectronic reactor is not ideal. The kinetics of TmGlyDH do not fit standard Michaelis-Menten kinetics, which will complicate mathematical modeling of the system. Modeling the reversible kinetics of a dehydrogenase-based biofuel cell system has been demonstrated (7), but modeling the reversible kinetics of cooperative enzymes would require creating a different, potentially more complicated model using the reversible Hill equation (5). The reversible rate equation for cooperative enzymes is empirical and does not provide mechanistic parameters (5). Another limitation is that the enzyme becomes inactivated by its product, losing all activity after 4 h in the presence of DHA at 50°C. To prevent inactivation of the enzyme catalyst, DHA would need to be continually removed from a catalytic reactor; this problem has been partially addressed by mutating the DHA reactive Lys and Arg residues. The TmGlyDH mutants produced have significantly increased stability to DHA at 50°C, but they lost thermostability. The best mutants, K104Q and K361Q, retained similar initial activity to the wild-type and maintained 90% of activity after 5 h with DHA. But K104Q and K361Q lost half their activity after about 2 h and 5 h at 50°C, respectively, compared to the wild-type enzyme, which lost only about 10% activity after 7 h at 50°C in the absence of DHA.

5.1.3 Suitability of N^6-immobilized NAD for use in bioelectrocatalytic systems

To determine which chemical groups on NAD^+ are accessible enough for binding with a linker for immobilization, NAD^+ was modeled into the crystal structure of TmGlyDH and into a homology model of TmMtDH. Based on a review of the literature pertaining to available chemistry to modify NAD and to the ability of enzymes to bind and use immobilized-NAD analogues, I chose the N^6-amine on the adenine moiety of NAD^+ for modification. N^6-carboxymethyl-NAD^+ (N^6-CM-NAD^+) was synthesized to allow binding to amines through

carbodiimide coupling. In Chapter 2, I demonstrated that TmGlyDH could use the immobilized cofactor and that the length of the linker tethering the immobilized-N^6-CM-NAD to the surface had little effect on the ability of the enzyme to use the immobilized NAD.

In Chapter 3, I showed that several different dehydrogenases could use sepharose-immobilized-N^6-CM-NAD and that the enzymes' active site structures could predict activity with soluble N^6-CM-NAD, but not with immobilized NAD. My results indicate that N^6-immobilized-NAD should have coenzymic activity with many dehydrogenases and that it is suitable for use in an electrochemical system.

5.2 FUTURE WORK

5.2.1 Immobilizing NAD on an electrode

Having demonstrated that N^6-immobilized NAD is usable by many different dehydrogenases, the logical next step is to immobilize it on an electrode. The electrode needs to be activated and modified to be a good NADH oxidation catalyst. Our collaborators have demonstrated that activated carbon electrodes with methylene green adsorbed onto the surface have excellent NADH oxidation activity (10). They incorporated carbon nanotubes that were previously functionalized by carboxylation, and then electrooxidized them by cyclic voltammetry. The carboxyl groups on the carbon nanotubes should provide active groups to which a diamine linker can be attached. After electroactivation of the carbon nanotube-modified electrode, methylene green can be adsorbed onto the surface and a diamino linker can be attached through carbodiimide-promoted coupling. This surface should be tested for catalytic NADH oxidation to confirm that the addition of a linker molecule does not decrease the NADH oxidation rate because the long carbon chain in the diamino linkers may act as an insulator,

inhibiting current flow. Then the N^6-CM-NAD can be immobilized to the terminal amine groups through carbodiimide-promoted coupling.

An alternative approach to modifying the electrode is to build up layers of polyelectrolyte (3). Because the carbon nanotube electrode has carboxyl groups, it is expected to have a negative charge. Thus, asorbing a layer of a positively charged polymer like polyethyleneimine on the electrode surface would provide primary amines to bind N^6-CM-NAD. Multiple layers of alternatively charged polymers could also be added, followed by NAD immobilization, although too many layers may hold NAD too far from the catalytic surface.

5.2.2 Engineering of TmGlyDH

Directed engineering of TmGlyDH was only marginally successful for improving activity with N^6-CM-NAD and for stabilizing the enzyme to DHA. For stability to DHA, there are many possible double mutants, or triple mutants, that could further improve stability. First, a 7-h time course for the single mutant K107Q should be performed, since the K107Q mutant retained almost as much activity after 2 h with DHA as the K104Q mutant did. Then combinations of K104Q, K361Q, and K107Q (if K107Q's increased stability to DHA is confirmed) should be prepared. Combinations of these mutations could further improve TmGlyDH's stability to DHA. The approach taken to stabilize TmGlyDH to DHA is limited by only modifying residues that react with DHA. An alternative strategy to stabilize the enzyme is to do directed evolution. Directed evolution could introduce mutations that counteract the effects of the Lys and Arg residues being modified by DHA instead of just mutating the specific residues that get modified. Error-prone PCR could be used to mutate the enzyme and then mutants could be screened by incubating them for several hours with DHA. Mutations that counteract the structure changes

that take place when DHA modifies the Lys and Arg residues would show increased residual activity.

5.2.3 Adding TmGlyDH to the bioelectronic interface

After NAD is immobilized onto the electrode surface, the next step is to immobilize the enzyme. TmGlyDH should have affinity for the electrode-immobilized NAD, and can then be cross-linked in place using glutaraldehyde. A similar approach to the kinetic based locking on strategy used for affinity chromatography with N^6-immobilized NAD-sepharose (2, 15) (see Chapter 1) could be employed to increase the enzyme's affinity for electrode-immobilized NAD. Adding a substrate analog like Tris (see Chapter 2) would allow the enzyme to form an inactive enzyme-Tris-(electrode-immobilized NAD) complex, holding the enzyme on the electrode surface. Then the addition of glutaraldehyde would fix the enzyme in place followed by washing the Tris away. With the enzyme and cofactor immobilized, the electrode should be usable for multiple catalytic cycles, thus reducing the operating costs. An added advantage to immobilizing TmGlyDH is that immobilization of the enzyme onto the electrode surface couldfurther stabilize TmGlyDH to DHA because the cross-linker may react with some of the DHA reactive Lys and Arg residues, immobilization could eliminate the aggregation and coagulation processes, and immobilization generally increases enzyme stability (13, 14).

5.3 ADDITIONAL USES OF THE BIOELECTRONIC INTERFACE

After the immobilization of NAD and TmGlyDH onto the electrode surface, the electrochemical properties would be tested. If the bioelectronics interface shows suitable current densities at moderate overpotentials and works for DHA production, it would be a proof of

concept for producing a dehydrogenase-based catalytic electrochemical reactor. The next step would be to apply other enzymes to the interface. I have demonstrated that a number of different dehydrogenases should be able to use N^6-immobilized-NAD and therefore the electrode interface should be adaptable to many different dehydrogenases. A working electrochemical connection could be used for many additional applications such as fuel cells and fuel cell powered implantable devices such as a blood glucose sensor and other biosensors (1, 3, 4, 6-9, 12, 16, 19). The breadth of reactions catalyzed and the wide acceptance of N^6-immobilized NAD by dehydrogenases would allow the adaptation of the bioelectronic system to many novel applications.

REFERENCES

REFERENCES

1. **Calabrese Barton, S., J. Gallaway, and P. Atanassov.** 2004. Enzymatic biofuel cells for implantable and microscale devices. Chem. Rev. **104:**4867–4886.

2. **Forde, J., L. Oakey, L. Jennings, and P. Mulchahy.** 2005. Fundamental differences in bioaffinity of amino acid dehydrogenases for N^6- and S^6-linked immobilized cofactors using kinetic-based enzyme capture strategies. Anal. Biochem. **338:**102–112.

3. **Hassler, B. L., N. Kohli, J. G. Zeikus, I. Lee, and R. M. Worden.** 2007. Renewable dehydrogenase-based interfaces for bioelectronic applications. Langmuir **23:**7127–7133.

4. **Hassler, B. L., and R. M. Worden.** 2006. Versatile bioelectronic interfaces based on heterotrifunctional linking molecules. Biosens. Bioelectron. **21:**2146–2154.

5. **Hofmeyr, J.-H. S., and H. Cornish-Bowden.** 1997. The reversible Hill equation: how to incorporate cooperative enzymes into metabolic models. Comput. Appl. Biosci. **13:**377–385.

6. **Jasti, L. S., S. R. Dola, N. W. Fadnavis, U. Addepally, S. Daniels, and S. Ponrathnam.** 2014. Co-immobilized glucose oxidase and β-galactosidase on bovine serum albumin coated allyl glycidyl ether (AGE)-ethylene glycol dimethacrylate (EGDM) copolymer as a biosensor for lactose determination in milk. Enzyme Microb. Technol. **64–65:**67–73.

7. **Kar, P., H. Wen, H. Li, S. D. Minteer, and S. C. Barton.** 2011. Simulation of multistep enzyme-catalyzed methanol oxidation in biofuel cells. J. Electrochem. Soc. **158:**B580–B586.

8. **Kulys, J. J., U. Bilitewski, and R. D. Schmid.** 1991. Reagentless biosensors for substrates of dehydrogenases. Anal. Lett. **24:**181–189.

9. **Li, G., N. Z. Ma, and Y. Wang.** 2005. A new handheld biosensor for monitoring blood ketones. Sens. Actuators, B **109:**285–290.

10. **Li, H., R. Li, R. M. Worden, and S. Calabrese Barton.** 2014. Facilitation of high-rate NADH electrocatalysis using electrochemically activated carbon materials. ACS Appl. Mater. Inter. **6:**6687–6696.

11. **Li, H., H. Wen, and S. Calabrese Barton.** 2012. NADH oxidation by electropolymerized azines on carbon nanotube modified electrodes. Electroan. **24:**398–406.

12. **Lobo, M. J., A. J. Miranda, and P. Tuñón.** 1997. Amperometric biosensors based on NAD(P)-dependent dehydrogenase enzymes. Electroanalysis **9:**191–202.

13. **López-Gallego, F., L. Betancor, C. Mateo, A. Hidalgo, N. Alonso-Morales, G. Dellamora-Ortiz, J. M. Guisán, and R. Fernández-Lafuente.** 2005. Enzyme stabilization by glutaraldehyde crosslinking of adsorbed proteins on aminated supports. J. Biotechnol. **119:**70–75.

14. **Mateo, C., J. M. Palomo, G. Fernandez-Lorente, J. M. Guisan, and R. Fernandez-Lafuente.** 2007. Improvement of enzyme activity, stability and selectivity via immobilization techniques. Enzyme Microb. Technol. **40:**1451–1463.

15. **Oakey, L., and P. Mulcahy.** 2004. Immobilized cofactor derivatives for kinetic-based enzyme capture strategies: direct coupling of $NAD(P)^+$. Anal. Biochem. **335:**316–325.

16. **Wang, Z., M. Etienne, F. Quilès, G.-W. Kohring, and A. Walcarius.** 2012. Durable cofactor immobilization in sol-gel bio-composite thin films for reagentless biosensors and bioreactors using dehydrogenases. Biosens. Bioelectron. **32:**111–117.

17. **Weckbecker, A., H. Groger, and W. Hummel.** 2010. Regeneration of nicotinamide coenzymes: principles and applications for the synthesis of chiral compounds. Adv. Biochem. Engin./Biotechnol. **120:**195–242.

18. **Wichmann, R., and D. Vasic-Racki.** 2005. Cofactor regeneration at the lab scale. Adv. Biochem. Engin./Biotechnol. **92:**225–260.

19. **Zhang, M., C. Mullens, and W. Gorski.** 2007. Co-immobilization of dehydrogenases and their cofactors in electrochemical biosensors. Anal. chem. **79:**2446–2450.